FRACTURE OF HSLA STEELS

MICROSTRUCTURAL ASPECTS OF THE FRACTURE PARAMETERS OF CONTROLLED ROLLED HSLA-STEELS

by

JON DAG EVENSEN, siv.ing.

A Thesis

Submitted to the School of Graduate

Studies in Partial Fulfilment of the

Requirements for the Degree

Doctor of Philosophy

McMaster University

February 1978

DOCTOR OF PHILOSOPHY (1978) McMaster University

(Metallurgy and Materials Science) Hamilton, Ontario

TITLE : Microstructural Aspects of the Fracture Parameters of Controlled Rolled HSLA-steels.

AUTHOR : JON DAG EVENSEN, siv.ing.
(Technical University of Norway)

SUPERVISOR: Professor J.D. Embury

NUMBER OF PAGES: 190 (xvi)

ABSTRACT

A combination of high strength and good fracture resistance is obtained in high strength low alloy (HSLA) steels by the use of controlled rolling and addition of micro alloying elements to refine the scale of the microstructure. In these fine grained materials traditional property-structure relationships do not adequately describe the fracture behaviour.

This thesis is concerned with the fracture properties of HSLA-steels at various temperatures and stress states. Three modes of failure are commonly observed. At low temperatures cleavage is the predominant fracture mode, whereas ductile failure by nucleation and growth of voids occurs at higher tempratures. In the intermediate temperature range delamination fracture on planes parallel to the rolling plane is observed. The various fracture mechanisms are discussed in terms of the detailed microstructure of the materials which has been characterized by the use of standard optical and electron metallography. In addition failure criteria for the most common fracture modes have been developed.

It is found that the condition for cleavage failure is adequately described in terms of a Griffith equation where the crack length is determined by an effective grain size of the order of twice the ferrite grain size. Further it is argued that the low temperature fracture toughness can be expressed by the cleavage stress and the size

of the process zone. For fine grained materials the process zone size is found to be independent of the scale of the microstructure.

The resistance to ductile fracture has been characterized in terms of a critical crack opening displacement (COD). It is argued that the COD value is determined by the size of the process zone which is independent of the scale of plasticity. The process zone size is related to the inclusion spacing.

Delamination is found to occur mainly by a grain boundary tearing mechanism. However, the presence of inclusion aggregates may reduce the fracture stress substantially. Delamination by the grain boundary tearing mechanism occurs at a critical value of the maximum shear stress indicating that crack nucleation is the critical event.

ACKNOWLEDGEMENTS

The author would like to express his graditude to his supervisor, Dave Embury, for continious advise and encouragement throughout this project.

Special thanks must also go to his colleagues in the mechanical metallurgy group for many fruitful discussions and to the deparmental technicians, all of whom rendered valuable assistance.

Further the efforts of Jon Lereim who performed the K_{IC} and COD tests reported in the thesis are greatly acknowledged.

Mention should also be made of Margaret Hopman and Anne Brit Fuglevaag for the typing, Tom Bryner for the photographs, Dave Hodgson for the diagrams and Bob Milsop (Stelco) for the assistance with the inclusion analysis.

Special thanks are also due to the Steel Company of Canada for providing the material and for financial support.

The financial support from NTNF (Norway) is also greatly appreciated.

Most important of all, the author would like to thank his wife, Britt Evensen.

TABLE OF CONTENTS

LIST OF FIGURES

LIST OF TABLES.

1. INTRODUCTION

Large tonnages of high strength structural steels are currently being used in the pipe line industry and as structural material in the form of plate. In addition, there is a large potential market in the automotive industry for thinner gauge HSLA-steel products. For these applications the following material properties are required: high strength, good toughness, good weldability and for sheet metal applications also good formability.

The economic aspects of utilizing higher grade steels for pipe lines have been considered by Beauchamp (1973). The weight savings that can be achieved for a 48 in (1.22 m) diameter pipe line operating at 70% of the yield stress, are shown in Table 1.1. It is seen that by going from an x-65 to an x-70 grade the weight reduction is 92 tons/mile. In addition to the material saving, similar cost reductions may be obtained in field welding and in pipe handling and transportation. Thus there is considerable impetus to develop higher strength materials that satisfy the property requirements without using higher alloy contents and expensive heat treatment.

Parrini et al. (1975) have discussed the economic aspects of the various possible processing routes for high strength structural steel. In figure 1.1 it is seen that the conventional quench and tempered steels and the normalized steels do not compare favourably in cost due to higher alloy content and additional heat treatments required after rolling.

The directly quenched and tempered steels have shown quite remarkable properties when produced on a laboratory scale (Parrini et al., 1975; Boyd, 1975). Further, they are of very lean compositions and thus very attractive from an economic viewpoint. Processing these materials in a reproducible manner on a commercial scale will, however, require very good control over rolling parameters and cooling rates.

The remaining alternative in figure 1.1 is the controlled rolled high strength low alloy (HSLA) steel, which combine good properties with low alloy cost and a minimum of time consuming processing. The physical metallurgy of controlled rolled HSLA steels has recently been described in a number of excellent reviews (Baird and Preston, 1973; Pickering, 1975; Gladman et al., 1975; Gray, 1972; Fukuda et al., 1973). The results of these investigations have brought into focus the need to understand the complex phase transformations occurring during continuous cooling of controlled rolled low alloy steels and the need to correlate the critical parameters governing the fracture behaviour with the existence and distribution of various microstructural constituents.

The improved properties of HSLA steels compared to conventional hot rolled structural steels are governed by the following factors.

1) The use of small amounts of alloying elements such as Nb, V, Ti, Al, N, which promote grain refinement in the austenite, and to some extent precipitation hardening in the ferrite. One major difficulty in predicting the effect of these alloy additions, i.e. the volume fractions precipitated in the austenite and ferrite, is the complex chemistry of these elements in the presence of both carbon and nitrogen (Johansen et.al., 1967) and the lack of suitable activity data in complex solutions.

2) The use of controlled rolling, involving close control of the degree of deformation, temperature and rate of cooling to optimize the yield of the alloying additions with respect to grain refinement and precipitation strengthening.

3) Further the trend has been to lower the carbon level to improve weldability. An inherent problem in low carbon steel making is the increase in available free oxygen and formation of oxide inclusions. In particular, one has to consider reoxidation of rare earth alloy additions when sulphide modification treatment is used (McLean and Kay, 1975).

4) The demand for cleaner steels with isotropic fracture properties has led to the use of both desulphurization and sulphide shape control. The objective of these practices has been to improve a number of factors such as ductile fracture toughness, through thickness ductility, cold formability and resistance to lamellar tearing during welding.

The dominant microstructures of controlled rolled HSLA-steels are conveniently divided into two groups, viz. polygonal ferrite structures and acicular ferrite structures. Often a mixture of the two structures is observed. The type of structure observed will be determined by the temperature of the austenite-ferrite transformation as illustrated in figure 1.2. Thus at higher transformation temperatures polygonal ferrite tends to form, whereas acicular transformation products are predominant at lower transformation temperatures. The transformation temperature will strongly depend on processing variables such as composition, thermo-

mechanical processing of the austenite and cooling rate. Variations in microstructure within the plate thickness is therefore often observed, both in terms of macroscopic variations due to change in cooling rate through the plate section and in terms of local variations due to differences in local hardenability. A further complication is introduced by the existence of non-ferritic transformation products such as carbide aggregates and islands of a mixed martensite retained austenite constituent. The volume fraction and distribution of these phases depend strongly on the processing schedule for the material.

Conventional correlations between the scale of the microstructural features and the fracture properties do not adequately describe the fracture behaviour of controlled rolled HSLA-steels. The fact that fracture is nucleated at heterogeneities in the material makes it difficult to obtain a complete and quantitative understanding of the fracture behaviour of the material. In order to establish criteria for failure it is thus of importance to be able to detect and characterize any heterogeneity in terms of its volume fraction and local distribution. Since the non-ferritic transformation products can act as preferential sites for fracture nucleation, a detailed knowledge of the transformation behaviour of the material and the correlation between transformation behaviour and processing variables is required. Further, the question arises how the quality control of the material can be performed when the microstructural features of interest are of submicron size. To date little attention has been devoted to this question, but the problem will become of increasing importance when designers start to demand an assessment of the material's fracture resistance in terms of critical stress intensities, crack arrest

properties and resistance to delamination.

The ability to relate the mechanical behaviour of a material and the detailed microstructural features is essential in alloy development and the optimization of processing schedule It is therefore important to achieve a detailed understanding of the various fracture modes observed in HSLA-steels and how they relate to the microstructure.

The objective of this investigation has been to delineate the predominate fracture modes in HSLA-steels occurring for various temperature and stress conditions. In order to quantify the fracture behaviour it has been necessary to develop fracture criteria that describe the various fracture modes in terms of the scale and distrubution of the various microstructural features of the material and the magnitude of the various stress components operating on the material.

In the present investigation three different steels have been considered. The steels are of commercial quality and have been controlled rolled on a full size mill. As these materials are used in the as rolled condition, no heat treatments were made and all mechanical testing was done on the plate as received. The advantage of this is that the results of the investigation are directly applicable to commercial materials. Further, the need for large quantities of material for mechanical testing would require rather elaborate facilities if the materials were to be produced on a laboratory scale. The problem with this approach is that the microstructures cannot be varied in a controlled and systematic manner to delineate the effects of the various microstructural components in a quantitative way. Also, there is the inherent problem of controlled rolled steels that the microstructure is very complex, thus making the interpretation of the

data more difficult. Since the microstructure could not be altered, three different materials with slight differences in composition and rolling schedule have been chosen. The steels are of comparable strength level, but their microstructural features show marked differences.

The approach taken in this study has therefore been to undertake a detailed characterization of the microstructure of the three steels, referred to as A, B and C, using a combination of standard optical microscopy, scanning electron microscopy, and transmission electron microscopy of thin foils and carbon extraction replicas. Further, small scale fracture tests have been used to assess the fracture resistance of the materials and the critical values of COD, K_{1C} and cleavage stress have been interpreted in terms of the characteristic microstructures.

TABLE 1.1

STEEL REQUIREMENTS PER MILE OF GAS PIPELINE

GRADE	X-52	X-60	X-65	X-70	X-75	X-80
WALL THICKNESS REQUIRED (in)	.970	.840	.775	.720	.675	.630
WEIGHT SAVING TONS/MILE BY GOING TO NEXT GRADE	0	164	92	71	60	58

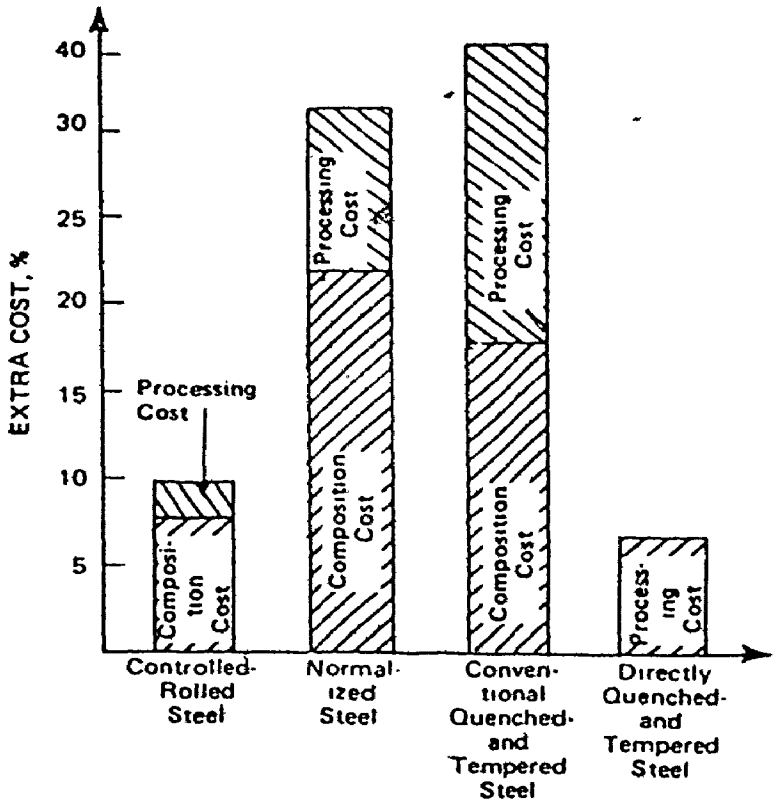

Figure 1.1: Diagram illustrating extra composition and processing cost for producing specially treated plates compared to production of C-Mn steels of the same quality. (from Parrini et.al., 1975)

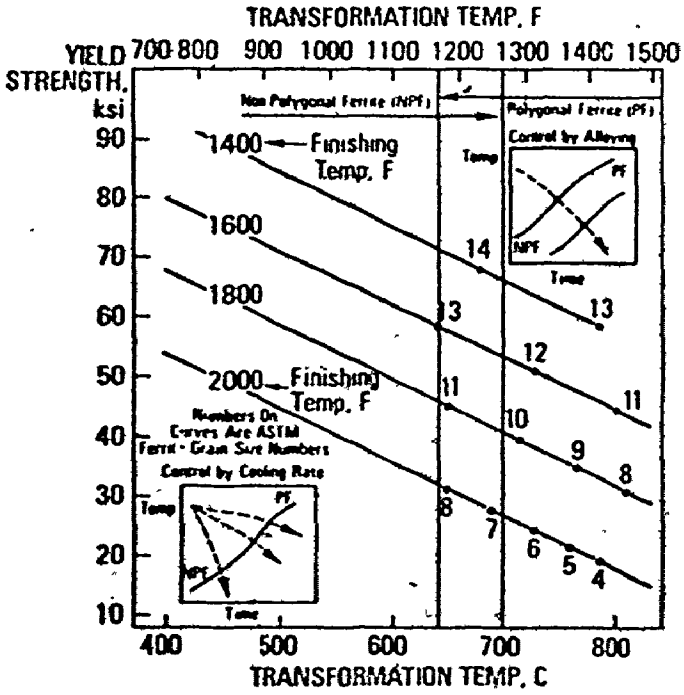

Figure 1.2: Diagram showing the influence of transformation temperature on the scale of the microstructure and the strength of controlled rolled HSLA-steels.

2. LITERATURE REVIEW

In this investigation of the microstructural aspects of fracture in HSLA-steels the objective has been to develop relations between fracture resistance and the detailed microstructure of the material. It is thus of interest to consider the various formats in which fracture resistance can be expressed, and how values of the fracture resistance can be obtained from relatively simple small scale experiments.

To introduce the microstructural aspects of fracture it is necessary to define the various fracture modes operating in HSLA-steels and to develop criteria which describe the fracture behaviour in a quantitative manner in terms of the magnitude and direction of the stresses and strains operative in the material. Further, the microstructure must be well characterized in terms of the heterogeneities that are responsible for nucleating the fracture process.

To provide a background for a discussion of the detailed fracture behaviour of HLSA-steels, some of the current ideas on fracture resistance and influence of microstructural features have been reviewed in the next sections together with a brief discussion on the development of microstructures in HSLA-steels.

2.1 MICROSTRUCTURE

The need for structural steels with improved strength and fracture toughness has led to the development of controlled rolling as a way of

refining the scale of the microstructure. The success of the controlled rolling technology is based on a delicate balance between thermal mechanical treatment and the use of small alloy additions to stabilize the structure. The action of the micro alloy additions, in addition to precipitation hardening in the ferrite, is to prevent grain growth and recrystallization in the austenite, the rationale being that transformation of a fine austenite structure will yield a fine ferrite structure. Most HSLA-steels are based on additions of either Nb, V, or Ti as a grain refiner. The majority of HSLA-steels for line pipe applications, however, are currently Nb treated. Thus the treatment of microstructures in controlled rolled steels will be restricted to Nb-bearing steels.

2.1.1. Deformation of austenite

In order to obtain a fine microstructure in the finished plate it is necessary to refine the austenite structure before transformation (Fukuda et al., 1973). In essence, this is done by allowing the structure to recrystallize between each rolling pass and trying to prevent grain growth at the same time. The various stages in the rolling sequence have been illustrated schematically in figure 2.1. In stage I at high rolling temperatures both recrystallization and grain growth will occur, thus there is no net refinement in the structure. By lowering the temperature recrystallization may still occur, but grain growth is prevented. The result is a refinement of the austenite grain size for each rolling pass. Further reduction in rolling temperature will prevent recrystallization and an elongated, heavily deformed austenite structure results (Teggart and Gittins, 1977).

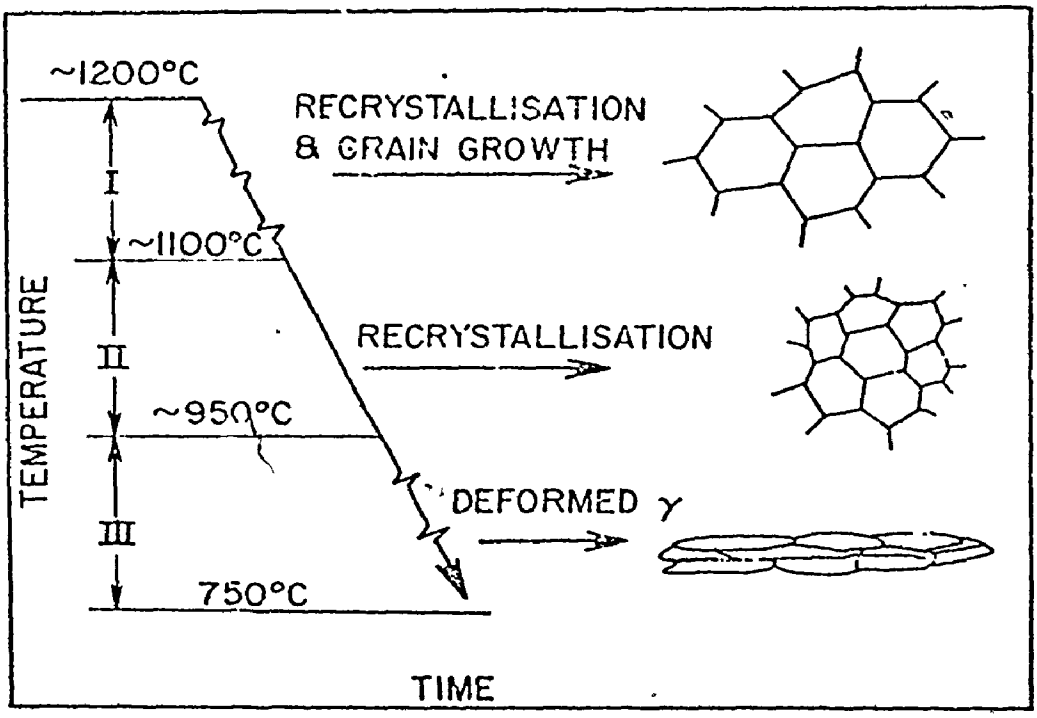

Figure 2.1: Schematic diagram showing the controlled rolling schedule for HSLA-steels.

The described rolling sequence is typical for Nb-bearing C-Mn-steels. For pure C-Mn steels, however, recrystallization, complete or partial, will take place even at the lower end of the temperature scale (Sekine and Maruyama, 1973). Thus the effect of Nb-additions in controlled rolling is to prevent recrystallization of the austenite. Two mechanisms have been proposed to account for the suppression of austenite recrystallization. The first involves Nb in solid solution which may retard the motion of dislocations and sub-boundaries via a solute drag effect (le Bon et al., 1975), thus retarding recovery and hence recrystallization of the deformed austenite. The second considers the influence of Nb(C,N) precipitates which form on the substructure produced during rolling and suppress recovery and recrystallization by a dislocation pinning mechanism. Work by Davenport et al. (1977) shows that the onset of retardation of recrystallization is accompanied by the formation of Nb(C,N)-precipitates, which supports the latter mechanism. There is, however, no definite rule to which mechanism should operate in each case.

In retarding grain growth in the austenite precipitation of Nb(C,N) on the grain boundaries seem to be the operating mechanism. Grain boundary precipitation in the austenite has been reported by Ohmori (1975) in a thorough investigation of Nb precipitation in low alloy steels.

At the start of transformation to ferrite the austenite may exist either in the form of a uniform fine grained recrystallized structure or in the form of an elongated, heavily deformed grain structure, depending on the temperature of the last rolling pass. In the latter case it is important that the structure is heavily deformed, as this will ensure that

the growing ferrite grains can only attain a certain size before impingement, and thus a fine grained ferrite is obtained.

The occurrence of partially recrystallized austenite or insufficient deformation of the austenite may lead to a duplex microstructure containing bands of large polygonal ferrite grains. These have been shown to have a detrimental effect on the mechanical properties, in particular on the delamination behaviour (Speich and Dabkowski, 1977).

2.1.2. Tranformation behaviour

It has been established that a uniform fine grained austenite structure is essential in order to optimize the ferrite mophology. Of equal importance, however, is the transformation temperature (Gray, 1972). This can be considered in terms of a simple nucleation and growth model for ferrite (Shewmon, 1969). At high transformation temperatures the nucleation rate is low and large polygonal ferrite grains are produced. As the temperature decreases the nucleation rate will increase and a gradual refinement of the structure occurs. At large degrees of undercooling more free energy is available for formation of non-polygonal structures. Although the acicular structures are thermodynamically unfavourable due to larger surface to volume ratio, they represent the faster growing species and will thus dominate the structure at lower transformation temperatures. The influence of the transformation temperature on the scale and morphology of the microstructure is illustrated in the diagram from Gray (1972) in figure 1.2.

The transformation temperature is determined by alloy additions and cooling rate, increased alloy content and cooling rate both lower the

transformation temperature. There is, however, a strong influence of the austenite condition in terms of grain size and dislocation structure, a heavily deformed structure tending to accelerate the transformation . (Coldren et al., 1972). Further, niobium left in solid solution has a marked effect on hardenability (Gray, 1972) making an a priori estimate of the transformation temperature difficult.

Polygonal ferrite with a grain size of 5.10^{-6} m (ASTM 12) and a carbon content of 0.15% has a yield strength of about 350 MPa and a transition temperature of about -50°F(Woodhead and Whiteman, 1972). By decreasing the carbon content the transition temperature can be improved; this, however, is at the expense of the strength. Similarly, the yield strength can be increased to about 550 MPa by precipitation hardening, but it is accompanied by a detrimental increase in transition temperature. If stronger materials are required it is therefore more satisfactory to suppress the transformation temperature to facilitate the transformation to an acicular structure.

Acicular ferrite is composed of groups of parallel ferrite laths of small misorientation arranged in colonies. The structure contains a very high dislocation density and is in general too complex to allow a quantitative assessment of either the dislocation density or the extent of alloy carbide precipitation by transmission electron microscopy.

The effect of Nb-addition is three-fold. Both the influence on the rate of recrystallization and grain growth in the austenite and the effect of niobium in solid solution on the hardenability have been considered. In addition, Nb(C,N) can precipitate in the ferrite to give a substantial increase in yield stress. Precipitation can occur both

during processing,i.e. during cooling or in the coiling operation for sheet material, or in a separate ageing treatment. Ageing to peak hardness is very rapid at high temperatures (about 5 minutes at 700°C) (Coldren et al., 1972) and an increase in yield strength of the order of 100 MPa can easily be obtained for a 0.05% Nb steel (McCutcheon et al., 1976). In order to have the beneficial effect of Nb on hardenability and precipitation strengthening it is important to avoid excess precipitation in the austenite (Coldren et al., 1972), care must therefore be taken to design a thermal-mechanical treatment to give optimum yield of alloy additions.

2.1.3. Carbon distribution

In addition to the morphology and scale of the ferrite, attention must be given to the redistribution of carbon during transformation and the formation of non-ferritic products. These may arise in the form of carbides or complex transformation products such as retained austenite or martensite formed by carbon rejection in the presence of alloying elements such as Mn.

The classical case of carbon redistribution is the pearlite banding due to segregation of alloying elements (Kirkaldy et al., 1962). In Nb-bearing HSLA-steels a similar effect is observed; this, however, is not related to the distribution of alloy elements (Herø et al., 1975), but to the austenite morphology. When heavily deformed austenite transforms, carbon is rejected by the advancing ferrite front towards the center of the original austenite grain where it transforms to pearlite. Thus a linear array of pearlite patches will form, giving rise to a

banding effect.

At lower transformation temperatures the pearlite is less well defined and has been referred to as non-lamellar pearlite (Tither and Lauprecht, 1977) or a mixture of pearlite and upper bainite (Speich and Dabkowski, 1977). Further, a tendency to precipitate cementite on ferrite grain boundaries is observed (Herø et al., 1975). The scale of the phase varies with the temperature of transformation but in some cases the carbide may form a continuous film which serve as a preferred fracture path in a manner analogous to the carbides formed in upper bainite (Pickering, 1967). Cementite may be formed in the austenite when the carbon concentration close to the advancing interface exceeds the extrapolated A_{cm} line. Lowering the transformation temperature will decrease the solubility of carbon in the austenite and give a higher concentration gradient of carbon in the remaining austenite due to inhibition of the diffusion process. Both these factors favour precipitation of carbide. Heterogeneous nucleation at the reaction front tends to precipitate cementite on the grain boundaries rather than inside the grains.

At intermediate cooling rates when carbon diffusion can occur over a greater distance in front of the advancing ferrite, a substantial carbon concentration may build up in the remaining austenite. If the condition for cementite precipitation is not met the transformation temperature for the remaining austenite may be lowered sufficiently to either stabilize the austenite or produce a high carbon martensite, as suggested by Biss and Cryderman (1971). The martensite constituent is often heavily twinned, indicating a local carbon content in excess of 0.5% wt. which is in agreement with calculations based on initial carbon content and volume fraction

of the martensite-austenite (M/A) constituent. The amount and distribution of the M/A-constituent depends both on the thermal history of the material and the detailed kinetics of the austenite ferrite transformation. In addition, factors such as the local hardenability, as defined by the homogeneity of the substitutional alloying elements, are of importance in determining the transformation behaviour of the retained austenite. A detailed study of the occurrence of the M/A-constituent in weld metal has been undertaken by Glover et al. (1977) where they demonstrate the importance of the austenite ferrite transformation kinetics on the distribution of the martensite-austenite phase. When the M/A-constituent is formed at intermediate cooling rates in an acicular ferrite matrix it has a blocky, irregular appearance, whereas increased cooling rates promotes transformation to bainitic ferrite and elongated discs of the M/A-constituent form between the ferrite laths. This is in agreement with observations by Habraken and Economopoulos (1967), but in contradiction to the view by Biss and Cryderman (1971), who argue that a transition to carbide formation should occur by increasing the cooling rate.

To date, there has been no definite study of the influence of the M/A-constituent on the fracture behaviour of HSLA-steels. It has been shown, however, (Embury et al., 1977) that the martensite austenite phase may play an important role both in terms of cleavage crack nucleation and as a source for void formation in fibrous fracture. Thus, if the propensity to fracture is considered in terms of volume fraction of second phase particles only, the occurrence of M/A constituents containing 0.5% C is more severe than having the carbon precipitated as cementite containing 6.7% C, which yields a lower volume fraction of particles. Further studies to delineate the characteristic structure and the

detailed mechanism of formation of the martensite austenite phase have long been due. It is believed, however, that introduction of the dual phase steels (Bucher and Hamburg, 1977) which utilize the M/A-constituent to modify the yielding behaviour and increase the formability, will increase the research effort being spent in this area.

2.1.4. Texture

Much effort has been devoted to studies of texture in structural steels and the work of Bramfitt and Marder (1973) has clearly demonstrated the importance of this aspect of the structure. The texture of the resultant ferrite may influence both the fracture behaviour, in particular delamination, and the plastic anisotropy and formability of the material. The texture may arise either from transforming pretextured austenite or from rolling in the ferrite range. The inheritance of texture from the austenite is very complex and depends both on the detailed morphology of the austenite and the austenite-ferrite orientation relationship. Lotter et al. (1976) have considered texture transformations both in hot rolled C, Mn-steels and in a Nb-bearing steel, the former being fully recrystallized before transformation and the latter consisting of heavily deformed austenite. Assuming a Kurdjumov-Sachs relationship they considered various possible fcc deformation and recrystallization textures and found that the observed ferrite textures, {100} <110> for C, Mn-steel, and {112} <110> for C, Mn, Nb-steel could be predicted from a "copper type" recrystallization texture, {100} <001> and a "copper type" rolling texture {112} <111> respectively. Similar results have been obtained by Inagaki (1977), who used the technique described by Kallend et al. (1976) to obtain

the texture transformations. For steels rolled after transformation to ferrite, Bramfitt and Marder (1973) observed increasing intensity of the {111} <uvw> texture at decreasing temperatures. Speich and Dabkowski (1977) however, observe an increasing {100} <011> component when the material is subjected to rolling in the ferrite range. This is consistent with cold rolling textures observed for mild steel (Akamutsa et al., 1966).

In addition to the crystallographic aspects of the ferrite the morphology of the prior austenite may determine the shape and distribution of the transformation products. This in turn may exert a marked influence on the mechanical properties of the final product.

2.1.5. Inclusion morphology

The existence of large fractions of inclusions has been a major problem in producing structural steels with an isotropic mechanical response. The problem arises both in terms of the volume fraction of second phase particles (Chapter 2.2.3) and because the inclusions, usually being plastic at hot rolling temperatures, occur in the form of stringers (Klevebring, 1974) thus giving rise to a strong anisotropy in the fracture behaviour. The approach taken in the HSLA-steel technology has been to use both desulphurization practices and to modify the inclusion shape. A detailed discussion of the various desulphurization processes is considered beyond the scope of this review. It is, however, of interest to consider briefly the various mechanisms of sulphide shape control.

The majority of sulphide shape control processes involve addition of elements such as Ti, Zr or rare earth compounds, the latter being used extensively for line pipe steel quality. Although these elements form

very stable sulphides, they all show a high affinity for oxygen (titanium also for nitrogen) thus requiring good deoxidation of the hot metal before addition (Luyckx et al., 1970). The possibility also exists that free oxygen may be provided from the slag and the refractory lining (Lu and McLean, 1974), thus facilitating the process of reoxidation. In addition, reoxidation may occur during pouring of the hot metal as described by McLean and Kay (1975). Reoxidation of rare earth (RE)-sulphides usually implies a sulphur reversion and a combination of RE-oxysulphides and MnS stringers may occur in the final products. In addition, the reoxidation products tend to precipitate as large units, and they often agglomerate to form large spatial networks of inclusions (Luyckx, 1975). During rolling these inclusion agglomerates are stretched out to form sheets of very high inclusion density which may be detrimental to the through thickness properties of the plate (Embury et al., 1977).

Although the use of sulphide shape control has resulted in great improvement in the isotropy of the mechanical response of HSLA-steel, care must be taken in the steelmaking practice to avoid reoxidation reactions and loss of alloy yield. From an economical viewpoint it is also of interest to define the extent to which the mechanical properties are improved with decreasing inclusion content, i.e., for very low inclusion content other mechanisms may limit the ductility. This problem requires a detailed knowledge both of the microstructural aspects and the fracture behaviour of HSLA-steel, but has to date received little attention.

2.2 FRACTURE BEHAVIOUR

The fracture behaviour of structural steels is characterized by a transition from the occurrence of ductile failure at higher temperatures to brittle failure at lower temperatures. This transition is illustrated schematically in figure 2.2 in terms of the energy absorbed in the fracture process at various temperatures. The low temperature failure process is often referred to as cleavage cracking where fracture occurs by nucleation and growth of microcracks at a critical stress level. The fracture stress (σ_c) is dependent on microstructural features such as the grain size and the scale and morphology of the carbides. At higher temperatures the critical fracture stress cannot be attained either by work hardening or by plastic constraint and other fracture mechanisms, referred to as rupture processes, will therefore take over. The ductile fracture mechanism is characterized by the occurrence of void nucleation at second phase particles and inclusions and growth and link-up of voids to the crack front. The energy absorption in ductile fracture is determined by the volume fraction and distribution of second phase particles in the material, giving rise to the upper shelf in the energy absorption curve in figure 2.2.

In controlled rolled HSLA-steels an additional fracture mode called delamination or splitting is commonly observed in the intermediate temperature range between ductile and brittle failure. The delamination fracture is similar to conventional lamellar tearing in that it occurs on planes parallel to the rolling plane, but the detailed mechanism of failure is different.

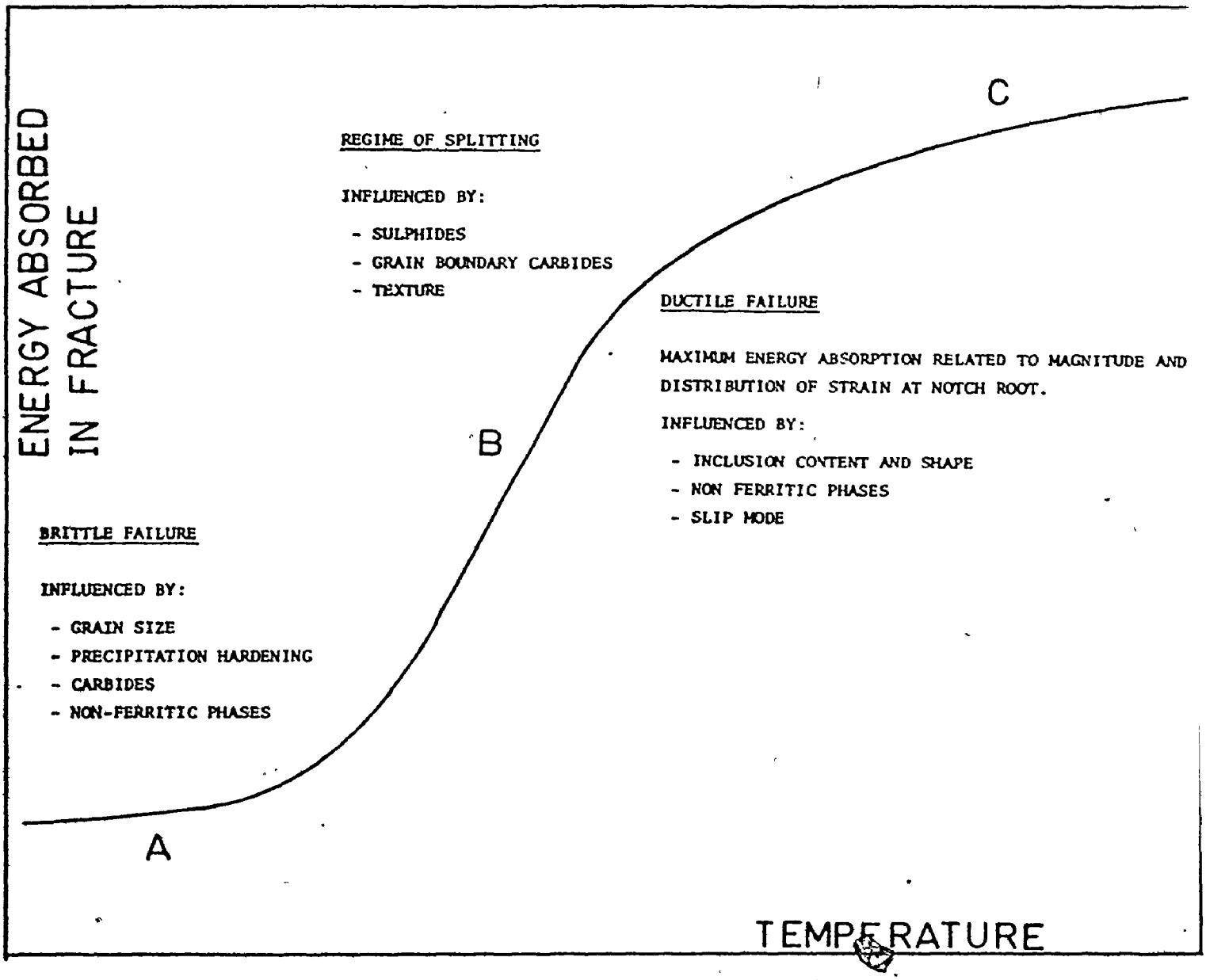

CRITERIA FOR FRACTURE

REGION	CRITERION	PROBLEMS
A	MAXIMUM NORMAL STRESS σ_1	DISTANCE OVER WHICH σ_1 ACTS, RELATIONSHIP OF MICROCRACK TO FAILURE EVENT
B	↑	NO UNIQUE MICROSTRUCTURAL ORIGIN
C	DISPLACEMENT TO JOIN VOIDS AT CRACK TIP	SLIP MODE, TYPE OF NUCLEI FOR VOIDS

Figure 2.2: Schematic diagram illustrating the various fracture modes observed in HSLA-steels.

Conventionally the only parameter used to describe the fracture properties of structural steels has been the ductile-brittle transition temperature (DBTT) as measured in a standard V-notch charpy test. The transition temperature can either be based on the attainment of a given energy absorption, or the attainment of a certain fracture appearance, e.g. 100% shear. The disadvantage of this treatment is that the transition temperature will scale with the size of the specimen and the strain rate (Lange, 1976) and the transition temperature in an actual structural assembly may be quite different from the transition temperature determined from charpy V-notch specimens. Further, the transition temperature is not of any quantitative use in design, i.e. it does not allow the designer to calculate the critical loads for a structure or the maximum allowable flaw sizes in the material. This leads to the problem of defining adequate parameters for fracture resistance that are independent of test procedure and specimen geometry.

2.2.1 Fracture Resistance

The concept of fracture resistance is best described in terms of a net energy balance between work done in advancing the crack and the potential energy release by crack propagation. The fracture condition can then be expressed as

$$G \geq R \qquad 2.2.1$$

where G is the rate of energy release and R is the rate of dissipating energy. In linear elastic fracture mechanics (LEFM) the energy release rate can be calculated in terms of the elastic stress-distribution in

front of a crack tip, and is given by

$$G = \frac{\sigma^2 \pi a}{E} (1-\nu^2) \qquad 2.2.2$$

where σ is the applied stress, a is the crack length and E the elastic modulus. By introducing the stress intensity factor $K = \sigma\sqrt{\pi a}$, eqn. 2.2.2 can be written: in plane strain

$$G = \frac{K^2}{E} (1-\nu^2) \qquad 2.2.3a$$

and by a similar argument in plane stress

$$G = \frac{K^2}{E} \qquad 2.2.3b$$

In terms of stress intensities the fracture condition (eqn. 2.2.1) can be written

$$K = K_{1C} \quad \text{for plane strain} \qquad 2.2.4a$$

$$K = K_C \quad \text{for plane stress} \qquad 2.2.4b$$

By the use of elastic stress analysis values of K as a function of applied load and specimen geometry can be calculated for various types of test specimens. Critical values of K (e.g. K_{1C}, K_C) can then readily be obtained from measurement of the fracture load in standard fracture tests.

A major problem in most structural material is that the attainment of the fracture condition will be accompanied by plastic deformation at the crack tip and an elastic evaluation of the crack tip stress distribution is strictly not valid. It has been found, however, that the LEFM

approach can still be used provided the extent of the plastic zone is small compared to the overall dimensions of the specimen. This is based on the requirement that the stress field from the effective crack, consisting of the original crack length and the plastic zone, does not interfere with the boundaries of the specimen and is usually expressed as

$$B,\ (W-a),\ a > 50\ r_{1y} \qquad 2.2.5$$

where a is the crack length, B is the specimen thickness, W is the specimen width and r_{1y} is the plane strain plastic zone size. For a typical HSLA-steel (σ_y = 500 MPa, K_{1C} = 150 MN $m^{-3/2}$) this would imply specimen dimensions of about 0.5 m.

The plastic zone in front of the crack tip will accommodate a crack opening displacement (COD). It has been suggested (Cottrell, 1965; Wells, 1965) that the value of this displacement at crack initiation is a characteristic parameter that can be used to describe the fracture resistance of a material. Alternatively, the fracture resistance can be expressed in terms of a critical fracture energy. By analogy to the potential energy release rate in LEFM a parameter, called the J-integral, can be defined which describes the energy release rate in a non-linear elastic material. This is assumed a reasonable approximation for the small scale yielding behaviour at the crack tip. The size requirements for COD and J-integral measurements are less severe than for a valid K_{1C} test. Griffis (1975) has shown that for a HY80-steel the J_i value is independent of specimen dimensions if

$$B,\ (W-a),\ a > 50\left(\frac{J_i}{\sigma_y}\right) \approx 0.02\ \text{m} \qquad 2.2.6$$

where J_i is the J value at crack initiation. An equivalent valid K_{1C} test would require a specimen over ten times this size. Analysis of failure under small scale yielding (Eagan, 1973; Robinson and Tetelman, 1976) have demonstrated that the concept of a critical crack opening displacement for fracture is consistent with the stress intensity approach, i.e.,

$$(COD)_i = \frac{K_{1C}^2(1-\nu^2)}{E\sigma_y} \qquad 2.2.7$$

where subscript i indicates that the value of COD at crack initiation should be used. Further, for the same assumptions it is found that

$$J_i = G_{1C} = \frac{K_{1C}^2(1-\nu^2)}{E} \qquad 2.2.8$$

or by combining the last two equations a linear relationship between J_i and $(COD)_i$ is found, viz.,

$$J_i = (COD)_i \, \sigma_y \qquad 2.2.9$$

Thus in the case of specimens suffering small scale yielding, three alternative approaches (K_{1C}, J_i, $(COD)_i$) can then be used to establish the critical fracture toughness for a material.

The COD approach has been extended to low and medium strength, high toughness materials suffering general yield in small scale tests (Smith and Knott, 1971; Robinson and Tetelman, 1976) and meaningful data have been obtained. The critical value of COD at crack initiation is found to be constant for specimen thicknesses down to about $5 \cdot 10^{-3}$ m. Similar results have been obtained for the J test (Landes and Begley,

1974), although the critical specimen size is larger.

The use of small scale tests to estimate the fracture resistance after general yield has proven very useful as a means of comparing the fracture behaviour of materials. These tests are thus extensively used in alloy developement and in the study of the detailed fracture mechanisms where the emphasis is to investigate the influence of various micro-structural features rather than produce reliable values for the fracture toughness. If, on the other hand, fracture resistance data are needed for design purposes, full scale J_{1C} or K_{1C} tests in accordance to recommended standards should be used. Valid results of fracture toughness obtained this way will allow the designer to calculate, by the techniques of elastic stress analysis, the maximum applied stress level and the critical defect size for a structure. Attempts have been made, however, to extend the fracture mechanics approach into the general yield regime (Heald et al., 1972). In the general yield fracture mechanics developed by Heald et al., the fracture condition is assumed to be a critical crack tip displacement which is determined by the local crack tip process and is assumed to be independent of the extent of the plastic zone. Using the Bilby, Cottrell and Swindon (1963) model the critical displacement is related to the applied stress. Standard fracture mechanics relations are then used to express the fracture resistance in terms of an apparent stress intensity factor, K_A. Thus the apparent fracture toughness in the post yield region is related to the plane strain fracture toughness by the following equation:

$$K_A = 2\sigma_{UTS}\left(\frac{c}{\pi}\right)^{\frac{1}{2}}\cos^{-1}\left[\exp-\left(\frac{\pi K_{1C}^2}{8\sigma_{UTS}^2 c}\right)\right] \qquad 2.2.10$$

where σ_{UTS} is the ultimate tensile stress and c is the crack length. Using equation 2.2.10 values of K_{1C} can be calculated from fracture toughness tests which do not fulfill the ASTM requirements.

In order to delineate the effect of various microstructural features on fracture resistance it is physically most attractive to express the resistance in terms of the energy absorbed in the fracture process (G_{1C} or J_{1C}). The parameters determining the energy dissipation are the stress and strain distribution in the plastic zone and the volume of the material deforming plastically. The limiting value of these parameters is determined by the detailed fracture processes occurring at crack tip, such as micro crack formation (cleavage), voiding at second phase particles or plastic collapse by strain localization. The concept of a plastic zone and a process zone, in which the critical fracture event is taking place, is illustrated schematically in figure 2.3 together with the stress distribution in front of the notch. It is seen from the figure that by allowing the material to yield at the crack tip the stress singularity predicted from LEFM is removed and the maximum tensile stress at the crack tip is given by the uniaxial flow stress. Inside the plastic zone the stress distribution is determined by the plastic constraint from the crack tip. In the following sections the microstructural features that limit the magnitude of the stresses and strains attained at the crack tip will be considered. Even though the various modes of failure in HSLA-steels, cleavage, ductile failure and delamination can occur simultaneously, it is convenient to treat them in separate subchapters.

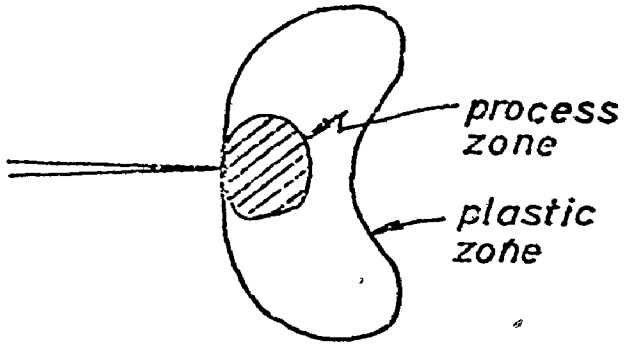

a

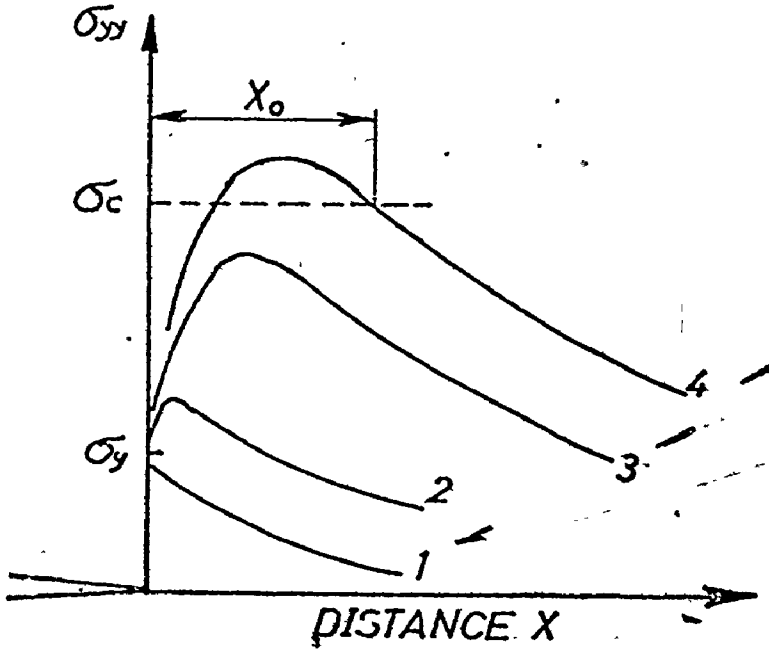

What are these numbers?

b

Figure 2.3: Schematic diagrams showing:
a, plastic zone and process zone in front of crack tip.
b, stress distribution in front of a sharp crack for increasing load.
X_o represent the distance over which the critical stress must be applied in order for cleavage failure to occur.

2.2.2 Cleavage Fracture

The failure of a material by cleavage consists of a series of events involving crack nucleation usually at carbides or some other heterogeneity, growth of crack nuclei to micro cracks of grain size dimensions, and linking up of the micro cracks to the main crack tip. The critical event is usually considered to be the growth step which occurs at a certain tensile stress. For structural steels the cleavage stress is substantially higher than the uniaxial yield stress and cleavage failure is rarely seen in tensile specimens. In notched samples or in front of a crack tip, however, a significant hydrostatic stress component is developed due to plastic constraint and the maximum tensile stress can be increased by a factor of about three (figure 2.3) in front of the crack tip. It should be noticed that this increase in tensile stress is due to plastic constraint only and that any work hardening will give an additional effect. Thus when the local tensile stress in front of the crack tip attains the same level as the critical cleavage stress the situation arises where a competition between continued plasticity and formation of micro cracks takes place. When micro cracks form, the condition for linking up to the main crack, i.e., complete fracture, depends on the detailed stress distribution (Ritchie et al., 1973). It is generally agreed that cleavage failure is induced by local plasticity, and Low (1954) has shown that for ferrite pearlite mild steels the cleavage stress is coincident with the yield stress for coarse grained materials and exceeds the yield stress for finer grain sizes. Based on the fact that cleavage cracks are slip nucleated, a variety of models have been proposed to clarify the mechanisms by which crack nuclei

grow to form micro cracks.

Cottrell (1958) has described a mechanism where two slip dislocations of the type $\frac{a}{2}\langle 111\rangle$ react to form a crack dislocation of the type $a\langle 100\rangle$. The condition for growth of this crack nucleus is given by an energy balance:

$$\frac{\partial}{\partial c}\left[-\frac{\sigma^2(1-\nu^2)}{E}\left(\frac{c}{2}\right)^2 - \tfrac{1}{2}nb\sigma c + 2\gamma c + \frac{\mu(nb)^2}{4\pi(1-\nu)}\ell n\left(\frac{2R}{c}\right)\right] = 0 \qquad 2.2.11$$

where the first term is the elastic energy released by forming a crack, the second term is the work done by the stress in moving the crack faces apart, the third term is the surface energy, and the last term represents the energy of the crack dislocation. Equation 2.2.11 is a quadratic equation in c (the crack length) which has one real root e.g. one stable crack length, when

$$\sigma nb = 2\gamma \qquad 2.2.12$$

By relating the displacement nb to the effective shear stress on the slip dislocations the final fracture condition appears as

$$\sigma_c = \frac{2\gamma\mu}{k_y} d^{-\frac{1}{2}} \qquad 2.2.13$$

where k_y is the slope in the Petch plot. The Cottrell model assumes an idealized material with uniform grain size and no heterogeneities, such that cracks are nucleated by slip bands inside the grains. Although the assumptions may be crude, the model does show good agreement with experimental data for conventional low carbon steels, and has been extensively used to characterize the fracture behaviour of these materials.

The technological response to the increasing demand for high strength, good toughness structural steels has been a continuous refinement of the scale of the microstructure. Thus the models used for evaluation of strength and toughness in conventional hot rolled ferrite pearlite steels are not necessarily applicable to the HSLA-steels. This is clearly demonstrated by applying the Cottrell model for cleavage fracture to steels with average grain size of 5×10^{-6} m, typical for controlled rolled micro alloyed steels, where a cleavage stress of about 4000 MN m^{-2} is predicted. The observed values for the cleavage stress are about half the predicted value, and the difference has been attributed to heterogeneities in the microstructure, carbides in particular. The influence of the carbides on the brittle fracture behaviour of steels has been considered in several articles in the literature (McMahon and Cohen, 1965; Smith, 1966; Almond et al., 1969(a,b)) and some of the fracture models that include the effect of second phase particles on cleavage stress will be discussed.

The fracture model proposed by Smith (1966) assumes, based on a Griffith criterion, that the stress concentration in front of a dislocation pile up is sufficient to crack carbide particles with low surface energy but too low to cleave a complete ferrite grain, which has a higher surface energy. Thus the fracture must be growth controlled and the extent of the micro cracks are given by a detailed energy balance. Expressed in terms of the grain size, d, the carbide thickness, t, the friction stress, τ_f, and the effective shear stress, τ_{eff}, the fracture criterion can be written

$$\frac{t}{d}\sigma_c^2 + \tau_{eff}^2\left(1 + \frac{4}{\pi}\left(\frac{t}{d}\right)^{\frac{1}{2}}\frac{\tau_f}{\tau_{eff}}\right)^2 \geq \frac{4E\gamma_m}{\pi(1-\nu^2)d} \qquad 2.2.14$$

where σ_c is the applied stress. This model emphasizes the combined effect of grain size and carbides on the cleavage stress, and indicates clearly the detrimental effect of large carbides. The influence of grain size is, however, less clear. If the effective shear stress is expressed in terms of the Hall-Petch relation

$$\tau_{eff} = \tau_y - \tau_f = k_y^s\, d^{-\frac{1}{2}} \qquad 2.2.15$$

and substituted for in eqn. 2.2.14 the fracture condition becomes

$$t\sigma_c^2 + k_y^{s2}\left[1 + \frac{4\tau_f}{\pi k_y^s}\, t^{\frac{1}{2}}\right]^2 \geq \frac{4E\gamma_m}{\pi(1-\nu^2)} \qquad 2.2.16$$

where k_y^s is the slope of the Hall-Petch plot. It is seen that the cleavage stress is now independent of grain size and only determined by the carbide thickness and the yield properties of the material. The fact that eqn. 2.2.14 still shows good agreement with experimental data must be attributed to the transformation kinetics in low alloyed steels that determine both the ferrite grain size and the carbide thickness. A constant t/d-ratio may therefore be expected for hot rolled ferrite pearlite steels. This, however, is not necessarily the case for the rather complex microstructures found in controlled rolled HSLA-steels.

A physically simpler and mathematically more tractable approach to the problem has been taken by Almond et al. (1969 a,b). Again, the model is based on a pile up of dislocations impinging on a grain boundary carbide as shown schematically in figure 2.4. A crack can form in the

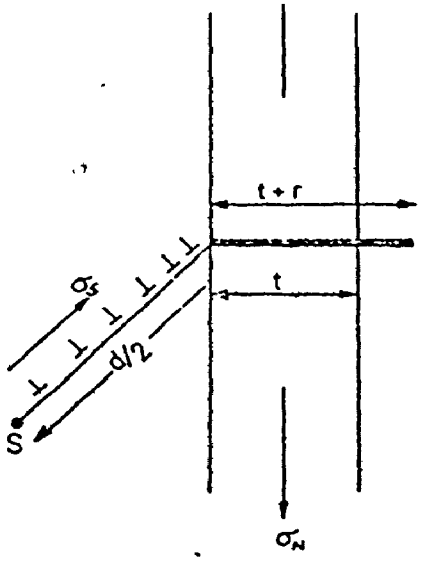

Figure 2.4: Schematic drawing illustrating the condition for ferrite microcrack formation by propagation of carbide cracks into the matrix.

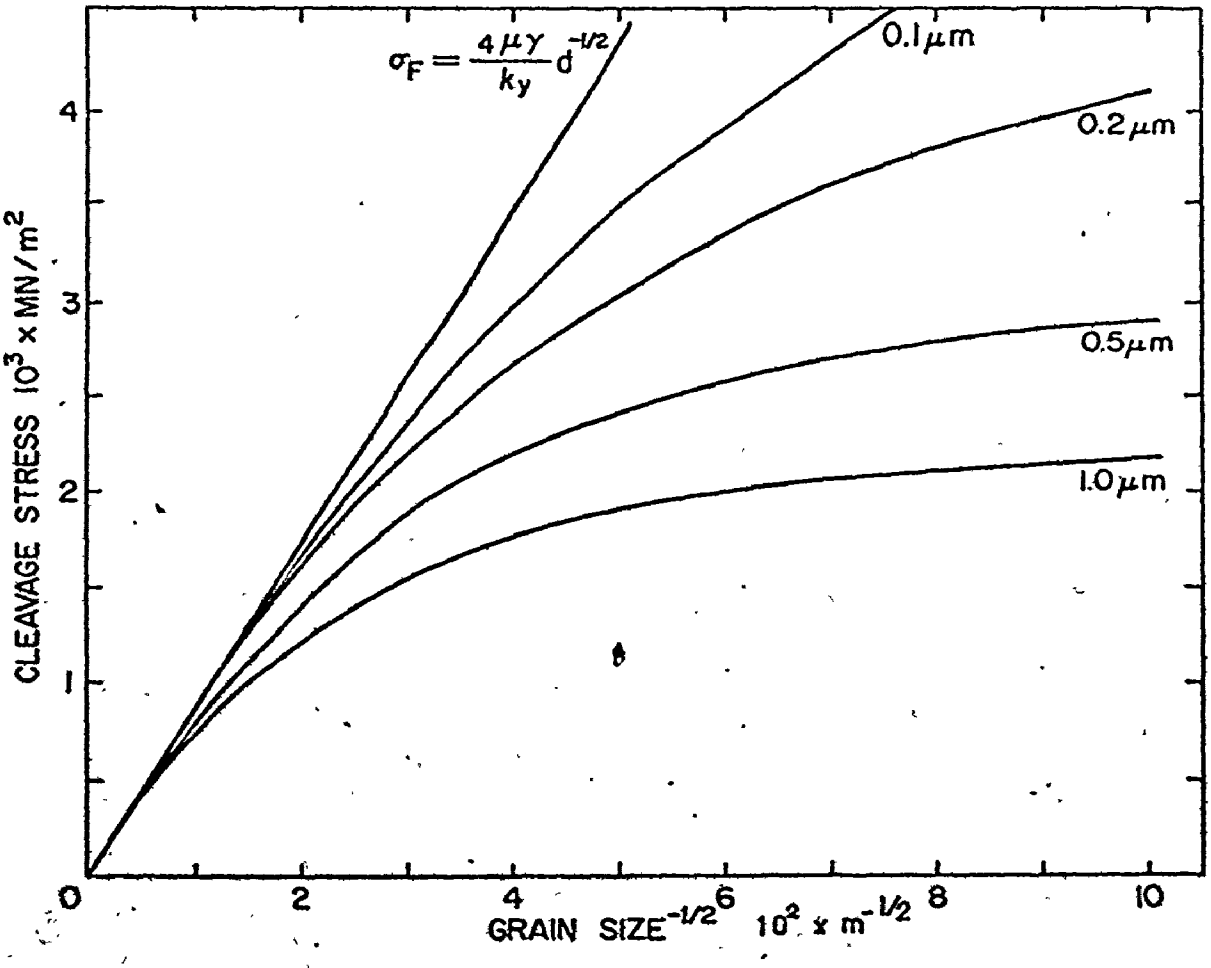

Figure 2.5: Diagram showing theoretical predictions of the critical cleavage stress as a function of grain size (Cottrell 1958) and grain size and carbide thickness (Almond et.al. 1969).

carbide with a surface energy γ_c, which is much less than the effective surface energy for formation of a cleavage crack in the matrix. Thus the critical event is propagating the crack a distance into the ferrite under the combined action of the applied stress σ, and the effective shear stress on the dislocation. As for the Cottrell equation there are four contributions to the total energy and an energy balance similar to equation 2.2.11 will result where (t+r) is substituted for the crack length, c. The result is a quadratic equation in r which has one real root, one stable crack length, when

$$\frac{\sigma na}{2\mu} + \frac{t\pi(1-\nu)\sigma^2}{8\mu\gamma} = 1 \qquad 2.2.17$$

By relating the opening displacement of the crack (na) to the shear strain in the pile up the following expression is obtained:

$$\sigma_c = \left[\frac{k_y^2 d}{4t} + \frac{8\mu\gamma}{\pi(1-\nu)t}\right]^{\frac{1}{2}} - \frac{kd^{\frac{1}{2}}}{2t} \qquad 2.2.18$$

It is seen from relation 2.2.18 that the occurrence of brittle carbides on the grain boundaries will strongly reduce the cleavage stress. When plotting cleavage stress versus grain size for a given carbide thickness according to eqn. 2.2.18 as in figure 2.5 it is seen that when the grain size is refined the influence of the grain boundary carbides in modifying the cleavage stress is becoming increasingly important. All the above models predict the cleavage stress for an idealized material with uniform grain size and no pronounced substructure, e.g. dislocation pile ups of the same length as the grain size are allowed to build up.

A further assumption is that the cleavage facets represent single grains and should be of the same size as the grain size. All these assumptions seem to hold reasonably well for low carbon ferrite-pearlite steels, but may well break down for steels rolled in the austenite/ferrite regime or when acicular ferrite is produced.

One of the major problems in trying to describe cleavage failure in the complex microstructures of the HSLA-steels, is choosing the correct value for the grain size. Recently evidence has been produced that the cleavage facet size does not correspond to the grain size in tempered martensite (Matsuda et al., 1972) and in bainite (Ohmori et al., 1974). These authors introduce the concept of a "covariant packet" of martensite or bainite laths, which is a bundle or packet of laths of the same Kurdjumov-Sachs orientation. They claim that the size of the cleavage facets correspond to the size of the covariant packets and use the term effective grain size to describe the fracture properties of the materials. Tanaka et al. (1975) found that the same concepts are valid for acicular ferrite structures in low alloy steels produced both by direct quenching after rolling and by a reheat and quenching treatment. These papers all discuss the influence of effective grain size in terms of the low temperature toughness expressed by the ductile brittle transition temperature. Matsuda et al. (1972) and Tanaka et al. (1975) find a linear relationship between DBTT and $L^{-\frac{1}{2}}$ (average cleavage facet size) whereas Ohmori et.al. (1974) find that the transition temperature is linearly dependent on $\ell nL^{-\frac{1}{2}}$ as expected from a Cottrell-Petch type model. Although these workers do not report the cleavage stresses of the steels investigated, the data indicate that the cleavage stress is determined by

the effective grain size. This concept has been studied in detail by Brozzo et al. (1977) who found that the cleavage stress depends on the effective grain size in low carbon bainitic steels. They claim that micro cracks can form at subcritical stress levels by some unspecified dislocation mechanism, and that the critical event in crack initiation is the propagation of these micro cracks through high angle grain boundaries. Thus the criterion for fracture is a version of the Griffith equation

$$\sigma_c = \left[\frac{2E\gamma_{eff}}{\pi c(1-\nu^2)}\right]^{\frac{1}{2}} \qquad 2.2.19$$

where the energy required to propagate the crack through the boundary is substituted for the surface energy. From their experimental data Brozzo et al. calculate an effective surface energy of 120 J m^{-2} using the Griffith equation. This is comparable to the fracture energy values obtained by Hahn et al. (1959), and indicate a strong fracture resistance from the high angle grain boundaries.

The cleavage stress for a material is most conveniently measured in a single edge notched (SEN) slow bend specimen where the stress distribution at the notch can be determined at fracture. This can be done either by performing the test at a temperature where fracture and general yield coincides and then apply a slip line field theory to find the stress distribution (Hill, 1950; Green and Hundy, 1956) or by using finite element methods (FEM) (Rice and Johnson, 1969; Griffiths and Owen, 1971). In either case, the fracture stress will represent the stress level when complete unstable crack growth occurs in the specimen,

whereas micro cracks may have formed at a subcritical stress.

To determine the fracture toughness specimens containing sharp cracks are normally used. The stress distribution at the crack tip will thus be somewhat different from the blunt notched specimen. When the uniaxial yield stress is attained at the sharp crack tip, blunting of the crack tip will occur and a plastic zone will be formed. The maximum tensile stress is then attained at some small distance from the crack tip (Rice and Johnson, 1969) depending on the size of the plastic zone (figure 2.5). It has been suggested (Ritchie et al., 1973) that the low temperature fracture toughness of the material may depend on the magnitude of this distance at the occurrence of fracture. Physically this may be interpreted as the ease by which microcracks formed at the point of maximum stress link up to the main crack tip. Rawal and Gurland (1977) have expressed the fracture toughness in terms of the critical cleavage stress and the critical distance (X_o) as

$$K_{1C} = \sigma_c \sqrt{2\pi X_o} \qquad 2.2.20$$

which is similar to the LEFM expression for the plane stress plastic zone. Using this equation some of the observed variations in fracture toughness with test conditions can be readily explained. For changing temperatures only minor variations in σ_c are observed (Oates, 1969) thus the critical distance X_o will be inversely related to the yield stress (figure 2.3). An increase in K_{1C} is therefore expected from eqn. 2.2.20 when the temperature increases.

A similar approach has been taken by Malkin and Tetelman (1971) who estimated the position of the stress maximum in a notched specimen

from a slip line field analysis and assumed that this corresponds to the extent of the plane strain plastic zone predicted from LEFM. The fracture toughness can then be expressed in terms of the notch root radius as

$$K_{1C}(\rho) = 2.9\sigma_y[\exp(\frac{\sigma_c}{\sigma_y} - 1) - 1]^{\frac{1}{2}}\sqrt{\rho} \qquad 2.2.21$$

Malkin and Tetelman measured K_{1C} for various root radii in a ferrite pearlite steel and found good agreement with their model for root radii greater than some critical ρ_o. For smaller values of ρ K_{1C} was independent of root radius. In terms of the distance from the notch tip to the stress maximum,which can be expressed as

$$X = \rho[\exp(\frac{\sigma_c}{\sigma_y} - 1) - 1] \qquad 2.2.22$$

(Hill, 1950), this means that when the micro cracks are formed closer to the crack tip than a certain distance, X_o, the fracture resistance becomes independent of the detailed stress distribution. It is also seen that when the value of X from eqn. 2.2.22 is substituted into eqn. 2.2.20, eqn. 2.2.21 is obtained, except for a constant due to Malkin and Tetelman's assumption of an average flow stress in the plastic zone.

Curry and Knott (1976) have determined the position (X) of the maximum in the stress distribution as a function of grain size in a high nitrogen steel using a finite element method. They found that for grain sizes over about $5 \cdot 10^{-5}$ m the ratio x/d is constant, whereas x becomes constant for smaller grain sizes. Again, the lower limit for

the x values is consistent with an optimum position for nucleation of the micro cracks. Various attempts have been made to elaborate on the microstructural significance of a lower limit of X_o (Tetelman, et.al., 1968; Ritchie et al., 1973; Curry and Knott, 1976; Ritchie et al., 1976) and critical values of one to two grain diameters have been suggested.

2.2.3 Ductile Failure

The majority of models of ductile fracture assume that the fracture event takes place by nucleation of voids at second phase particles and growth of individual voids until the voids coalesce and join up to the crack tip. The three different stages of fracture, i.e. nucleation, growth and coalescence, are commonly considered separately and a variety of models describing these events have been published in the literature.

Argon et al. (1975,a) have described the condition for void nucleation in terms of a critical interface strength (σ_i) between the second phase particles and the matrix such that the normal stress (σ_N) at the interface must exceed σ_i for voiding to occur. The critical stress is normally higher than the yield stress of the matrix which has to work harden locally to reach the condition for voiding. It is thus convenient to describe the nucleation condition in terms of a critical macroscopic strain, ε_n. The Argon model is based on a continuum-plasticity approach and does not involve a description of the local work hardening mechanism.

Ashby (1966) has proposed a dislocation mechanism that accounts for the local work hardening and the increase in flow stress at the particle. The local tensile stress at the interface is expressed

in terms of the number of dislocation loops piled up against the particle and thus related to the macroscopic strain.

Both the Argon and the Ashby models assume interface decohesion as the mechanism of void nucleation. Cracking of second phase particles or inclusions has, however, commonly been observed to result in voiding, in which case the nucleation criterion should be similar to the fiber loading model of Lindley, Oates and Richards (1970).

The majority of models describing growth of voids express the change in void geometry in terms of the macroscopic values of stress, strain and initial distribution of voids. McClintock (1968) has described how an array of cylindrical voids will grow in a hydrostatic stress field. This model does not provide a mechanism for void coalescence and local impingement of voids is therefore assumed as a fracture criterion. This, however, tends to seriously overestimate the total fracture strain.

Thomason (1969) has proposed a model for ductile fracture by internal necking between cavities in the material. This model assumes that the array of pre-existing voids deforms uniformly with the matrix until the condition for local necking of the remaining ligaments is attained. The condition for coalescence is expressed in terms of the intercavity spacing or the volume fraction of cavities.

A purely geometric model has been suggested by Brown and Embury (1973) where they consider voids growing along the major strain axis in the specimen. The voids will elongate until the length equals the spacing of the voids, taken to be the average initial spacing of the particles, at which point unconstrained plastic flow along planes of maximum shear stress can occur, thus leading to void coalescence and fracture.

A comparison between models describing ductile failure and available data on failure strain for various materials has been undertaken by LeRoy (1977). This invetigation indicates that for a broad range of materials the Brown and Embury model describes the experimental results very well. It should be noted, however, that the majority of ductile failure models only describe the straining process until linking of voids or some sort of strain localization occurs and do not include the strain increment during void coalescence. The reason why predictions of macroscopic fracture strains still can be made is that the coalescence strain, although of appreciable magnitude, is only affecting a small volume close to the fracture surface and will thus not significantly change the macroscopic fracture strain as measured by the reduction in area. However, it is pertinent to consider the shortcomings of the current models before attempting to utilize them to estimate the fracture toughness expected for fibrous fracture models. A common feature for the void growth models is that the coalescent stage is considered in purely geometric terms such that the growth strain is limited by the initial volume fraction of particles or cavities. However, there is now much evidence (Ernst and Spretnak, 1969; Clayton and Knott, 1976; Embury et al., 1977) to suggest that at higher yield strengths void coalescence occurs by localized shear deformation. The strain localization is attributed to the low work hardening rate relative to the applied stress on the ligament and results in a lower ductility than predicted from any geometric model of total strain to failure. In terms of fracture toughness the occurrence of strain localization will severely reduce the magnitude of the predicted COD-value for fibrous fracture. A further approximation

is the assumption of a uniform distrubition of void nucleating particles. In most structural materials these will be grouped together in a non-uniform fashion resulting in a reduction both in the effective nucleation strain (Argon et al., 1975,b) and in the growth strain (Brown and Embury, 1973). As discussed in section 2.2.1 of this chapter, the fracture resistance can be expressed in terms of the stress intensity factor K_{1C}, the fracture energy J_{1C} or the crack opening displacement COD at fracture. In fibrous fracture the latter approach is attractive since the criterion for failure is one of critical strain.

The attainment of a critical displacement at the crack tip is accommodated by the plastic zone in front of the crack. It is therefore expected that variations in geometry that affect the local stress, strain distribution and the size of the plastic zone will influence the magnitude of the COD value. In terms of linear elastic fracture mechanics this is given by

$$COD = \frac{K_{1C}^2(1-\nu^2)}{\sigma_y E} = \frac{6\pi\sigma_y(1-\nu^2)}{E}\, r_{1y} \qquad 2.2.23$$

where r_{1y} is the plane strain plastic zone. The extent of the plastic zone or the maximum value of COD is limited by the amount of strain the material can sustain at the crack tip, and thus by the initial root radius of the notch. Smith and Knott (1971) and Chipperfield and Knott (1975) have measured the critical COD values as a function of the notch root radius for several steel qualities and did indeed find a constant ratio between COD and root radius. Below a critical notch root radius, however, the opening displacement is constant indicating an increasing fracture strain for decreasing root radius. The fact that COD is constant and equal to

the sharp (fatigue) crack COD for small root radii is of interest in determination of COD since fatigue cracking could be avoided and machined notches used instead. Rice and Johnson (1969) have explained the occurrence of a lower shelf for the COD values in terms of the plastic zone size. Thus the condition for voiding to occur is that particles exist inside the plastic zone, i.e., the extent of the plastic zone must be of the same magnitude as the interparticle spacing. Cracks of sub-critical radius therefore have to blunt sufficiently for the plastic zone to envelop the void nucleating particles. A simple geometric argument giving the same net result could also be put forward. In terms of the Brown and Embury model the condition for void linking is a local displacement of the same magnitude as the particle spacing. To obtain COD values equal to the particle spacing the crack may have to blunt substantially beyond what is predicted from a constant strain criterion. This suggests the possibility that for a constant volume fraction of second phase particles a coarse particle distribution will be beneficial in terms of fracture resistance, whereas the total strain, as measured by the reduction in area in a tensile test depends on the volume fraction of particles.

In HSLA-steels the microstructure is very complex and a variety of second phase particles exist that may produce void nucleation, the most important being sulphides and islands of M/A-constituents. The extent to which removal of sulphides, the primary source of voids, is economical must therefore be considered in terms of the other available mechanisms of void nucleation and linkage. In particular, large volume fractions of the M/A phase and the occurrence of strain localization have been observed to reduce the ductility of some HSLA-steels (Embury et al., 1977).

2.2.4 Delamination

In the transition range between brittle and ductile failure, splitting or delamination is often observed along planes parallel to the rolling plane in controlled rolled plate and sheet. This can be a serious problem because it prevents the attainment of the maximum energy absorption value, i.e. it produces a sloping region in the Charpy curve.

The occurrence of delamination is due to planes of weakness oriented parallel to the rolling plane. The origin of these planes of weakness has been described in the literature in terms of cleavage on (100) planes oriented parallel to the rolling plane (Miyoshi et al., 1974), grain boundary decohesion (Herø et al., 1975; Hornbogen and Beckmann, 1976) or decohesion along sheets of inclusions (Embury et al., 1977). The latter case does not represent the traditional problem of elongated sulphides or silicates being formed during hot rolling, but is due to the agglomeration of rare-earth (RE)-oxy-sulphides precipitated in the melt. During rolling these clusters are deformed to sheets of very high inclusion density, which will severely reduce the through thickness properties of the material. Delamination by the cleavage mechanism seems to be confined to steels rolled to low finishing temperatures. This is consistent with the development of a (100) texture when the material is subjected to rolling in the ferrite range (Coleman et al., 1973; Miyoshi et al., 1974). If, however, the plate is finished rolled in the austenite range the transformation texture is not expected to show any strong (100) component in the rolling plane, although delamination may still occur. Herø et al. (1975) showed by careful metallography that the splits propagated along ferrite grain boundaries. This observation

was attributed to the formation of voids at grain boundary carbides. Due to the transformation kinetics in these materials a large fraction of the carbides may precipitate on grain boundaries parallel to the rolling plane, thus producing planes of weakness when voiding occurs.

Hornbogen and Beckmann (1976) have considered the influence of rolling finishing temperature on delamination in terms of a recrystallization mechanism. When rolled in the ferrite range the deformed material tends to recrystallize and carbides precipitate on the recrystallization front. Since nucleation of new grains starts in the maximum strained material, which is assumed to be the elongated ferrite boundaries, planar arrays of carbides will be produced. This mechanism may operate in coiled sheet where ample time is available for the recrystallization-precipitation process. In plate material where the cooling rate is faster, little precipitation is observed in the ferrite (McCutcheon et al., 1975). It is important to realize that no unique microstructural feature is responsible for the occurrence of delamination, e.g. a variety of microstructural constituents can provide planes of weakness parallel to the rolling plane. It is therefore difficult to define a criterion for delamination failure. The majority of reports of delamination assume that the critical condition for splitting is the attainment of a critical tensile stress normal to the plane of weakness. It has been suggested, however, (Embury et al., 1977; Groom and Knott, 1975) that the strain may be of importance in the nucleation of splits by the ferrite grain boundary mechanism.

2.2.5 Summary

The predominant fracture modes for HSLA-steels are cleavage failure at low temperature, ductile failure by voiding at ambient temperatures and the occurrence of delamination for intermediate temperatures(figure 2.2).

A variety of models describing both cleavage and ductile fracture have been developed for simple materials with a uniform grain structure and a well defined inclusion and carbide morphology. There is a question, however, as to whether these models adequately describe the fracture behaviour of the more complex materials produced by controlled rolling or if other parameters have to be included in the analysis.

This suggests that there is an advantage in terms of applicability of results, in studying the fracture behaviour of commercial materials rather than using laboratory heats where the microstructure is easier to control. It does, however, require a detailed characterization of microstructure in terms of grain size and shape, inclusion distribution, carbide morphology, and non-ferritic phases produced during transformation.

For cleavage fracture a series of questions remain to be answered regarding the microstructural origin of the cleavage stress, e.g. influence of carbide distribution, effective grain size and non-ferritic transformation products. Further, there is the problem of relating the cleavage stress to the low temperature fracture toughness, and the size of the process zone necessary to accommodate the fracture process. This suggests an experimental determination of cleavage stress and fracture toughness for materials with different microstructures, and detailed fractography to relate the critical fracture events to the microstructural

features.

A major problem in ductile failure is the range of microstructural constituents that can nucleate voids during straining, e.g. at non-metallic inclusions precipitated from the melt, carbides and the M/A constituent. These have to be characterized both in terms of size and distribution, and in terms of their mechanical response, i.e. nucleation strain, for various stress states. Further, the mechanism of void linking is of major importance in determining the maximum value of COD that can be attained in a fracture test. The following experiments should yield further insight in the problems described: A metallographic investigation of the nature of the microstructural constituents involved in the voiding process in tensile and notched specimens. Determination of the fracture strain in tension and correlation with COD values obtained from notched bend samples.

Delamination failure or splitting may occur by a variety of mechanisms such as fracture along elongated inclusions or inclusion sheets, cleavage in (100) textured material, and grain boundary tearing. It is thus necessary in each case to determine the microstructural origin of the delamination failure. Failure by the grain boundary tearing mechanism does not seem to obey a simple critical tensile stress criterion. Tests involving different stress and strain states at failure may delineate the influence of the various stress components and allow a fracture criterion to be formulated.

3. EXPERIMENTAL PROCEDURE

The scope of this investigation is to describe the fracture behaviour of controlled rolled HSLA-steels in terms of the detailed microstructure. The fracture behaviour is studied in single edge notched (SEN) bend specimens and in tensile specimens deformed at various temperatures.

The mechanical behaviour is correlated to the detailed microstructure of the material as revealed by standard optical metallography, transmission electron microscopy (TEM) and X-ray techniques. Additional information about the detailed fracture behaviour is obtained from an extensive scanning electron microscopy (SEM) study of fractured specimens.

3.1 MATERIALS CHARACTERIZATION

The materials used were supplied by the Steel Company of Canada, Ltd., Hamilton, and consisted of controlled rolled plate of 3/4" thickness. Three different materials, referred to as steel A, B and C, were studied. The plates obtained from steel A were from two different heats with identical rolling schedule and composition except for a small difference in sulphur level. Material from the two heats was kept separate and is referred to as steel A1 and A2. The compositions and rolling practice for the various materials are listed in ble 3.1.

The cleanliness of the materials was assessed by optical metallography. Three perpendicular sections, longitudinal, transverse

TABLE 3.1

COMPOSITION AND ROLLING PRACTICE

	C	P	S	Mn	Si	Nb	Mo	Al	Ce	Ni	Rolling Practise
STEEL A1	0.05	0.006	0.017	1.92	0.07	0.06	0.32	0.03	0.022	-	Reheat temperature 1130°C 74% reduction below 840°C
STEEL A2	0.05	0.006	0.011	1.80	0.08	0.06	0.32	0.03	0.011	-	As A1
STEEL B	0.05	0.009	0.007	1.98	0.30	0.06	0.55	0.04	0.004	0.22	Reheat temperature 1140°C 55% reduction below 840°C
STEEL C	0.05	0.003	0.018	2.08	0.23	0.06	0.41	-	-	0.24	Reheat temperature 1175°C 55% reduction below 790°C

and short transverse, were viewed in the as polished condition. Steel C containing thin elongated manganese sulphides was etched in oxalic acid (10 gr oxalic acid 100 ml water) to reveal the sulphides. A quantitative assessment of the inclusion morphology, size and distribution was obtained using the Quantimet 720 image analyzer at Stelco Research.

The microstructure was studied by optical metallography using 2% nital or saturated picral etchants. The ferrite morphology was best revealed by the nital etch whereas the picral etch gave additional information on carbide distribution and the morphology of the martensite austenite constituent. Further information on the detailed structure of the carbides was obtained by the use of SEM on samples polished, etched lightly in nital and plated with gold. The gold plating prevented charging effects at the carbides and allowed high magnification microscopy to be performed without disturbances in the image.

Transmission electron microscopy was used to reveal the finer details of the microstructure. Longitudinal sections, 1 mm thick, were cut from all materials and the specimens thinned mechanically to about 0.1 mm. From these samples 3 mm discs were cut and thinned electrolytically to perforation in a Struers Tenupol using a solution of 10% perchloric acid in methanol. The solution was cooled to -40°C and thinning performed using 30 V applied voltage. The samples were investigated in a Philips 300 electron microscope operating at 100 kV accelerating voltage. In addition to the thin foils, direct carbon extraction replicas were studied in the TEM, revealing information on the detailed morphology of the non-ferritic phases at lower levels of magnification (<5000 X) not easily obtained using thin foils.

Crystallographic texture has been proposed as a source for the initiation of splitting failure and was thus investigated in the materials used in the delamination study. The degree of directionality was assessed using a Philips 1080W texture goniometer and CoKα radiation. The intensity distribution of the (200) and (110) reflexions was recorded and plotted as pole figures. The intensity was normalized to random intensity as measured in a compacted iron powder sample.

Extensive SEM fractography was carried out on all types of specimens broken at various temperatures. This involved a detailed study of fracture surface features such as cleavage facet size, dimple type and size, and inclusion morphology. To prevent corrosion and damage of fracture surfaces all fracture surfaces were laquered with "Microstop laquer" immediately after testing. The specimens were then cleaned in an ultrasonic cleaner using acetone before inspection in the SEM.

Further information on the detailed correlation between fracture path and microstructural features was obtained using the techniques described by Almond et al. (1969) and Chessnut and Spurling (1977). The former is a technique where fracture surface and microstructural features can be studied simultaneously by polishing and etching a tapered section of the specimen. The technique described by Chessnut and Spurling utilizes electrolytic polishing and etching of selected areas of the fracture surface. The latter procedure, originally used for titanium alloys, was modified for HSLA-steels by using a 10% perchloric in methanol solution for electrolytic removal of material and subsequent etching in 2% nital. This gave a very sharp edge between the fracture surface and the etched section, thus allowing a one to one matching of fracture surface features

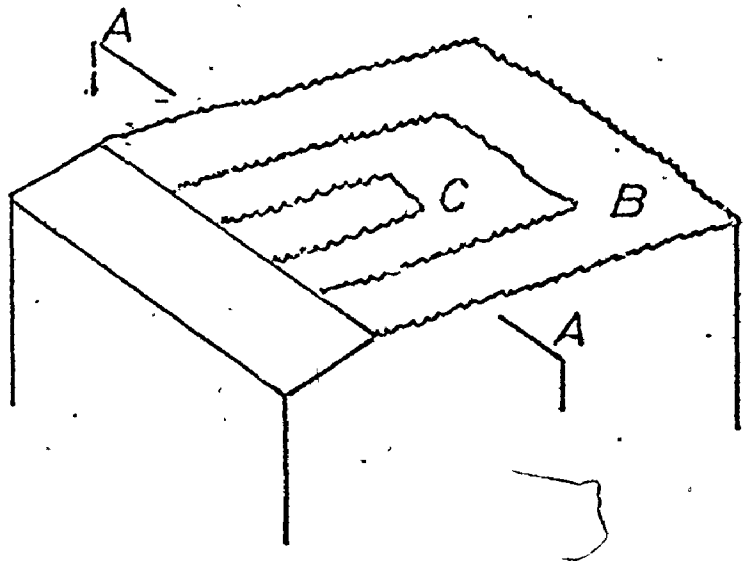

a: Sketch showing specimen preparation technique for revealing fracture surface and microstructural features. Region B is the original fracture surface and region C the electro-polished and etched surfac

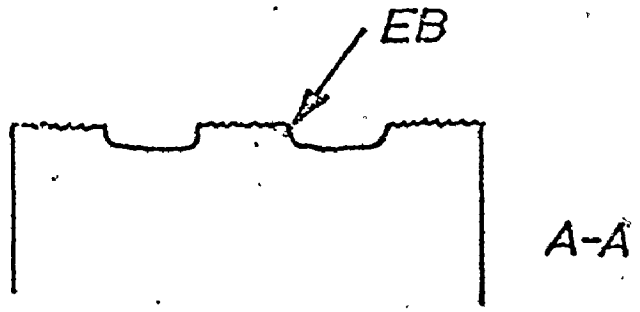

b: Section A-A showing profil of electropolished specime Arrow EB indicate directio of electron beam in the SE

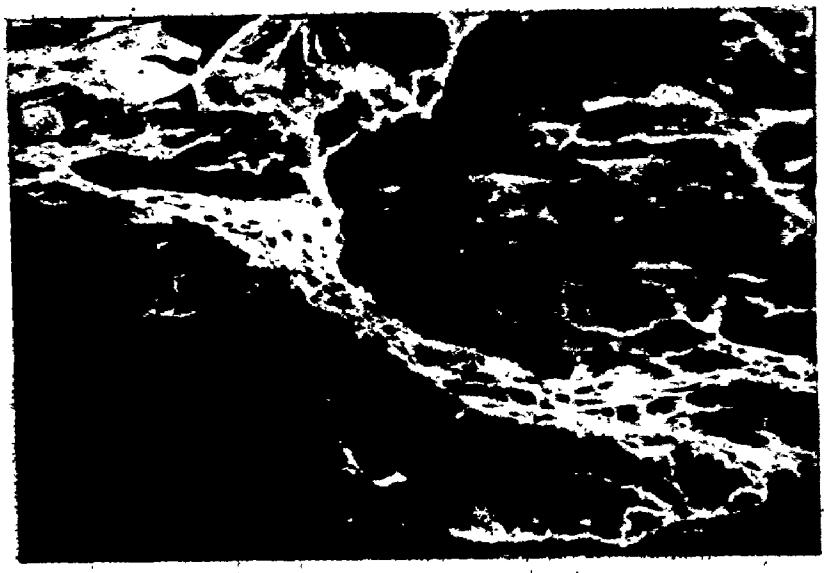

c: Example of results that can be obtained by this technique: Slow bend specimen of steel B.

and microstructural components as shown in figure 3.1.

Additional information was obtained from nickel plated and sectioned specimens where both the fracture path and the damage accumulated in the specimen prior to fracture could be studied. Nickel was deposited electrolytically on the fracture surface from a solution containing 250 ml nickel sulphamate, 10 gr nickel chloride, and 10 gr boric acid. The bath temperature was held constant at 70°C and a current density of 0.9 Amp/cm^2 was used.

3.2 MECHANICAL TESTING

In the brittle fracture regime the usual criterion assumed for failure is the attainment of a critical stress (figure 2.2) and the determination of the cleavage stress is thus of major importance. For HSLA-steels the cleavage stress is usually higher than the fracture stress in tension at all convenient test temperatures ($T > 77°K$) and a simple tensile test will therefore not reveal the critical cleavage stress. The critical stress is, however, attained in notched specimens where the plastic constraint gives a significant stress amplification (Knott, 1966). The specimen chosen was a SEN (single edged notched) bend specimen with dimensions as indicated in figure 3.2. The specimen was loaded in a three point bending rig fitted to a floor model Instron testing machine (figure 3.3) in a cage under the crosshead. This allowed various cooling media to be used. At temperatures above -78°C the cage was immersed in a mixture of dry ice and acetone, at lower temperatures cooled nitrogen vapour was sprayed on the rig and the specimen through a copper

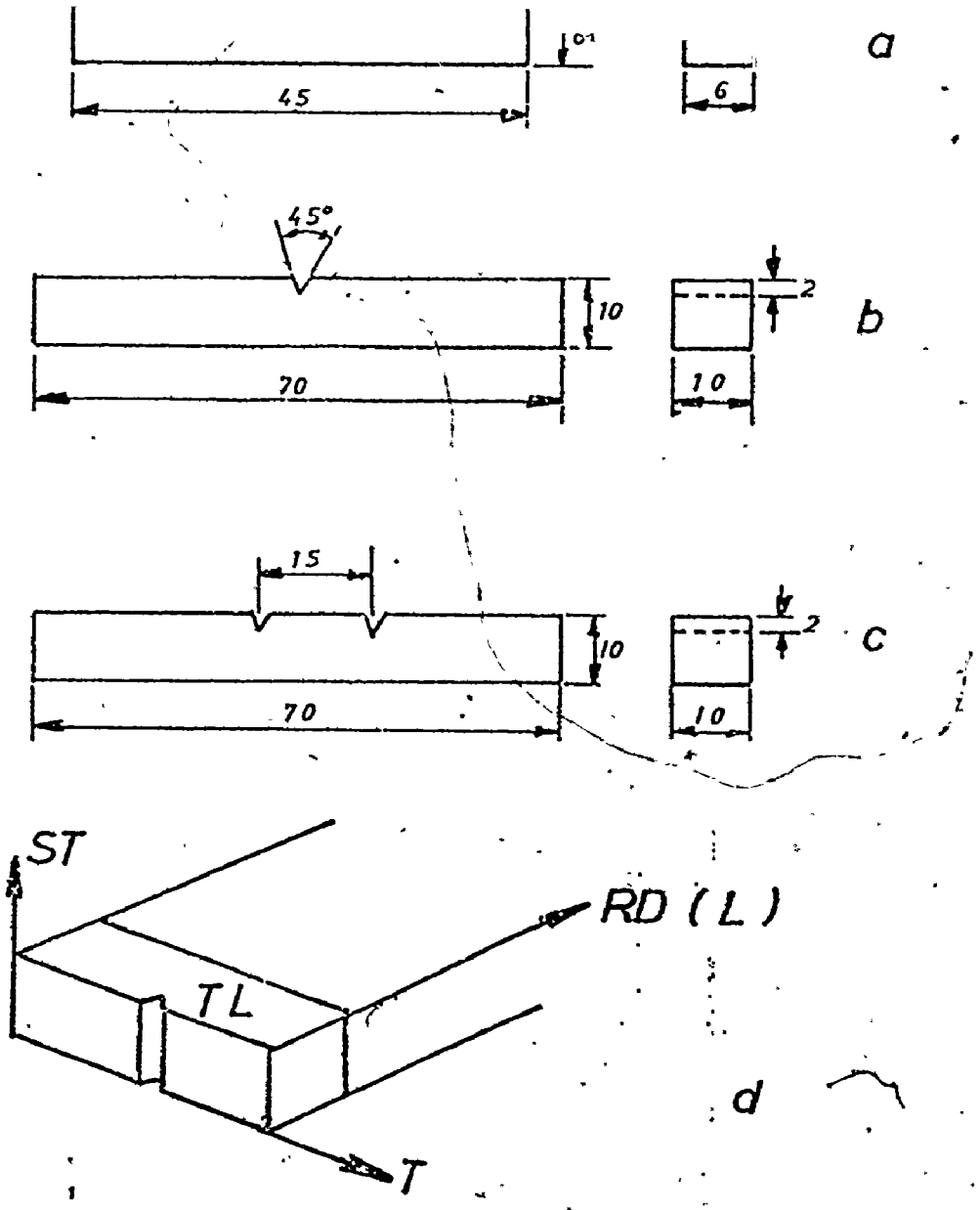

Figure 3.2.a,b,c,d: Drawings showing the specimens used to assess the fracture behaviour of HSLA-steels.

a: Subsize Charpy specimen used to determine the cleavage stress.

b: Single edge notched (SEN) bend specimen used to assess COD and K_{1C} values.

c: Double notched bend specimen used for metallographic studies of the fracture process.

d: Definition of orientations in the plate.
RD: rolling direction, L: longitudinal direction,
T: Transvere direction, ST: short transverse direction.
Orientation of bend specimen TL, specimen oriented in the transverse direction with crack propagating in the longitudinal direction.

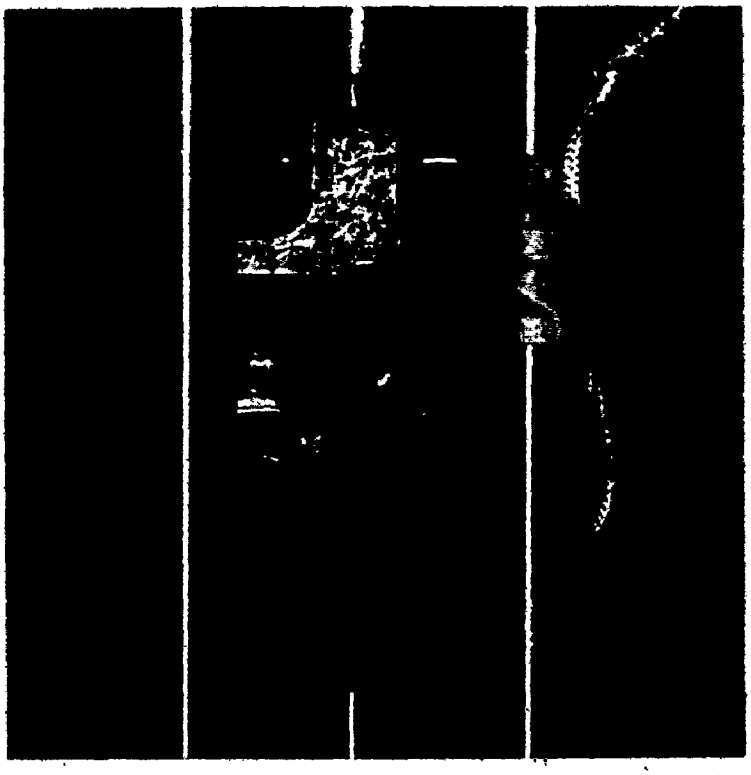

Figure 3.3: Photograph showing the three point bending rig mounted in a cage under the cross head on the testing machine.

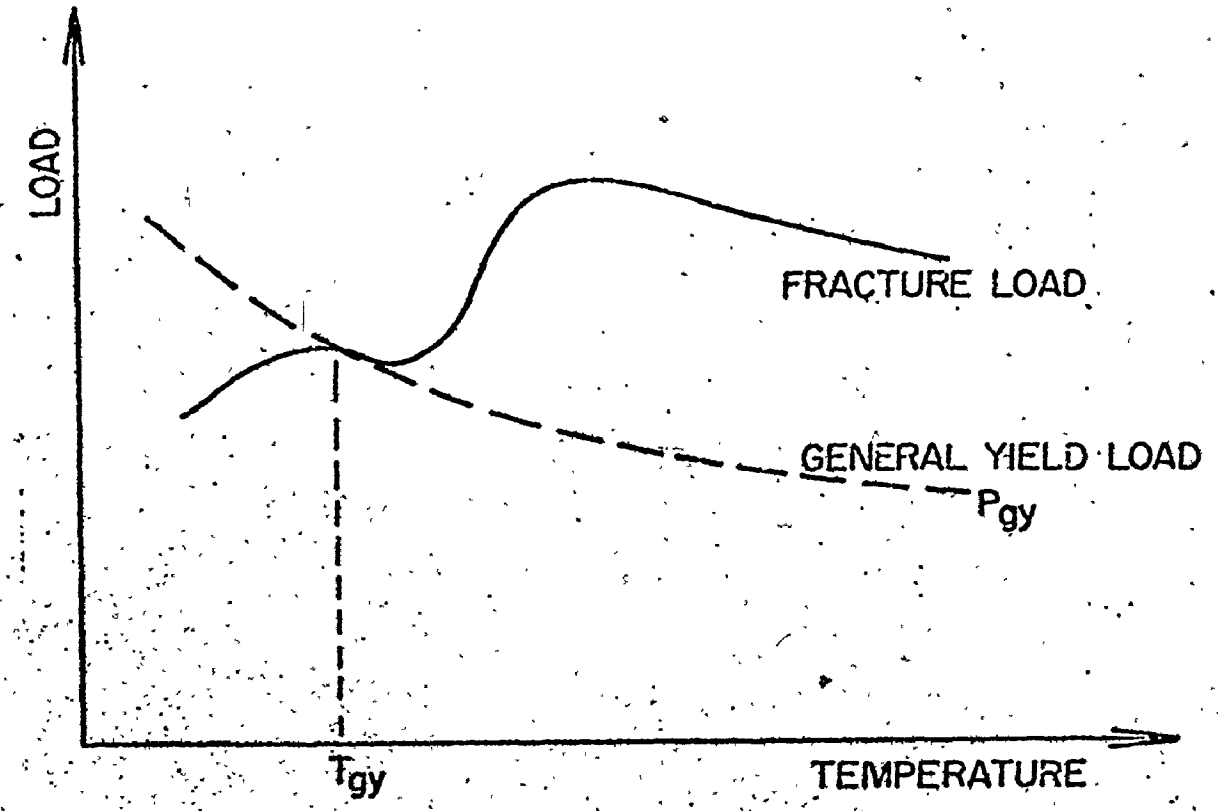

Figure 3.4: Schematic diagram showing variation in fracture and general yield load versus temperature in a

spiral surrounding the specimen. To increase the cooling efficiency the cage was covered in a styrofoam box of approximately 3/4" wall thickness. The temperature was measured by a thermocouple inserted in a dummy specimen attached close to the actual test sample and recorded on a digital voltmeter. The temperature was held constant to within ±2°C during the test.

The use of a SEN bend specimen to determine the cleavage stress is based on the assumption that maximum stress in front of the notch can be deduced from a slip line field theory at general yield (Green and Hundy, 1956). It is thus necessary to do tests at various temperatures until the condition for coincidence between fracture and general yield is established, e.g. at T_{gy} in figure 3.4. At this point the fracture stress can be expressed as $\sigma_F = R\sigma_y$ where R is the plastic constraint factor which can be estimated from slip line field theory, e.g. $R = (1 + \frac{\pi}{2} - \frac{\theta}{2})$ where θ is the included notch angle. Preliminary tests showed that it was necessary to use $\theta = 30°$ to get $T_{gy} > 77°K$, which is the lower limit for test temperatures that can be readily obtained.

Values for fracture toughness in the ductile and cleavage regime were obtained from precracked SEN bend specimen (figure 3.1) loaded in four point bending. A detailed drawing of the bending rig and the attachment to the Instron crosshead is shown in figure 3.5.

At low temperatures values of K_Q were calculated from the fracture load using the following equations as suggested by Tada et al. (1973)

$$K_I = \frac{6M}{W^2}\sqrt{\pi a}\, F(a/W) \qquad 3.1$$

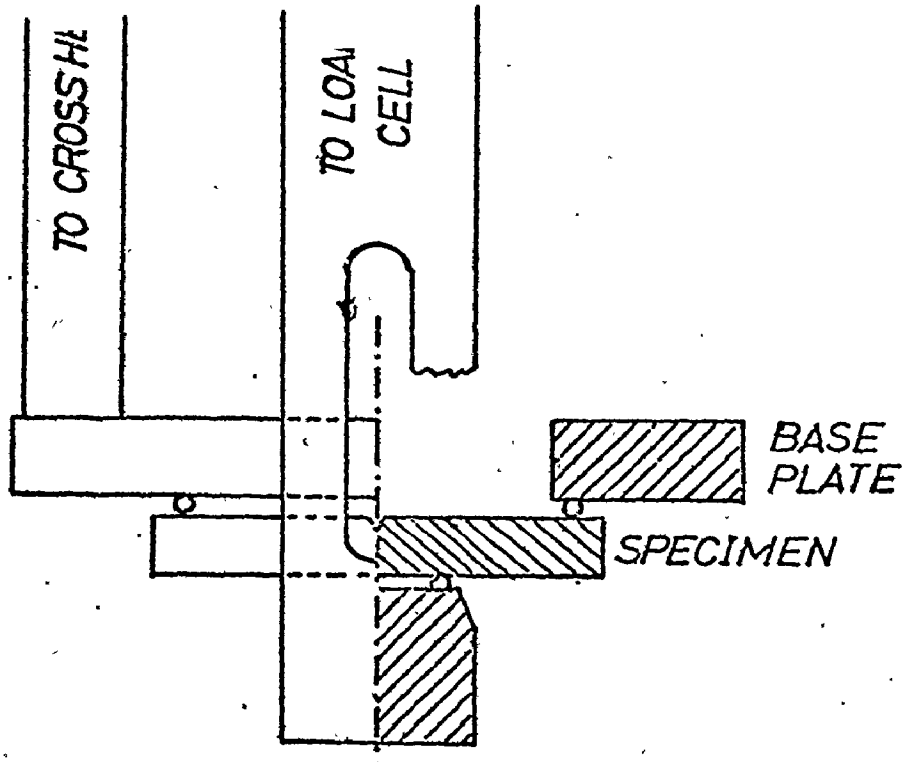

Figure 3.5.a.

Figure 3.5.b.

Figure 3.5.a,b: Illustration of four point bending rig.

a: Drawing showing assembly of the rig. The hatched areas represent the midsection.

b: Photograph showing specimen mounted in the bending rig.

$$F(a/W) = 1.122 - 1.40(a/W) + 7.33(a/W)^2 - 13.08(a/W)^3 + 14.0(a/W)^4 \qquad 3.2$$

where M is the bending moment, a is the crack length, W is the specimen width and F(a/W) a geometric factor. In the fibrous fracture regime toughness was estimated from measurements of the crack opening displacement (COD). The crack tip opening displacement was measured using the technique described by Robinson and Tetelman (1976) where a silicone rubber compound (Kerr citricon) is allowed to penetrate into the crack under load and subsequently harden. By subtracting the initial slot width and any crack opening displacement due to stable crack growth a value for the crack opening displacement at initiation $(COD)_i$ was obtained (figure 3.6). The dimensional stability of the epoxy was checked by making an impression of the gap between the points of a micrometer and subsequently measuring the thickness of the hardened epoxy on the same travelling microscope used for measuring COD values. It was found that the dimensions could be measured to within ±1% of the original gap opening.

The influence of the notch geometry on the stress and strain distribution at the notch tip was discussed in chapter 2, where it was argued that the volume over which a critical stress or strain is operating depends on the root radius of the notch. It was thus of interest to investigate the correlation between plastic zone and process zone size and the scale of the microstructure, e.g., inclusion spacing, grain size etc. The fracture resistance, expressed in terms of COD or K_{IC}, was measured in SEN-specimens in four point slow bending. Slot widths from 60 μm to 500 μm were obtained by wire cutting using a silicon carbide

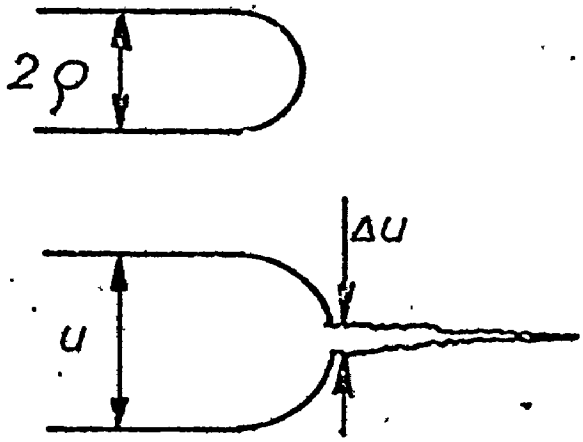

Figure 3.6: Schematic drawing showing measurement of COD values using the rubber impregnation technique. The opening displacement is given by COD = u - 2ρ - Δu where u is the slot width on load, 2ρ is the original slot width and Δu is the opening displacement associated with stable crack growth.

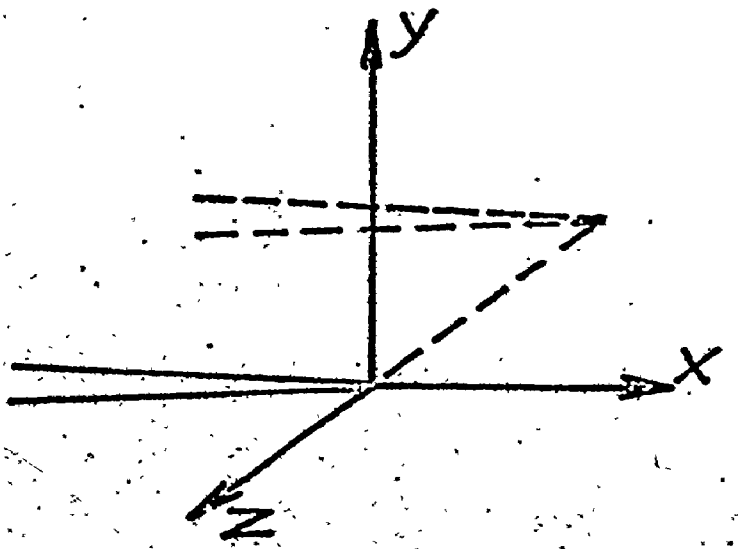

Figure 3.7: Schematic drawing showing orientation of the coordinate system used to describe the crack tip stress field.

abrasive. The precracked specimens, having an effective root radius of zero, were fatigued in the floor model Instron at a constant strain amplitude corresponding to a ΔK-level of about 15% of the room temperature K_{1C} value which is well below the upper limit given by Knott (1973).

To further investigate the nature of the damage introduced in a material during crack initiation, double notched specimens were broken in four point bending. With the specimen dimensions shown in figure 3.2, both notches will see the same bending moment during the initial loading and it is assumed that both notch tips go through the same loading history. When a crack propagates from one notch the other can be sectioned and prepared for metallography thus revealing the detailed fracture initiation mechanism, i.e., micro crack formation, voiding, localized shear etc. Sectioned specimens were studied in the SEM after etching lightly in 2% nital and gold plating to avoid charging effect at non-conducting particles. The behaviour of various microstructural features in the notch tip strain field were studied and correlated to the strain gradient in front of the notch. The strain gradient was determined by micro hardness measurements in front of the notch after first establishing a calibration curve between micro hardness and strain as measured in samples deformed in uniaxial compression.

Delamination has been studied in a variety of tests where stresses develop normal to the rolling plane of the plate. In the slow bend tests used to evaluate the cleavage stress splitting occurred at intermediate temperatures between the regime of completely ductile and brittle failure. Splitting was usually accompanied by a load drop in the load deflection curve allowing the maximum stresses in front of the

notch to be estimated from the slip line field theory. Assuming a Tresca yield criterion the maximum values of the principal stresses are given by

$$\sigma_{yy} = \sigma_y(1 + \frac{\pi}{2} - \frac{\theta}{2}) = \sigma_y R \qquad 3.3a$$

$$\sigma_{xx} = \sigma_{yy} - \sigma_y = \sigma_y(R - 1) \qquad 3.3b$$

$$\sigma_{zz} = \tfrac{1}{2}(\sigma_{yy} + \sigma_{xx}) = \sigma_y(R - \tfrac{1}{2}) \qquad 3.3c$$

where the coordinates are defined in figure 3.7. In a notched bend specimen of the T-L orientation (figure 3.2) the σ_{zz} component will be acting on planes parallel to the rolling plane and is thus believed to cause splitting under certain conditions.

A more accurate determination of the normal stress at delamination can be obtained from a short transverse tensile test. This method is restricted to heavy gauge plate where sufficient wall thickness exists to allow machining of tensile specimens. In the present case tensile specimens with 5 mm gauge length were used (figure 3.8) to assess the through thickness tensile properties. To make sure no stress concentration effect developed due to the small length to diameter ratio (1:1) longitudinal specimens of similar geometry were pulled and the tensile behaviour compared to results from standard tensile tests (5:1 length to diameter ratio) performed at the same strain rate.

Delamination is also observed in longitudinal tensile specimens where radial stresses develop in the necked region. The radial stress component can be calculated from Bridgeman's analysis (1952) and is given by:

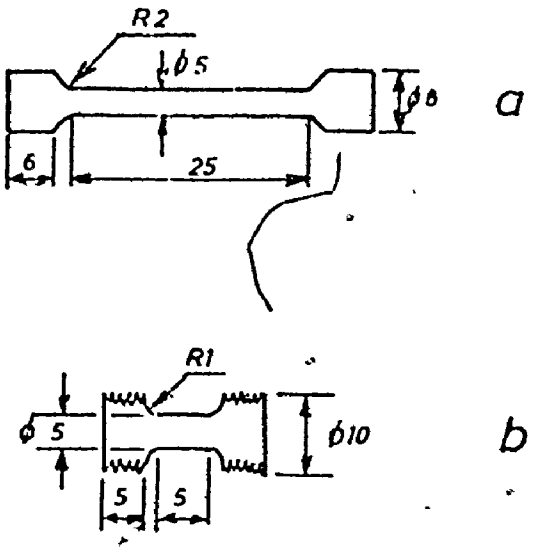

Figure 3.8: Drawing showing tensile specimen used to assess mechanical properties.

a: Longitudinal tensile specimen.

b: Short transverse tensile specimen.

The specimen used in the transverse direction is the same as in a except for a 20 mm gauge length.

$$\sigma_{rr} = \sigma_f \, \ell n\left(1 + \frac{a}{2R}\right) \qquad 3.4$$

where σ_f is the flow stress in the neck, a is the radius of the minimum cross section of the neck and R is the radius of curvature of the neck. According to Bridgeman the flow stress can be expressed in terms of the average tensile stress in the neck, i.e., the true fracture stress at the occurrence of delamination (σ_F^*). Equation 3.4 can then be rewritten as

$$\sigma_{rr} = \frac{\sigma_F^*}{1 + \frac{2R}{a}} \qquad 3.5$$

Values of R and a were determined using a shadow graph where the shadow of broken specimens were projected onto a glass screen at 20X magnification. a could then be measured directly on the screen whereas R was determined by comparing the magnified neck profile to circles of known diameter. Values of the delamination stress (σ_{rr}) have been determined at a variety of temperatures between -196°C and room temperature using tensile specimens of 25 mm gauge length and 5 mm diameter (figure 3.8).

The large differences in true strain to failure in the longitudinal and short transverse tensile tests suggested that the influence of strain on the delamination behaviour be investigated further. Thus short transverse tensile samples were pre-deformed in compression to a strain of about 0.5. The specimens were then remachined to the original original diameter (5 mm) and pulled in tension at -70°C.

During the analysis of the delamination data it became apparent that the results could be described in terms of a critical shear stress criteria for the nucleation of splits.

Two different mechanisms involving the shear stress can be envisaged. Either the shear stress in the plane of weakness can nucleate a shear crack (mode II crack) or the occurence of delamination may be due to the increase in flow stress during straining. The latter is expressed by the radius of the von Mises yield surface ie, the maximum shear stress. In order to separate the two mechanisms tensile specimens were cut with various orientations to the plate. Tensile specimens with the tensile axis in the longitudinal and the short transverse direction have no shear stress component parallel to the rolling plane whereas specimens machined with the tensile axis at 45^{o} to both the rolling direction and the rolling plane normal have the maximum shear stress component in the rolling plane. Due to limited plate thickness these were only 4 mm diameter (figure).

In addition to the tensile [illegible] described in connection with the delamination tests transverse tensile specimens were pulled in order to correlate the true strain in tension with COD values obtained for SEN-bend specimens in the T-L orientation. These specimens were slightly shorter than the standard specimens since they were made from the halves of broken bend specimens (figure 3.8).

4. MICROSTRUCTURES - RESULTS AND DICUSSION

The compositions and hot working scheduled for the steels used in this investigation are summarized in table 3.1. In this section the detailed microstructural characterization will be discussed in terms of current theories for phase transformations in low alloyed structural steels which were described in chapter 2.

In this work, emphasis has been given to the microstructural features directly involved in the detailed fracture processes. Thus many microstructural aspects of HSLA-steels, e.g. precipitation kinetics, the nature of the dislocation substructure etc. have not been treated in any detail. Although worthy of more detailed investigation, these phenomena are considered outside the scope of the present study.

A summary of the detailed literature review in chapter 2 concerning the most important microstructural features in determining the fracture behaviour of HSLA-steels is given in figure 2.2. At low temperatures brittle failure processes are influenced by the scale and morphology of the ferrite, distribution of carbides and the occurrence of non-ferritic transformation products. In the case of ductile failure the critical parameters are the magnitude and the distribution of strain at the crack tip which is influenced by the inclusion content and shape, the mode of slip and again the occurrence of non-ferritic transformation products. The occurrence of delamination depends on microstructural features such as the type and distribution of sulphides, the existence of grain boundary carbides and the crystallographic texture of the plate.

The work on materials characterization has thus been concentrated on the microstructural features mentioned above.

For clarity the various microstructural constituents have been treated separately when possible.

4.1 FERRITE MORPHOLOGY

The scale and morphology of the ferrite structure in the various steels have been studied by optical metallography using samples etched in nital and by transmission electron microscopy. The low magnification composite micrographs in figure 4.1 show the general features of the microstructures. Steel A consists of polygonal ferrite whereas steel C shows a duplex microstructure consisting of a mixture of polygonal and acicular ferrite and steel B is almost fully acicular with a few polygonal grains distributed throughout the microstructure. Further, a banded ferrite structure is apparent in figure 4.1, in particular in steels A and C where layers of polygonal ferrite and a mixture of acicular structures and non-ferritic phases seems to alternate through the thickness of the plate. In addition, large variations in grain size are observed both between the various steels and within each plate as seen from the grain size distribution fucntions plotted in figure 4.2.

Banding in hot rolled structural steels is normally attributed to the occurrence of segregation of solute elements, e.g. Mn and Si, during solidification (Kirkaldy et al., 1962). The effects of the solute elements is twofold. During soaking an equalization of carbon activities will take place thus leading to a segregation of carbon in the austenite.

Figure 4.1.a,b,c:

Composite micrographs illustrating banded microstructures in three orthogonal sections. (nital etch,

a [illegible]

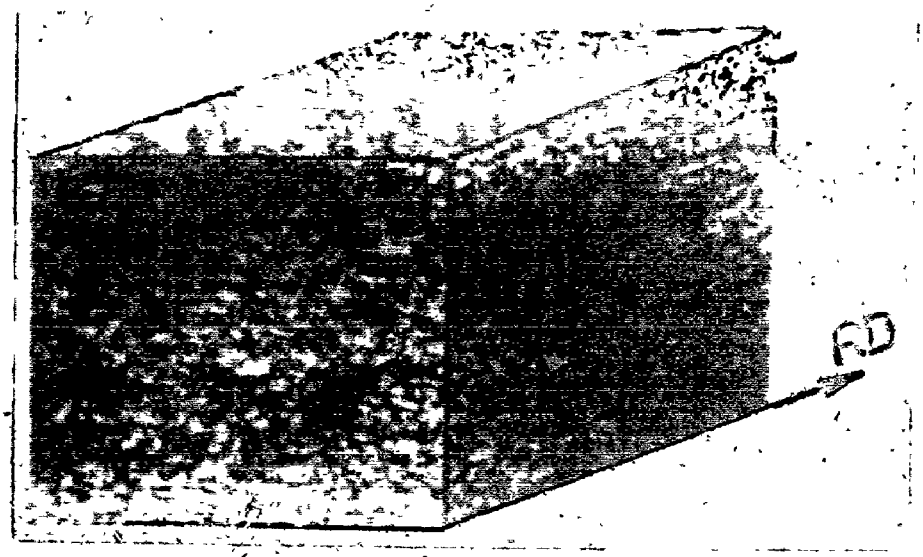

b: Steel B,
300x magnification

c: Steel C,
300x magnification.

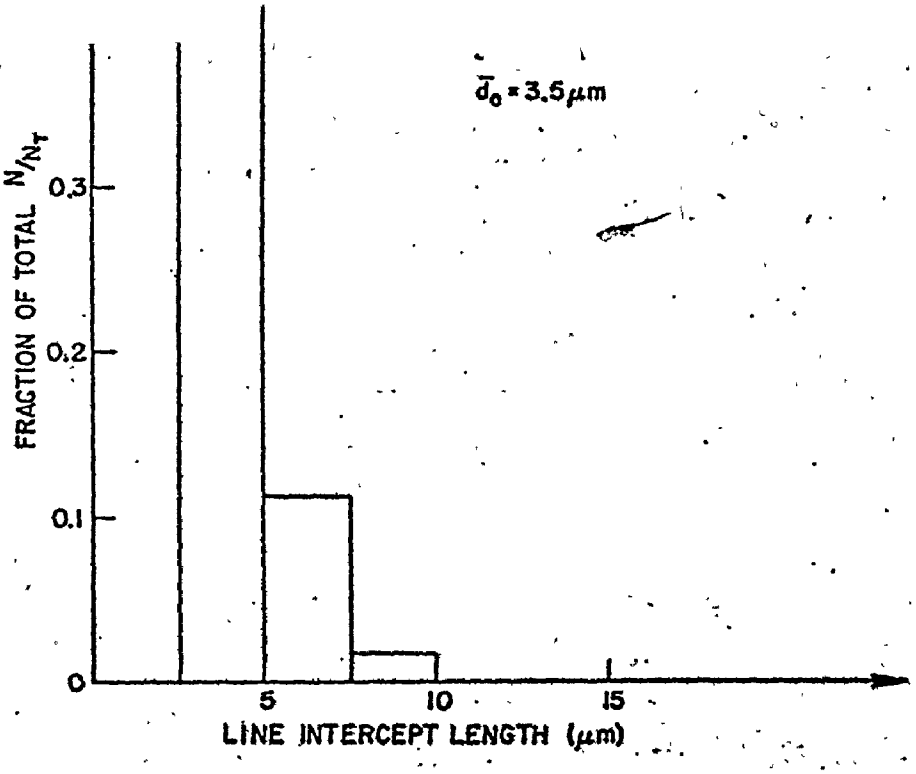

Figure 4.2.a

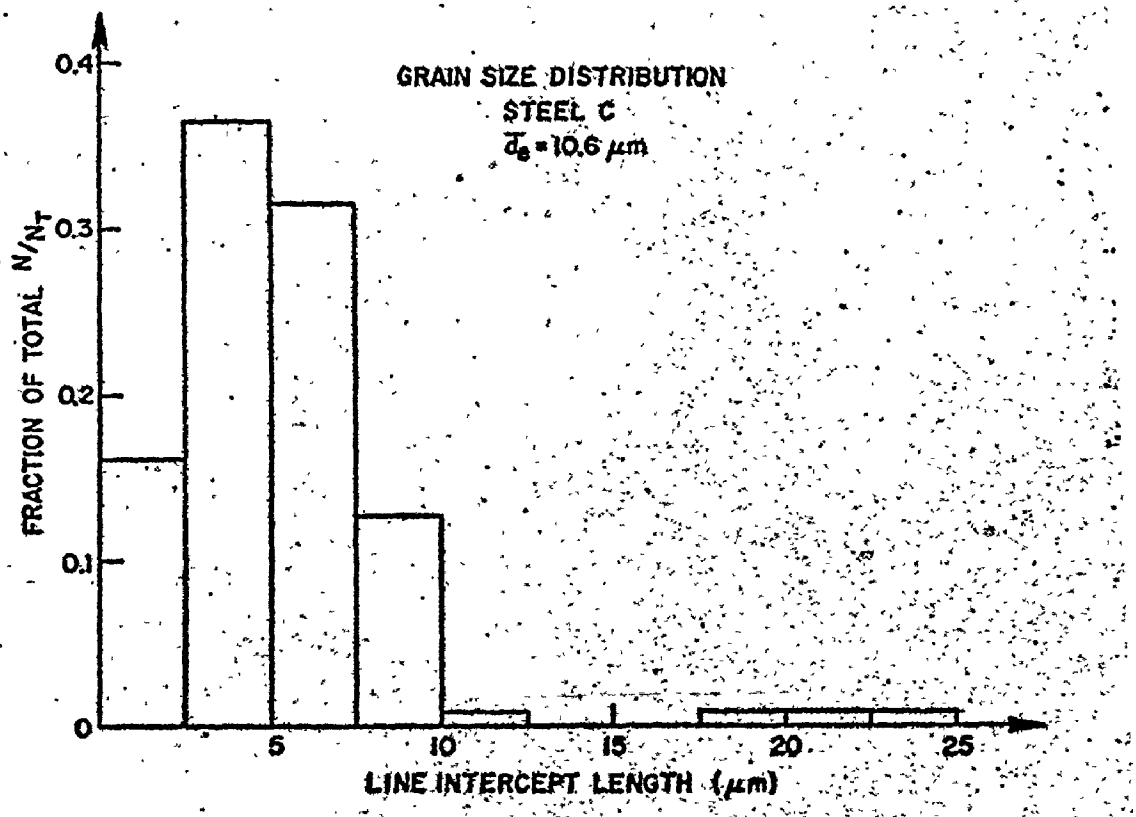

Figure 4.2.b

Figure 4.2: Ferrite grain size distribution for steel A and C determined by the line intercept method.

This effect has been shown by Darken quoted by Shewmon (1963) in diffusion couples of critical constant carbon content but with different levels of Si. In the case of Si "uphill diffusion", i.e., diffusion of carbon against the concentration gradient will take place (figure 4.3). Rather more important, however, is the influence of solute segregation and pre-segregation of carbon on the transformation temperature. In the case of manganese segregations, ferrite nucleation will start in regions with lower alloy content and carbon rejection will occur at the advancing ferrite front.

In the present investigation microprobe point analysis for Mn, Mo and Si was done along lines parallel to the rolling plane normal, i.e., normal to the band structure, but no significant variation in the composition was observed. This is in accord with results reported by Biss and Cryderman (1971) and previous work by Herø et al. (1975).

An alternative mechanism for development of banding in the ferrite structure can be described in terms of the detailed austenite morphology during controlled rolling. As discussed in chapter 2, one of the main reasons for using Nb additions is to retard recrystallization and grain growth during the last stages of rolling. The three steels studied are all heavily deformed below 850°C which is the lower limit for recrystallization (Sekine and Maruyama, 1973) and transformation will thus start from an unrecrystallized austenite with elongated grains. Ferrite nucleated at the austenite grain boundaries will reject carbon in front of the advancing transformation front according to the phase diagram shown schematically in figure 4.4. In the case of elongated austenite grains, bands of higher carbon content will form along the

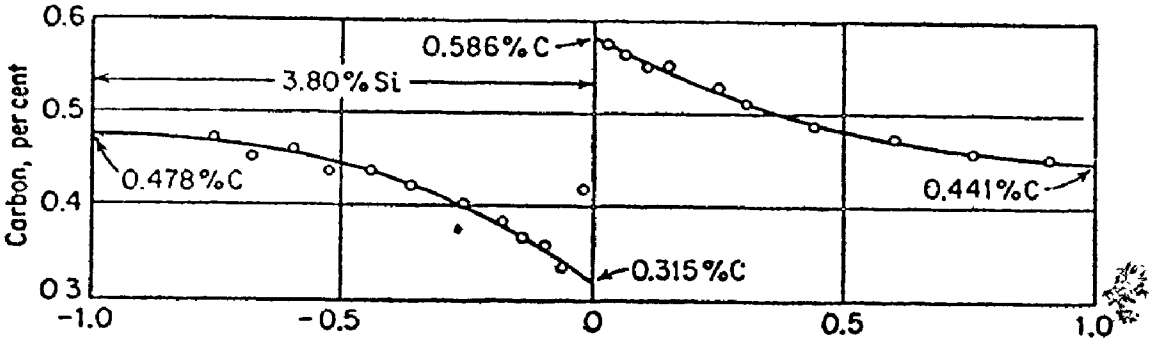

Figure 4.3: Distribution of carbon after annealing in a diffusion couple containg different amounts of Si. (Shewmon 1963)

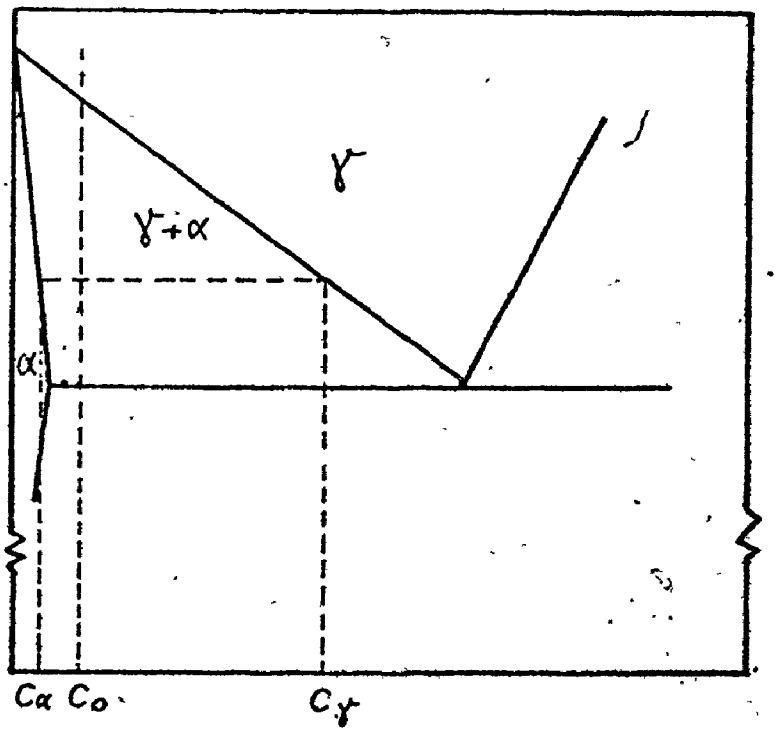

Figure 4.4: Schematic Fe-C phase diagram illustrating the redistribution of carbon between ferrite and austenite during isothermal transformation.

center of the original austenite grains. These regions will have a higher hardenability due to the increased carbon content and non-polygonal ferrite and carbide aggregates will tend to form there. This is illustrated in steel C, figures 4.1 and 4.5, where rows of polygonal grains seem to delineate the original austenite grain boundaries.

When the hardenability is increased by alloy additions as in steel B, the transformation temperature will be sufficiently low for acicular ferrite to nucleate at orginal austenite boundaries and the banded appearance of the ferrite,observed in steel A and C disappears. There is still, however, a tendency for banding of the carbon rich phases.

Of the steels used in the current study, steel A is characterized as polygonal, although a small volume fraction of acicular structures is recognized (table 4.1). Steel B, having a higher alloy content, is almost fully acicular with only a small fraction of polygonal ferrite grains. The duplex microstructure observed in steel C, e.g. about 40% acicular ferrite, corresponds to the intermediate composition (table 3.1).

The degree of acicularity in controlled rolled HSLA steels depends strongly on the composition, e.g. transformation temperature, of the material. McCutcheon et al. (1976) have attempted to describe the structure in terms of a hardenability factor which is simply given by Σ(Mn + Mo + Ni + Cr + Cu) expressed in percent. They observe a linear correlation between volume fraction of acicular ferrite and the hardenability factor. Although this factor fails to recognize any difference in hardenability potency for the various elements, it yields a qualitative prediction of the structure. In the study by Kirkaldy (1973) a weighted sum is used to describe the hardenability. This

Figure 4.5.a,b,c:

Optical micrographs showing the ferrite structure of steels A, B and C in longitudinal sections (nital etch).

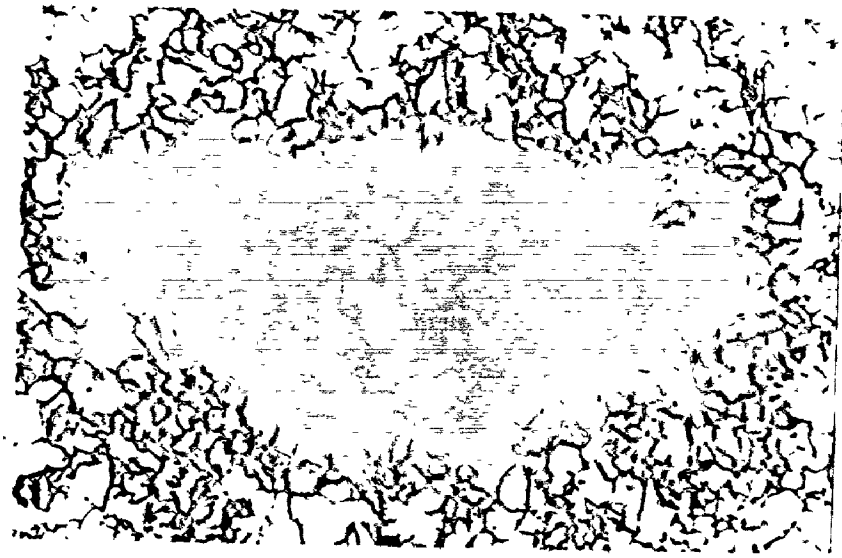

a: Steel A,
630x magnification.

b: Steel B,
630x magnification.

c: Steel C
630x magnification.

treatment also recognizes the strong potency of Mo in producing acicular structures (Coldren and Mihelich, 1977).

In addition to the hardenability expressed as some function of the composition, the scale and morphology of the austenite plays an important role in determining the structure. A prediction of the detailed structure from thermodynamic data is therefore extremely difficult for controlled rolled steels.

In the materials treated in this work the applied cooling rates are assumed to be the same due to similar rolling schedules and more important the final plate thickness is the same. Further, the chemistry of the three steels is almost identical except for a slight differnce in Mo-level (table 3.1). Thus, based on the above discussion the observed differences in acicularity may be attributed largely to the difference in Mo-content.

It is apparent from figures 4.1 and 4.5 that large variations in polygonal grain size exist thus making it difficult to characterize the materials in terms of grain size. In the acicular steels the grain boundary structure is not well defined in the optical microscope, and a characteristic grain size cannot readily be ascribed to these materials. Considering only the polygonal ferrite the following grain sizes have been determined from the line intercept method (Brandon, 1966) on longitudinal sections. Steel A has an average grain size of 3.5 μm, but larger grain diameters are frequently observed (figure 4.5a). Steel C has coarser polygonal structure with average grain size of 10.6 μm. The grain size distribution function for steel C is duplex, however, with one maximum around 4.5 μm and a second smaller maximum around 20 μm accounting

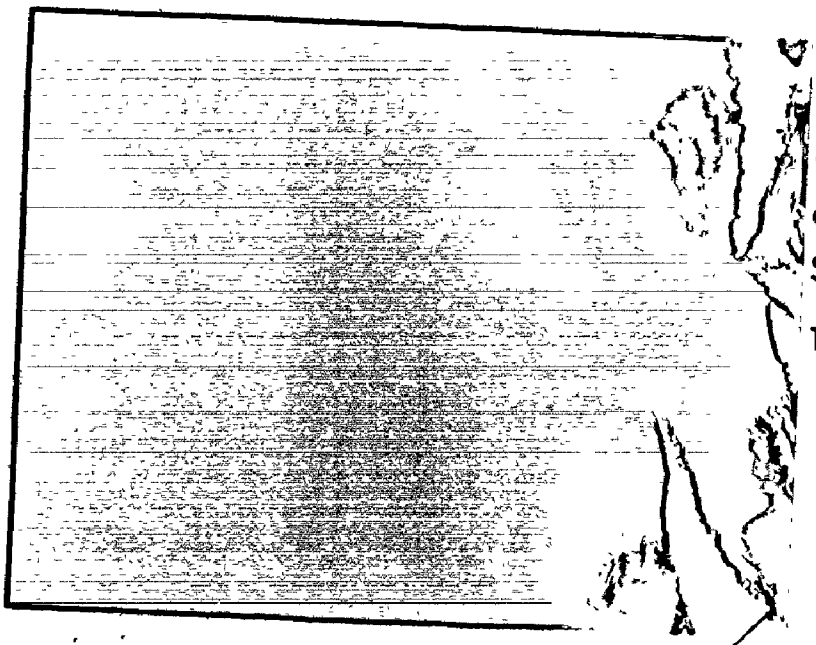

Figure 4.6:

Transmission electron micrograph showing polygonal ferrite structure exhibiting low dislocation density. Steel A.

18500x magnification.

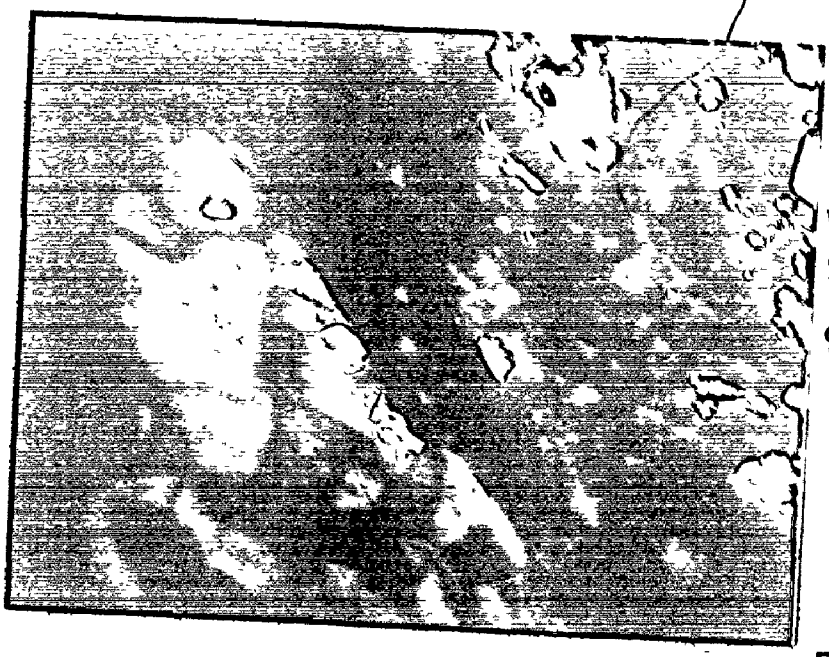

Figure 4.7:

Transmission electron micrograph showing acicular ferrite structure consisting of laths with high dislocation density Steel B.

9200x magnification.

Figure 4.8:

Transmission electron micrograph showing mixed polygonal acicular ferrite structure. Steel B.

3200x magnification.

for the high average grain size. Since steel B is almost fully acicular no attempt has been made to determine the ferrite grain size from optical micrographs.

The grain size of the polygonal ferrite depends not only on the transformation temperature but the scale and morphology of the austenite seem to be of equal importance. Assuming that ferrite nucleates at the austenite grain boundaries the number of nucleation sites per unit volume will depend on the austenite grain boundary area. Thus a heavily deformed austenite with strongly elongated grains will provide more nucleation sites and a finer grain size results. There is also the purely geometric argument that ferrite nucleated in austenite grains with a high aspect ratio only can grow a small distance before impingement occurs. The fact that steel A exhibits the finer grain size may be explained in a qualitative manner in terms of these arguments when the rolling schedules of steels A and C are compared (table 3.1).

The structure of the polygonal ferrite is very different from the acicular ferrite. The former is equiaxed and has a low dislocation density (figure 4.6), whereas the latter consists of a lath structure with very high dislocation density as shown in figure 4.7. The lath structure is not very regular and can at times be difficult to distinguish due to the dislocation substructure (figure 4.8). The heavily dislocated acicular structures are typical for Mn-Mo-Nb-steels that transform during continuous cooling (Coldren and Mihelich, 1977). The effect of Mn and Mo is to lower the transformation temperature such that the fully acicular steels transform at temperatures just above the bainitic start temperature (Boyd, 1977). This is illustrated in a schematic CCT

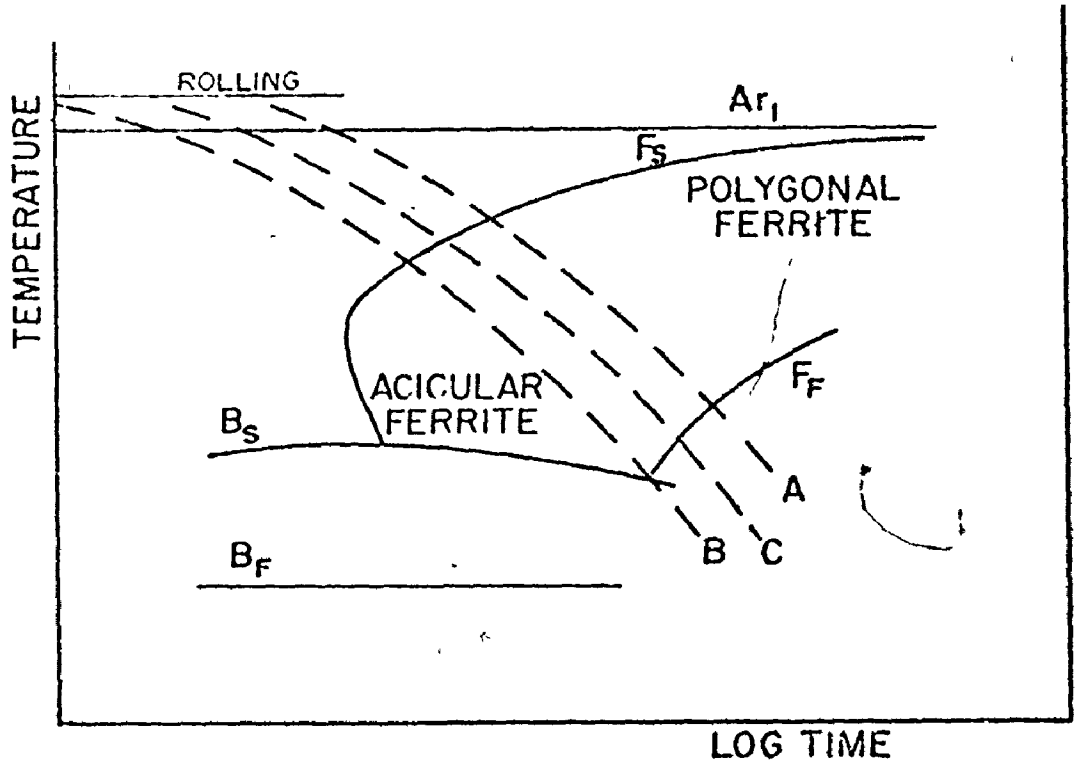

Figure 4.9: Schematic CCT-diagram for HSLA-steels. The difference in hardenability for steels A, B and C is represented by a relative shift in the cooling curves.

TABLE 4.1

FERRITE MORPHOLOGY

STEEL	FRACTION ACICULAR FERRITE(%)	POLYGONAL GRAIN SIZE(μm)	LATH WIDTH(μm)
A	14	3.5	-
B	97	-	0.3
C	42	10.6	-

diagram in figure 4.9 where the relative differences in hardenability are indicated in terms of different cooling curves, although it must be assumed that the actual cooling rate is identical for air cooled plates of the same thickness.

4.2 NON-FERRITIC PHASES

One of the major problems in describing the microstructure of controlled rolled HSLA-steels is to characterize the type and distribution of the various carbon containing phases. In the present materials carbon appears in the form of granular pearlite, grain boundary cementite, alloy carbides, and in the martensite austenite (M/A)-constituent. As these microstructural constituents influence the mechanical properties through vastly different mechanisms it is important to understand under what conditions they form, and how to combine the composition and the processing schedule to produce a material of optimum properties.

In steel A the carbon appears in isolated patches of granular pearlite and in the form of islands of M/A-constituent. In addition, some grain boundary precipitation of cementite is observed. The carbide morphology of steel A is illustrated in figure 4.10a-c using various metallographic techniques. As discussed in the previous section, banding may occur both in the ferrite structure and in the carbide distribution. This effect is seen clearly in figure 4.10a.

At lower transformation temperatures the formation of granular pearlite is suppressed and a larger fraction of the M/A-constituent is observed. Also, the formation of grain boundary cementite is enhanced

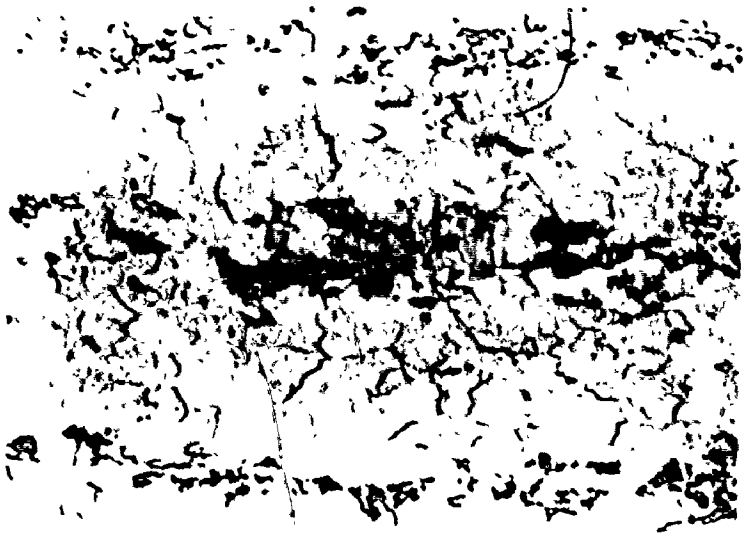

Figure 4.10 a,b,c:

Carbide morphology in steel A.

a: Optical micrograph showing the banded distribution of carbides and M/A-phase. (picral etch).

820x magnification.

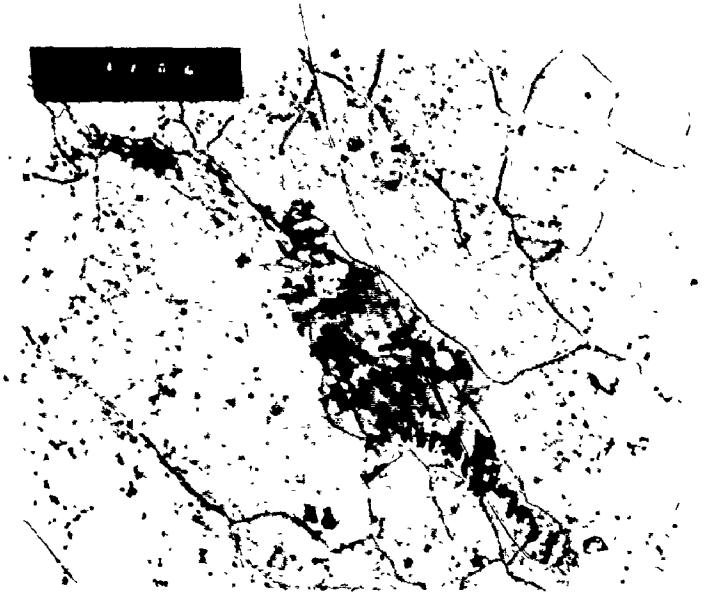

b: Carbon extraction replica showing granular pearlite colony.

5000x magnification.

c: Transmission electron micrograph showing detail of granular pearlite colony.

27800x magnification.

Figure 4.11.a,b,c:

Carbide morphology in steel B.

a: Optical micrograph showing distribution of M/A-constituent in a longitudinal section. (picral etch).

820x magnification.

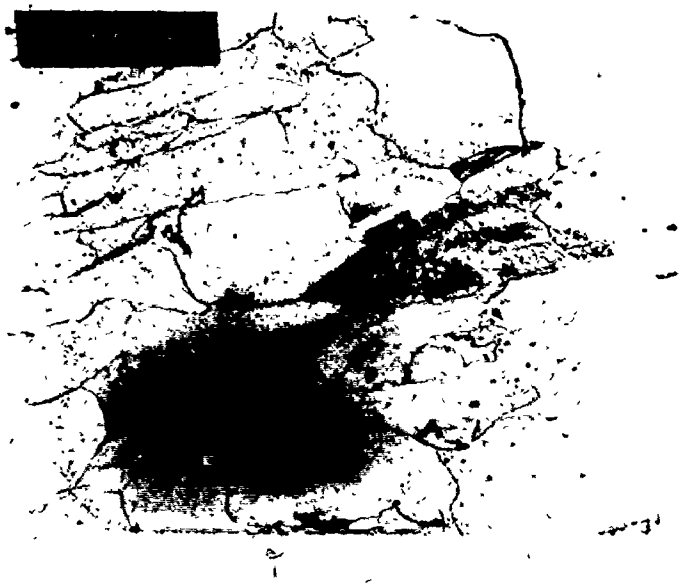

b: Carbon extraction replica showing details of the M/A-phase and grain boundary carbides.

4100x magnification.

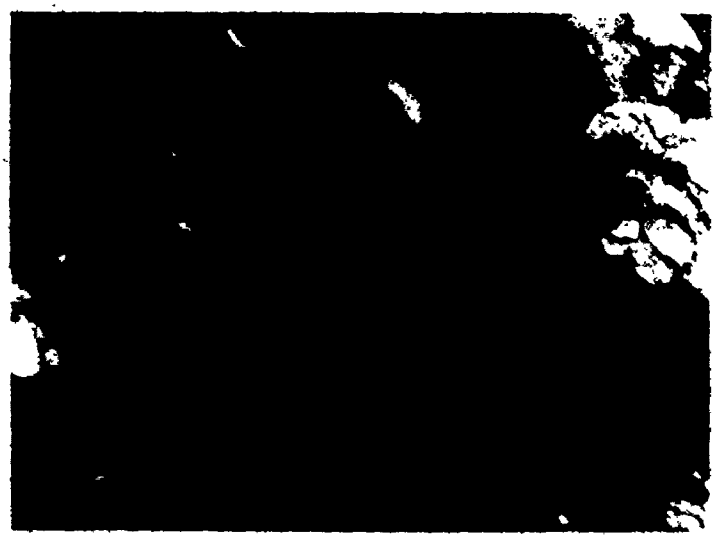

c: Transmission electron micrograph showing M/A-islands in an acicular ferrite matrix. (black regions).

9200x magnification.

Figure 4.12.a,b,c:

Carbide morphology in steel C.

a: Optical micrograph showing banded distribution of carbides and M/A-phase. Regions of polygonal ferrite are virtually carbon free. (picral etch).

820x magnification.

b: Optical micrograph showing detail of carbide morphology. Granular pearlite (P) and an elongated structure resembling upper bainite (B). (picral etch).

1600x magnification.

c: Transmission electron micrograph showing a granular carbide colony and grain boundary precipitates.

16300x magnification.

when the transformation temperature decreases. This is illustrated for steel B in figure 4.11a-c. When picral etchant is used the M/A-phase appears slightly darker than the ferrite matrix and is outlined by black etching phase around the perimeter (figure 4.11a). The grain boundary carbides also appear as black lines in the optical microscope. The M/A-islands in steel B are rather finely dispersed, the average size being about 1-2 μm. However, the volume fraction of M/A is found to be 12%, by the line intercept method, which is a substantial volume fraction of a second phase capable of producing voids during straining (Embury et al., 1976).

In steel C carbon is present both in the form of granular pearlite and M/A-islands. The granular pearlite seem to be associated with polygonal ferrite (figures 4.5c and 4.12a) whereas the M/A-phase occurs predominantly in the bands of acicular ferrite.

The observed carbide morphology can be raticnalized in a similar manner to the ferrite structure in terms of a schematic CCT diagram (figure 4.9). At higher transformation temperatures polygonal ferrite and bands of granular pearlite patches form. Since ferrite is nucleated in strongly elongated austenite grain boundaries, bands of high carbon austenite form in the center of the original austenite grains due to carbon rejection from the growing ferrite. If a CCT diagram is plotted for the remaining austenite this will shift continuously during transformation as the carbon content increases. Thus the transformation temperature for the last transforming regions may be substantially lower than predicted from the initial composition. The occurrence of granular pearlite, as compared to the lamellar pearlite observed in C-Mn steels, is

then due to the combined effect of lowering the transformation temperature and the addition of molybdenum and niobium. The low transformation temperature for the granular pearlite patches has also been indicated by Tither and Lauprecht (1977) who observed a mixture of upper bainite and granular pearlite in a pearlite reduced steel of slightly leaner composition than steel A but cooled at a faster rate.

In steels with higher alloy content and lower initial transformation temperature, viz. steel B, acicular ferrite structures tend to form. Carbon will still be rejected by the growing ferrite but the macroscopic banding of the carbon containing phases seem to be reduced due to retardation of long range diffusion at lower temperatures. Instead, carbon seems to either precipitate on ferrite grain boundaries or it is concentrated in small regions of austenite which eventually transform to produce a mixture of high carbon martensite and retained austenite (M/A) as seen in figure 4.11a.

The average carbon content of the M/A-phase can be estimated from the volume fraction of the phase and the initial carbon content assuming that no carbides form. In steel B this gives a carbon content of 0.5%. This is also indicated by the appearance of the M/A-constituent in the transmission electron microscope where heavily twinned martensite, usually seen in materials with carbon content in excess of 0.5% (Christian, 1971), is observed (figure 4.13). In principle it is possible to measure the carbon content of the M/A-phase by ageing the material to precipitate the carbon and measure the volume fraction of carbides in the M/A-constituent. Figure 4.14 shows the structure of steel B after ageing at 620°C for 1 hour. Some precipitation of grain

Figure 4.13: Transmission electron micrograph showing twinning in the M/A-constiuent.
27800x magnification.

Figure 4.14: Transmission electron micrograph showing the structure of steel B after annealing at 620°C for 1 hour.
18500x magnification.

boundary cementite has occurred and a small fraction of the acicular ferrite has recrystallized. However, no recovery in the dislocation structure of the M/A-phase has occurred, thus making any quantitative metallography very difficult. Ageing at a higher temperature to completely recrystallize the structure may circumvent this problem. A substantial increase in alloy carbides was not observed in the present case although this has been observed in steels of similar composition by Coldren and Mihelich (1977).

There has been some question in the literature to whether the martensite austenite constituent or grain boundary carbides should form at low transformation temperatures. It has been suggested by Pickering that cementite will precipitate when the local carbon concentration exceeds the A_{cm} line in the phase diagram. The height of the carbon spike in front of the advancing austenite ferrite inferface depends on the cooling rate. Fast cooling and thus a low transformation temperature will not allow any long range diffusion and a high and narrow carbon spike results. At slower cooling rates, i.e., higher transformation temperature, a wider carbon distribution with lower maximum concentration results. In the former case the local carbon concentration may exceed the A_{cm} level and precipitation of cementite results (Biss and Cryderman, 1971; Herø et al., 1975). In the latter situation, however, the carbon level may build up over an appreciable volume and formation of the M/A-constituent will result. On this basis Biss and Cryderman suggested that the volume fraction of the M/A-phase may be reduced if the cooling rate is sufficiently increased. This, however, assumes that the morphology of the ferrite does not change, i.e., the same nucleation and growth

TABLE 4.2

CARBIDE MORPHOLOGY

STEEL	VOLUME FRACTION M/A PHASE (%)	CARBIDE THICKNESS (μm)
A	3.5	<.2
B	12.2	<.2
C	5.8	<.2

mechanism of ferrite formation is operative over the cooling rates of interest. Glover et al. (1977) have studied the transformation products in weld metal of HSLA plates as a function of cooling rate and found that for cooling rates substantially higher than observed in plate production the ferrite morphology changes to a bainitic structure. In this case the M/A-constituent is present on the ferrite lath boundaries and the actual volume fraction of M/A is larger than observed at lower cooling rates. They also observed that increasing the initial carbon content tends to favour precipitation of grain boundary cementite which is in accord with the view of Biss and Cryderman (1971) and Herø et al. (1975). An additional effect of increasing the carbon content is to lower the M_S-temperature which also favours carbide formation.

Although precipitation of alloy carbides represent an important strengthening mechanism in the HSLA-steels, a detailed study of the alloy carbides was not undertaken as these only influence the fracture behaviour by altering the yield stress. Further, the alloy carbides are not readily observed and a detailed investigation will usually involve dark field transmission electron microscopy using calculated positions for the precipitate electron diffraction reflections (Davenport, 1977).

4.3 TEXTURE

The occurrence of strong (100) textures in controlled rolled HSLA-steels has been proposed as a mechanism for delamination or splitting failure by cleavage (Miyoshi et al., 1973). This suggested that the textures be determined in steels A and B which were used in the delamination

study. The distribution of intensities of the (200) and (110) reflections were plotted as pole figures as shown in figures 4.15 and 4.16 for steels A and B, respectively. It is seen from the pole figures that a weak (100) [110] texture is present in steel A. In addition, the texture component (112) [110] appears. It is difficult to differentiate between the strength of the various texture components as the pole distributions tend to overlap both in the (200) and (110) pole figure, however, the (112) [110] orientation seems to be the stronger texture component. In steel B the (100) [110] component is very weak and can hardly be recognized at all (figure 4.16a). The (112) [110] component, however, is stronger than in steel A.

Since the rolling finish temperature was well above the transformation temperature for both steel A and B the ferrite texture must have been inherited from the austenite. Two posibilities then arise, the ferrite can either transform from a heavily deformed non-recrystallized austenite or the austenite may have recrystallized in part or completely. The possible rolling and recrystallization textures of austenite have been reviewed by Jones and Walker (1974) and are shown in table 4.3. By introducing the Kurdjumov-Sachs relationship between austenite and ferrite, Jones and Walker calculated the ferrite textures from the possible austenite textures listed in table 4.3. They found that the (100) [110] ferrite texture, which is observed in steel A, could be derived from the "pure metal" recrystallization texture (100) [001] in the austenite. Further, the "pure metal" orientations (123) $[\bar{4}12]$ and (146) $[\bar{2}\bar{1}1]$ for rolled austenite will transform to give the (112) [110] ferrite texture observed in both steel A and B. The "alloy type" rolling

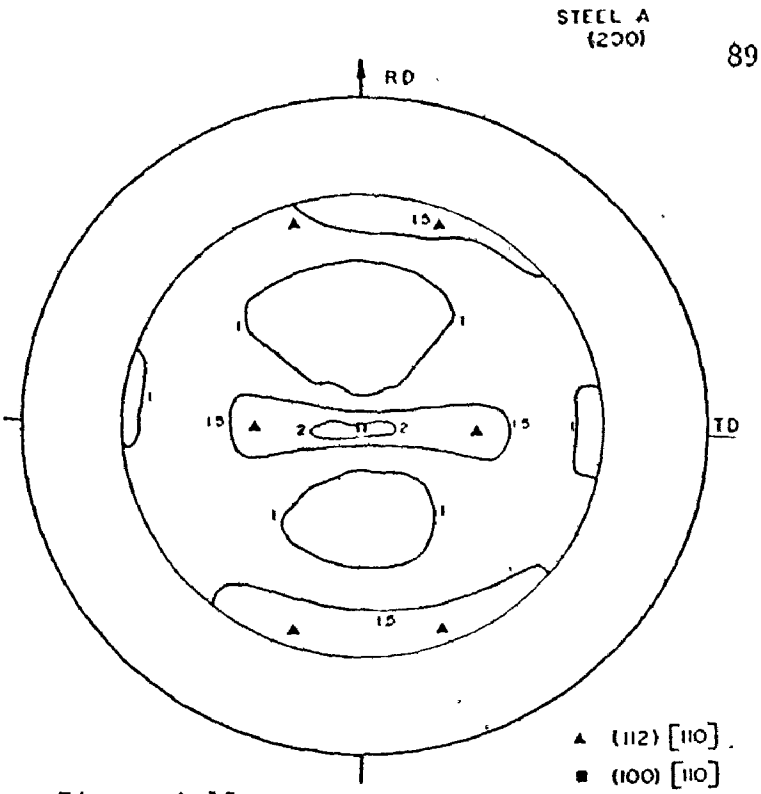

Figure 4.15.a

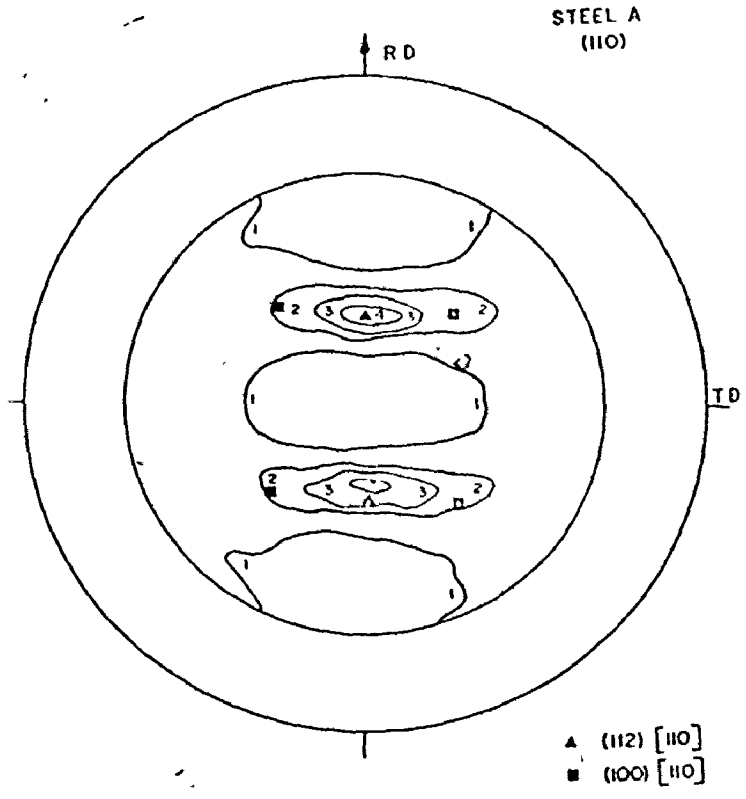

Figure 4.15.b

Figure 4.15.a,b: Polefigures showing the texture components of steel A at midthickness.
a: 200 polefigure,
b: 110 polefigure.

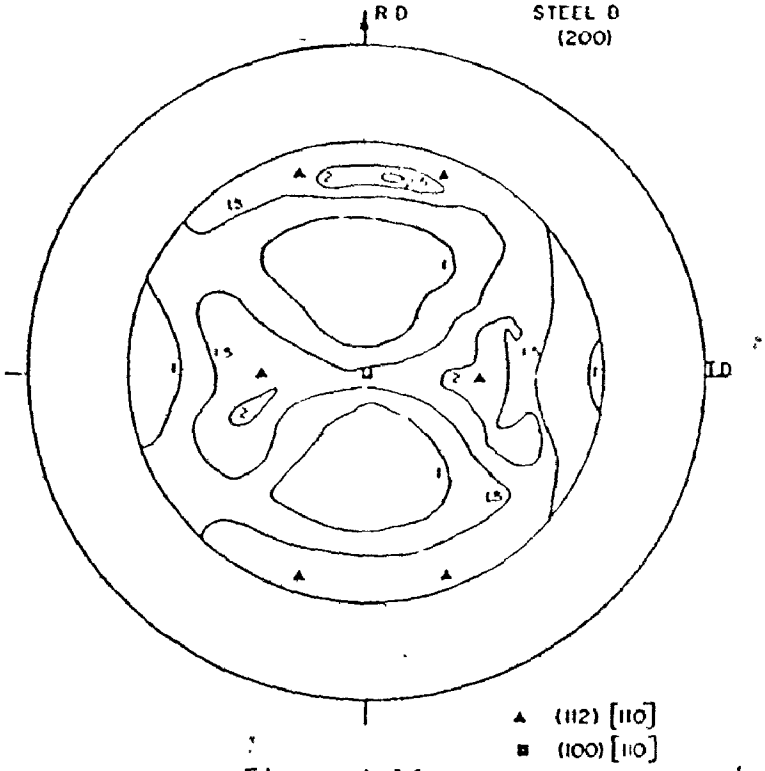

Figure 4.16.a

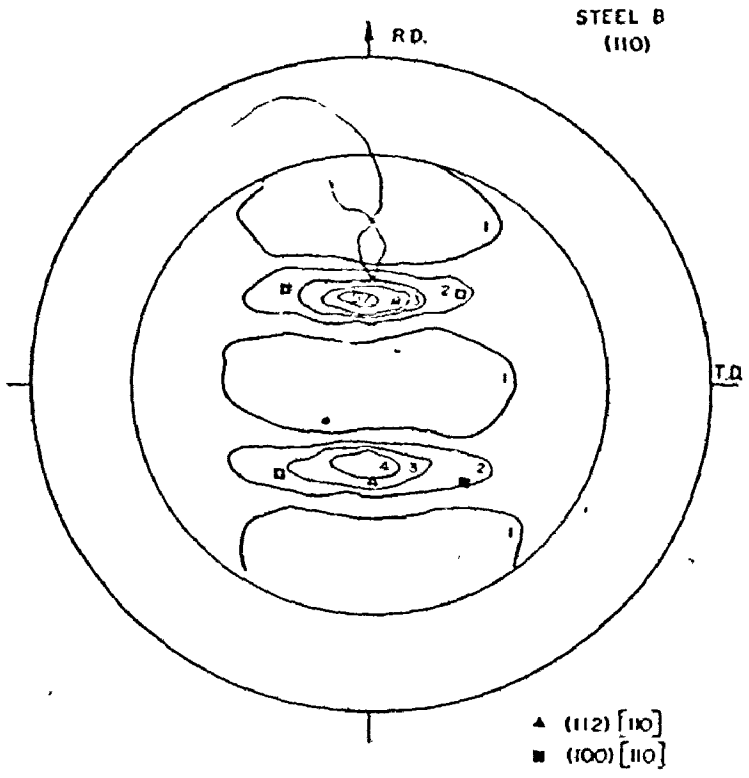

Figure 4.16.b

Figure 4.16.a,b: Polefigures showing the texture components of steel B at midthickness.
a: 200 polefigure,

and recrystallization textures listed in table 4.3 do not compare favourably with the observed ferrite orientations. Similar conclusions were drawn by Lotter et al. (1976) who studied texture development in hot rolled micro-alloyed strip of various compositions.

Based on the observed pole figures, figures 4.15 and 4.16 and computations by Jones and Walker (1974) and Lotter et al. (1976) it can be concluded that recrystallization of the austenite had started before transformation in steel A, whereas steel B transformed from non-recrystallized austenite. This is probably due to the heavier deformation schedule for steel A (table 3.1), which therefore has more stored energy available for recrystallization.

The use of pole figures to compare computed and measured textures may not be the best way of modelling texture development in ferrite. The two main problems are the accuracy with which the pole figure itself can be plotted, the second arises because of the overlap of texture components in the pole figure. With regards to the first problem the error in plotting the pole figure is estimated to be within $\pm 3^{\circ}$ for any point in the pole figure for the technique used. This will not distort the general appearance of the pole figure but may cause problems when a detailed matching of pole figures is attempted. The difficulty with overlapping intensity distributions can be circumvented by using a computerized representation of the texture components (Kallend et al., 1977). Davies et al. do, however, observe the same texture components for the controlled rolled Nb bearing steels using the crytallite orientation distribution function, i.e., a (hkl) [110] fibre texture centred around (112) [110].

TABLE 4.3

POSSIBLE AUSTENITE TEXTURES[x]

{123} <412> {146} <211>	Main orientation of a "pure metal" or "copper" type rolling texture.
{110} <112>	"Alloy" type rolling texture.
{100} <101>	The main orientation produced by recrystallizing a "pure metal" type rolling texture.
{112} <212>	Secondary orientation produced by recrystallizing a "pure metal" type rolling texture.
{113} <332> {112} <534>	Main orientations produced by recrystallizing an "alloy" type rolling texture.

x From Jones and Walker (1974)

4.4 NON-METALLIC INCLUSIONS

The inclusion morphology of HSLA-steels is usually dominated by the sulphides and oxy-sulphides in rare earth (RE) treated steels. The stability of the various RE-compounds at 1600°C is shown in figure 4.17. Steels A1 and C have relatively high sulphur contents (table 3.1), whereas steels A2 and B show substantially lower sulphur levels. Further all steels but C have been rare earth treated for sulphide shape control. Typical inclusion shapes are shown in figure 4.18a,b. Steel C exhibits long stringers of MnS produced during hot rolling, whereas the oxy-sulphides shown in steel A1 are rigid at hot rolling temperatures and thus keep their equiaxed shape.

One of the major problems in using RE-sulphide shape control is the affinity of these elements to oxygen, and thus their propensity to reoxidation if oxygen is available from sources such as slag, refractory lining or air entrainment during pouring (Kay and McLean, 1975). The reoxidation products tend to agglomerate in the ingot and form large inclusion clusters (Luyckx, 1975). Although the individual inclusions are rigid during hot rolling, the clusters are flattened out to form large sheets of very high inclusion density. These inclusion sheets were observed occasionally in steel B and rather frequently in steel A1. An example is shown in figure 4.19, the high magnification inset show that the inclusions consists of a mixture of various components as often observed in oxy-sulphides (Wilson and Wells, 1973). When these inclusion sheets occur the through thickness properties of the material are drastically reduced.

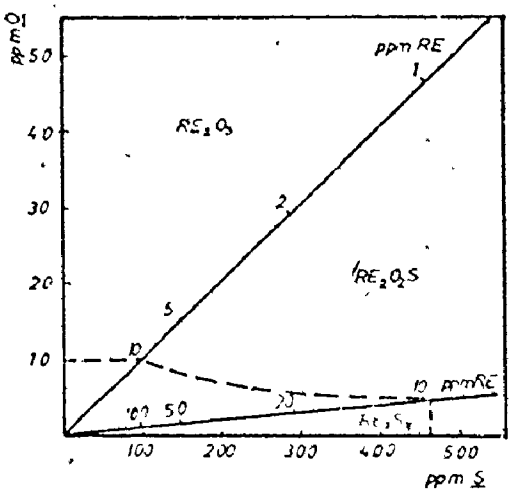

Figure 4.17:

Rare earth oxygen, sulphur relationships with respect to oxide, oxysulphide and sulphide stability fields at 1600°C. The broken line corresponds to an iso-rare earth concentration of 10 ppm. (data from McLean and Lu, 1974).

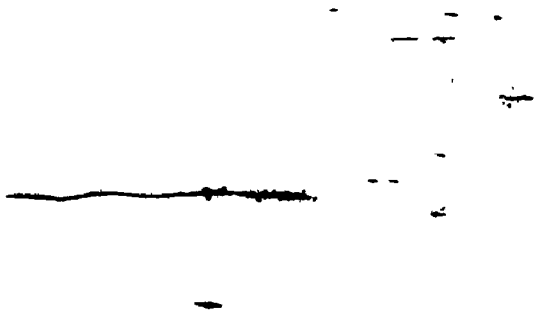

Figure 4.18.a,b:

Optical micrographs showing typical inclusion morphologies in HSLA-steels.

a: MnS-stringers

formed during rolling of steel C.
(Oxalic acid etch).

85x magnification.

b: Rare earth

oxysulphides in steel B.

500x magnification.

Figure 4.19:

Optical micrograph of a polished section of steel B. Showing planar arrays of inclusions.

85x magnification.

Figure 4.20.a,b:

SEM-fractographs showing features of lamellar tearing.

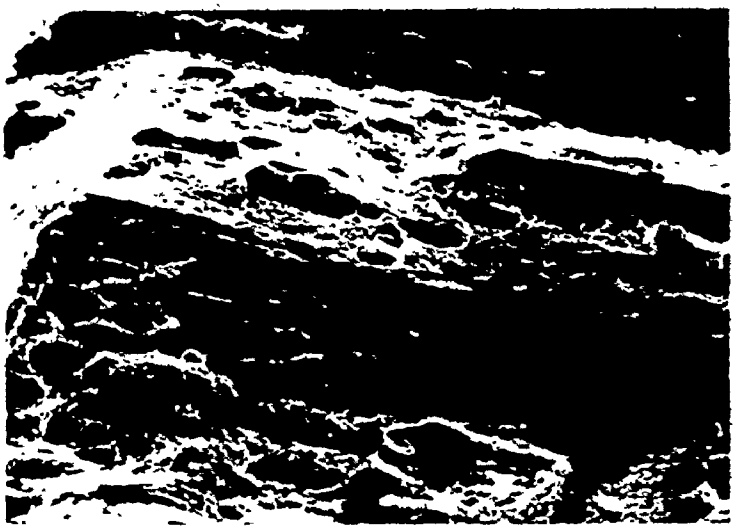

a: Tearing along MnS-stringers.

630 x magnification.

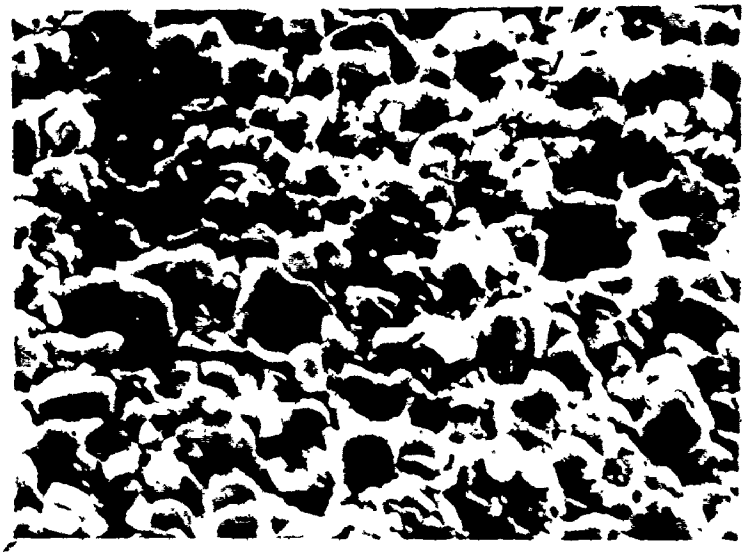

b: Planar array of rare earth oxysulphides on fracture surface.

2500x magnification.

Further reversion of sulphur to the melt may occur during reoxidation products and manganese sulphides will result due to loss of RE-additions. This was observed occasionally on fracture surfaces of through thickness tensile specimens of steel A1 and B as shown in figure 4.20.

It was not possible to characterize in detail the chemistry of all inclusions observed. However, when SEM fractography was performed the X-ray energy dispersive analysis attachment was used to identify inclusions of typical appearance. This technique does not, however, differentiate between RE-sulphides and RE-oxy-sulphides, since oxygen is not detected. RE-oxides on the other hand could be separated due to the lack of sulphur. Study of fracture surfaces containing inclusion sheets revealed a high density of both RE-oxides and RE-oxy-sulphides. In addition, alumina inclusions were observed occasionally. These also have a tendency to agglomerate in the ingot and form inclusion sheets in rolled material (Luyckx, 1975).

In order to correlate the ductile fracture behaviour of the materials to the inclusion morphology, a quantitative analysis of inclusion number, shape and area fraction was undertaken using the Quantimet 720. The results are shown in table 4.4. The volume fractions of inclusions are calculated from the average area fractions from three orthogonal sections in the plate. It is noted that the volume fraction of inclusions in steel A1 is about twice that of steel C, although the sulphur levels are the same. This is attributed to the occurrence of oxides and oxysulphides in steel A1, whereas the inclusions in steel C are predominantly MnS.

TABLE 4.4.a

RESULTS FROM QUANTIMET ANALYSIS

Steel	Section[x]	Total number/mm^2	Individual length(μm)	Total area fraction(%)	Inclusion aspect ratio
A1	L	260	3.923	0.385	1.20
	T	234	3.314	0.255	1.47
	ST	451	2.539	0.296	1.03
A2	L	325	2.288	0.136	1.51
	T	323	1.714	0.094	1.28
	ST	321	1.684	0.098	1.19
B	L	149	2.093	0.069	1.72
	T	162	1.824	0.065	1.37
	ST	202	2.428	0.179	1.64
C	L	218	3.736	0.221	2.09
	T	229	3.510	0.166	2.06
	ST	145	1.941	0.122	0.99

x L: longitudinal, T: transverse, ST: short transverse

TABLE 4.4.b

Steel	A1	A2	B	C
Volume fraction(%)	0.30	0.11	0.11	0.17

The COD specimens used to assess the resistance to fibrous fracture were cut in the T-L orientation (figure 3.2), thus the inclusion parameter of interest is the inclusion spacing observed in the short transverse section. Assuming elliptical inclusions with major and minor semi axes a and b respectively the area fraction of inclusions is given by.

$$A_f = \frac{\pi ab}{\lambda_T \lambda_L} \qquad 4.4.1$$

where λ_T and λ_L are the centre to centre inclusion spacings in the transverse and longitudinal direction, respectively. Further, if it is assumed that the ratio of the spacings equals the aspect ratio of the particles, i.e., $F = \frac{a}{b} = \frac{\lambda_L}{\lambda_T}$ equation 4.4.1 can be solved with respect to the spacings yielding.

$$\lambda_T = \frac{a}{F} \sqrt{\frac{\pi}{A_f}} \qquad 4.4.2\ a$$

$$\lambda_L = a \sqrt{\frac{\pi}{A_f}} \qquad 4.4.2\ b$$

Values for the inclusion spacings have been calculated according to equation 4.4.2 using data from the Quantimet analysis of the inclusion distribution in the short transverse sections, and are reported in table 4.5.

The majority of models for ductile failure by void nucleation and growth consider a uniform distribution of spherical particles in which case the values of λ_T and λ_L are identical. Good correlation

between COD and inclusion spacing have thus been found both using the spacing in the x-direction (Rice and Johnson, 1969; Brown and Embury, 1973) and in the y-direction (Smith and Knott, 1972) (orientations defined in figure 3.7). It is believed, however, that the former approach is physically better founded, and will therefore be used in this work.

A further problem arises when attempting to apply the theoretical models to controlled rolled HSLA-steels. Due to the propensity to clustering of the oxysulphides in the melt elongated clusters of inclusions with a very small local spacing often occur (figure 4.18.b). In this case the condition for instability is given by the coalescense of super voids formed at the inclusion clusters. Hence the fracture condition should be described in terms of the cluster spacing rather than the average inclusion spacing which is calculated from equation 4.4.2. This parameter is difficult to determine in a quantitative manner as subjective judgement always will be involved in defining the cluster size. However, microscopic investigation of several metallographic sections indicate an average cluster length of about four times the average particle length. The cluster spacing will thus be four times the spacing calculated in equation 4.4.2 b assuming the other parameters constant. (table 4.5).

TABLE 4.5

INCLUSION SPACINGS

Steel (short transverse section)	Longitudinal inclusion spacing(μm)	Transverse inclusion spacing(μm)	Longitudinal spacing between inclusion aggregates(μm)
A1	41.3	40.1	165
A2	49.8	41.9	199
B	50.0	31.0	200
C	43.3	49.6	170

5. FRACTURE BEHAVIOUR - RESULTS AND DISCUSSION

The occurence of fracture in HSLA-steels can usually be devided into three main groups as illustrated in figure 2.2. At low temperatures the fracture behaviour is dominated by cleavage failure, whereas ductile failure by nucleation and growth of voids is the mechanism observed at higher temperatures. In the transition between these two fracture modes a third mechanism referred to as delamination or splitting is frequently observed. Figure 2.2 also list some of the fracture criteria applicable to the various fracture modes and the various microstructural features which influence the fracture processes. However, the majority of the models describing both brittle and ductile failure have been developed for normalized or hot rolled ferrite pearlite steels with well characterized microstructures and are not necessarily applicable to the complex microstructures exhibited by the controlled rolled HSLA-steels. In this investigation attention has thus been focused on the predominant fracture modes as illustrated in figure 2.2 in order to develop criteria for fracture and to delineate a detailed correlation between microstructure and fracture properties.

For clarity the results for the various fracture modes are presented in separate subchapters together with

a discussion of the parameters used to relate experimental data to current theoretical models.

5.1 CLEAVAGE FAILURE

The majority of quantitative models available in the literature describe cleavage failure in terms of the attainment of a critical stress (Cottrell, 1958; Smith, 1966; Almond et.al., 1969). The value of the critical stress can be related to microstructural features such as grain size and carbide thickness (eqns. 2.2.13 and 2.2.18) or in materials with a less well defined grain structure to an effective grain size defined by the cleavage facet size (Brozzo et.al., 1977). Further the models describing low temperature fracture toughness all evaluate the fracture resistance in terms of the cleavage stress σ_c and some critical length (eqns. 2.2.20 and 2.2.21). A detailed understanding of the microstructural aspects of the cleavage stress is thus of major importance in developing structural steels with good low temperature fracture properties.

In the fine grained materials used in this work the cleavage stress could not be attained in pure tension. A single edge notched (SEN) bend test where the stress level is raised by a factor of about two to three due to the plastic constraint in front of the notch was therefore used. The maximum

stress value can be evaluated either by a finite element method (Griffiths and Owen, 1971) or by a slip line field analysis (Green and Hundy, 1956). The latter method as described in chapter three was used in this study.

Further the fracture toughness at -196°C was determined using SEN-specimens in four point bending. The specimen dimensions were not sufficient for valid K_{1C}-tests according to ASTM specification E 399, but approximate (K_a) values were determined. The influence of specimen geometry on the fracture toughness was studied by varying the notch root radius from zero (fatigue crack) to about 0.3 mm. These results are compared to theoretical predictions from eqn. 2.2.21. and calculated values for the process zone size or the critical distance.

5.1.1 Results

The results of the slow bend tests performed to determine the critical cleavage stress are shown in figure 5.1 a-c for steels A, B and C respectively. The fracture and general yield loads for tests performed at various temperatures are plotted, and the critical stress calculated from the fracture load for the condition that fracture and general yield coincide. Values of the critical cleavage stress are listed in table 5.1 together with the critical temperature and interpolated values of the yield stress at the same condition. It is noted that both the polygonal

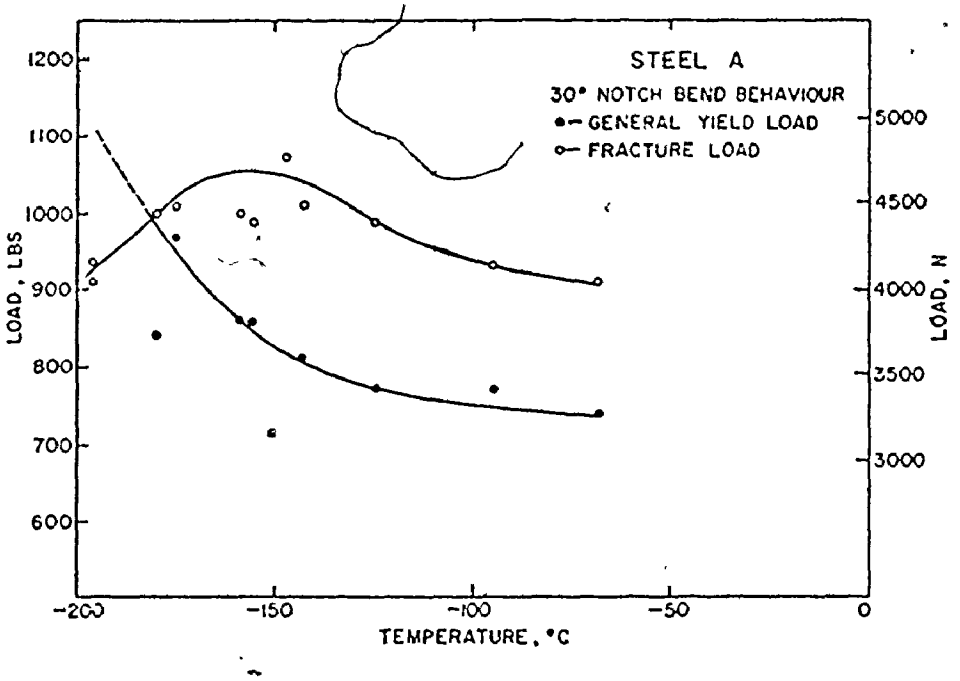

Figure 5.1.a

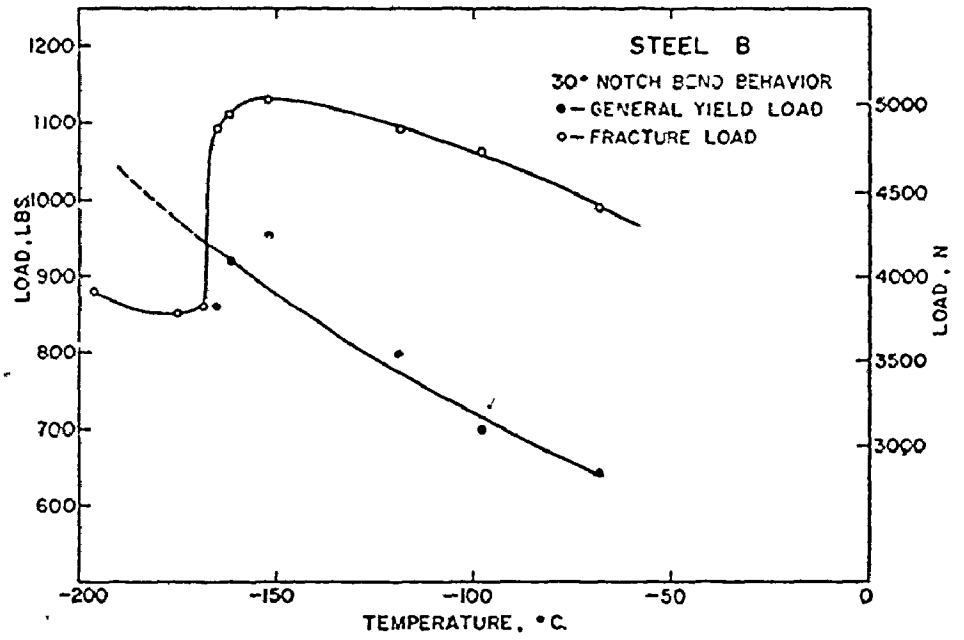

Figure 5.1.b

Fracture and general yield load for notched slow bend specimens of steel A and B.

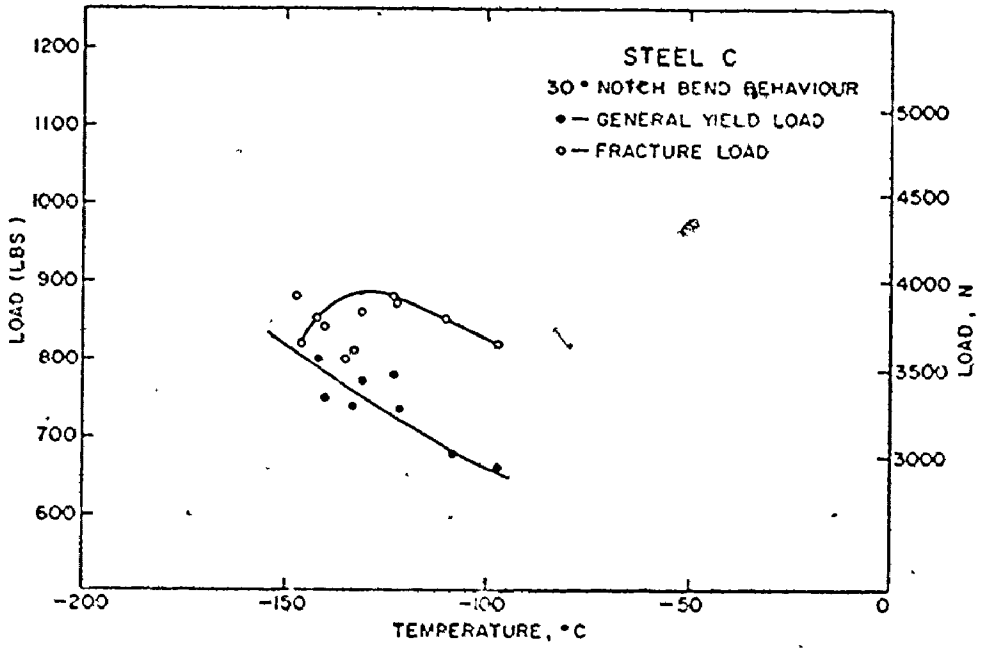

Figure 5.1.c: Fracture and general yield load for notched slow bend specimens of steel C.

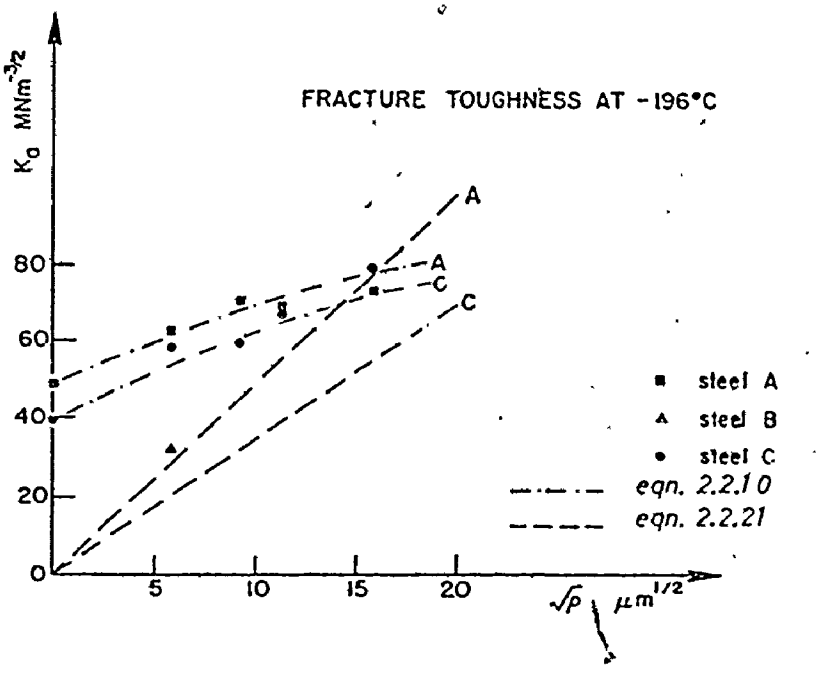

Figure 5.2: Apparant fracture toughness measured in four point bending for various root radii.

steel A and steel B which is almost fully acicular have cleavage stresses of the same magnitude whereas steel C shows a substantially lower cleavage stress.

A correct evaluation of the low temperature fracture toughness according to the ASTM standards (E399) was not possible due to a lack of material. Thus both the specimen dimensions and the number of specimens available are insufficient to give statisticly dependable results. However, the results obtained are of great value in determining the microstructural aspects of cleavage fracture resistance. In figure 5.2 values of the apparant fracture toughness K_a are plotted versus the square root of the notch root radius according to equation 2.2.21. The experimental results are compared to theoretical predictions of the fracture toughness based on the critical cleavage stress. These are shown as dotted lines marked A and C in the figure and represent solutions of equation 2.2.21 using the cleavage stresses from table 5.1.

In order to relate the failure event to the scale of the structure critical parameters such as grain size and carbide distribution were determined in chapter four (figures 4.2 and 4.10-4.12). The critical values of the cleavage stress are plotted versus the inverse square root of the grain size in figure 5.3 and compared to theoretical predictions from the Cottrell model (eqn. 2.2.13) and the

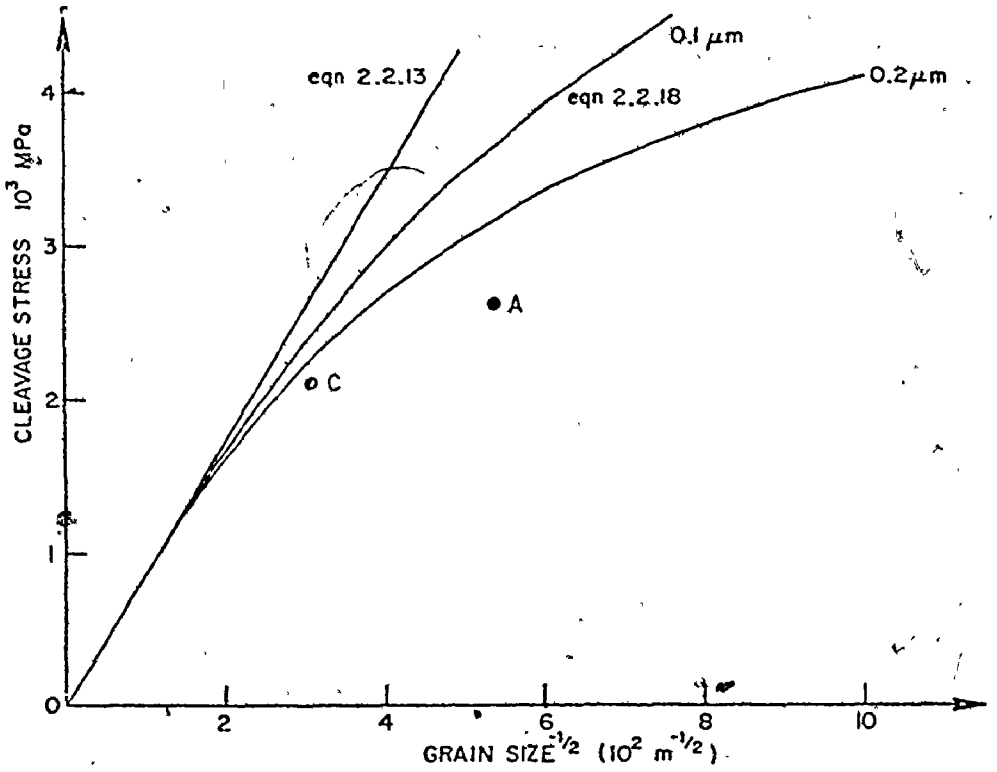

Figure 5.3: Critical cleavage stress as a function of ferrite grain size for steel A and C. Theoretical predictions by Cottrell and Almond et.al. included for comparison.

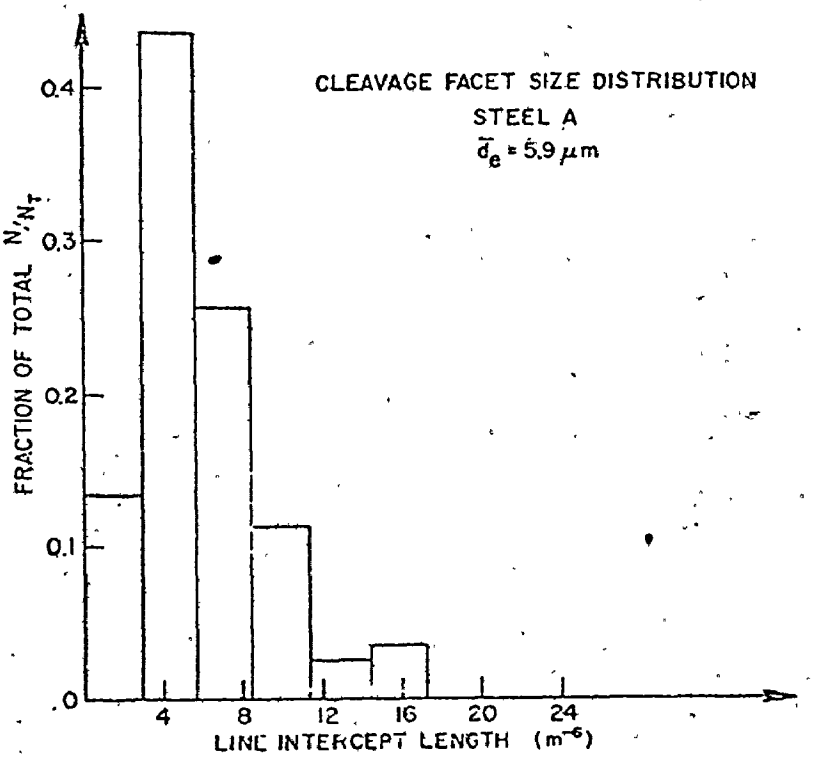

Figure 5.4.a: Cleavage facet size distribution for steel A.

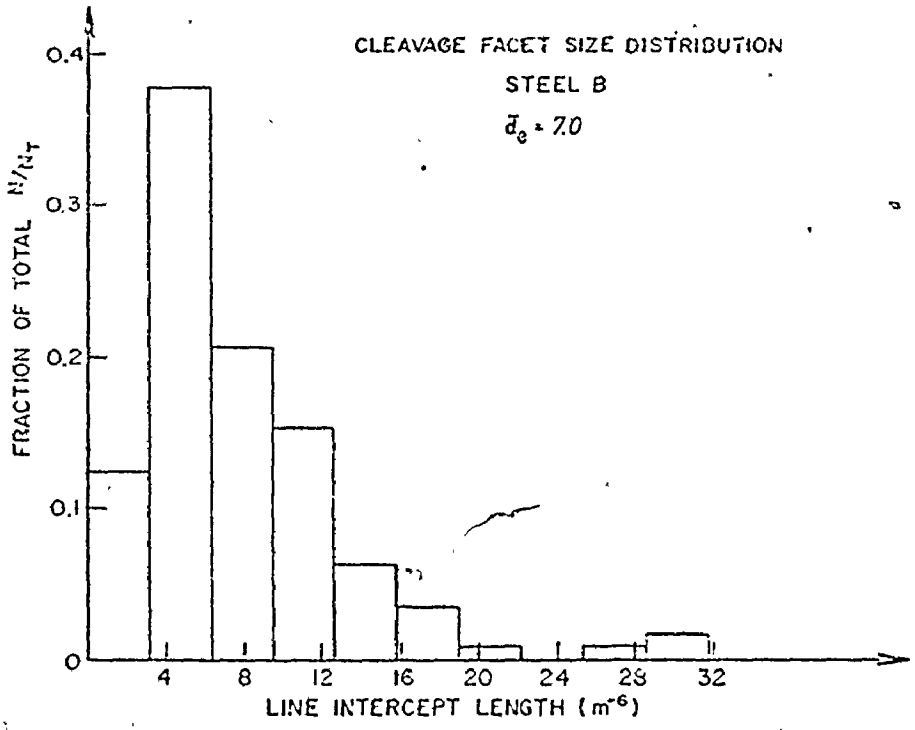

Figure 5.4.b: Cleavage facet size distribution for steel B.

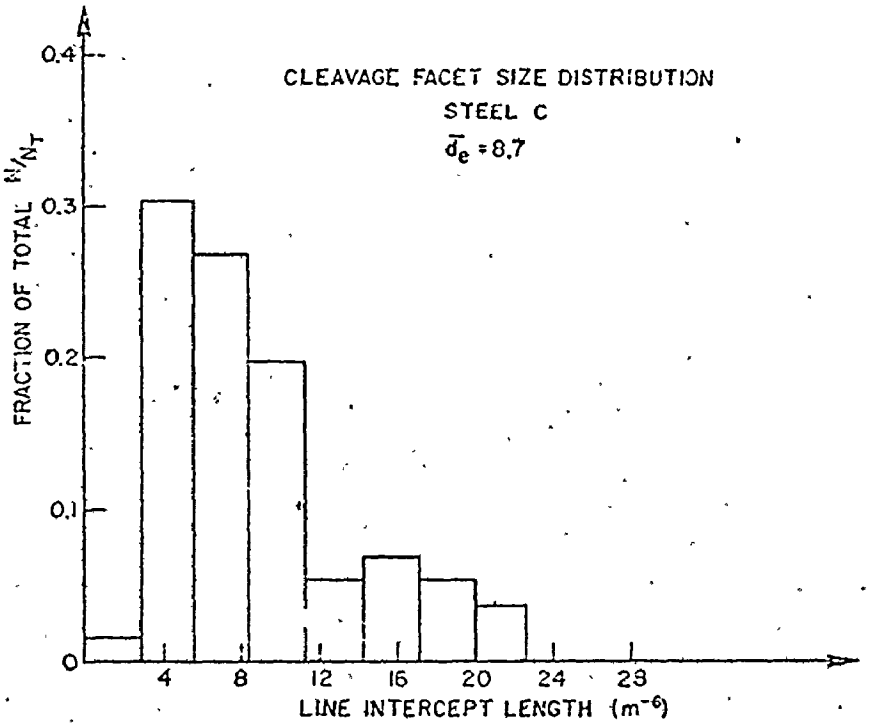

Figure 5.4.c: Cleavage facet size distribution for steel C.

model by Almond et.al. (eqn. 2.2.18) using carbide thicknesses of 0.1 and 0.2μm in accord with the observed values. Due to the difficulty in assessing a grain size value to the acicular structure of steel B (figure 4.1 b) only steels A and C are represented on figure 5.3. A relatively poor fit between theoretical predictions and experimental results is observed.

Brozzo et. al. (1977) have suggested that the cleavage stress is determined by the effective grain size as determined from the cleavage facet size on the fracture surface. Figure 5.4 a-c shows the size distribution of cleavage facets in steels A, B and C respectively. When plotting the critical values of the cleavage stress versus the effective grain size figure 5.5 is obtained. The line deduced by Brozzo et.al. for brittle failure of bainitic steels is included in the diagram for comparison. The stress levels determined by Brozzo et. al. are however, calculated using a finite element method which yields results that are lower than the slip line field data by a factor of 1.12. In order to facilitate a direct comparison the present data are reduced by the same amount and represented by the open symbols in figure 5.5. Calculation of the effective surface energy then yields a value of 109 Jm^{-2} which is very close to the value of 120 Jm^{-2} deduced by Brozzo et al. The lower limit of the present results are indicated by the dotted line (γ = 103 Jm^{-2}), thus all the current data are within

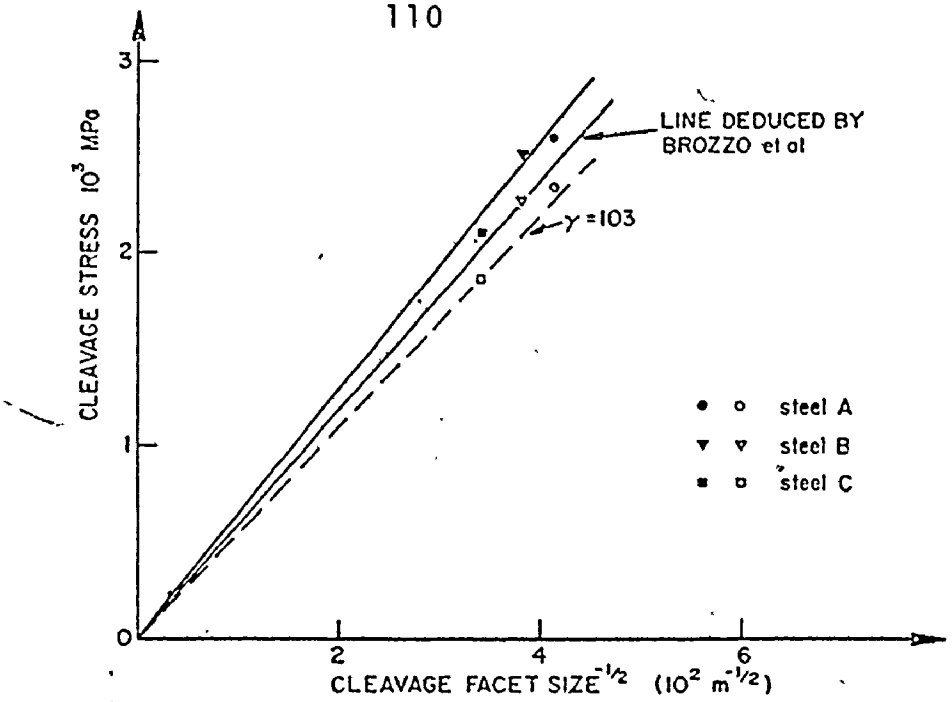

Figure 5.5: Critical cleavage stress plotted against effective grain size as determined from the cleavage facet size distribution.

Figure 5.6: Optical micrograph from sectioned Charpy specimen (steel A) showing non propagating microcracks in polygonal ferrite. Cracks are nucleated in grain boundary carbides (arrow). (Nital etch).

14% of the effective surface energy determined by Brozzo et al.

The fracture resistance measurements at -196°C are reported in figure 5.2. Apparant fracture toughness values of 49. $MNm^{-3/2}$ and 40.5 $MNm^{-3/2}$ were obtained for steels A and C respectively. Due to lack of material precracked specimens of steel B were not available, but one specimen with slotwidth 60 μm gave a toughness value of 32 $MNm^{-3/2}$. Further the influence of the notch root radius is demonstrated in figure 5.2 for steels A and C. The lower shelf in fracture toughness described by Malkin and Tetelman (1971) is not observed in this investigation for the range of root radii studied. Lines representing the theoretical correlation between apparant fracture toughness (K_a) and root radius (ρ) according to models by Malkin and Tetelman (1971) (eqn. 2.2.21) and Heald et al. (1972 b) (eqn. 5.1.1) are included in figure 5.2 for comparison.

In order to relate the magnitude of the critical cleavage stress and the fracture toughness to the scale of the microstructure, studies were made both of the fracture surfaces and the structure beneath the notch in the double notch bend samples. It appeared from these observations that the average cleavage facet size and the length of the non-propagating microcracks were about two times larger than the scale of the ferrite

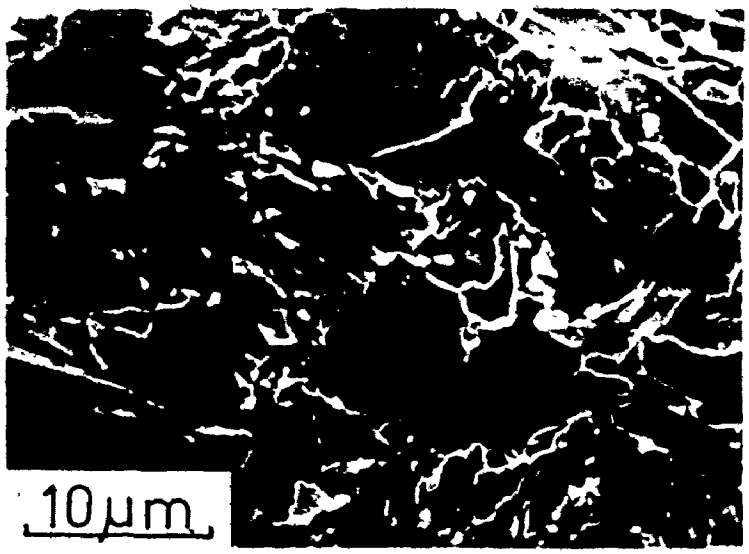

Figure 5.7: SEM-micrograph from sectioned slow bend specimen (steel B) showing microcrack in acicular ferrite. (Nital etch) (2400x magnification).

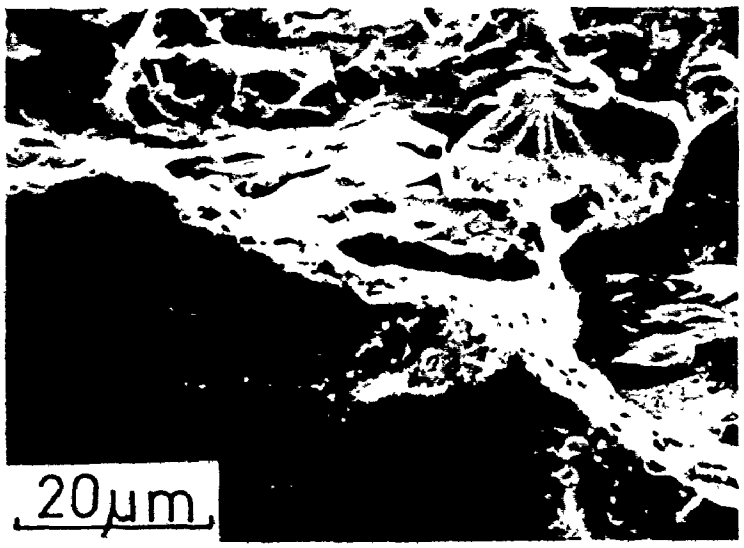

Figure 5.8; SEM-micrograph showing correlation between fracture path and microstructural features.
Fracture surface and polished and etched section revealed simultaniously by preferential electro polishing and etching in nital.

grain size. These features are illustrated in the micrographs figures 5.6 to 5.8. The same result appears by comparing the grain size distributions and the cleavage facet size distribution in figures 4.2 and 5.4 respectively. For steel C the average value of the grain size and the cleavage facet size is about the same.

5.1.2 Discussion

The theoretical models for cleavage stress described in chapter two, except the Smith model, indicate that the cleavage stress depends on the inverse square root of the grain size. The physical reasoning behind the various equations presented in chapter two is however different. In the mechanisms described by Cottrell (1958) and Almond et al (1969) it is assumed that the critical event is growing a microcrack through a ferrite grain under the combined action of the applied stress and the stress concentration at the tip of a dislocation pile up. Thus the microstructural features of importance are the mean free ferrite path (eqn. 2.2.13) and the carbide thickness (eqn. 2.2.18). For polygonal ferrite structures the mean free ferrite path corresponds to the grain size, and the cleavage stress is assumed to scale with the ferrite grain size as determined in chapter 4 (figure 4.2) As seen from figure 5.3 however the Cottrell model,

which takes no account of second phase particles, tend to seriously overestimate the cleavage stress for fine grained materials, eg. a factor of two for steel A.

By taking the carbide size into account a somewhat better fit is obtained. The carbide thicknesses observed are typicly about 0.1 μm (figure 4.10 - 4.12). When this value is introduced in the Almond model (eqn. 2.2.18) and plotted in figure 5.3 an overestimate of the cleavage stress of about 40% is still observed.

It has been argued (Knott, 1977) that not only the average grain size, but also the detailed grain size distribution is of importance, i.e., for a wide grain size distribution there may be a sufficient number of large grains to trigger off a complete fracture although the stress level may be subcritical with respect to the average grain size. Observations of secondary microcracks nucleated away from the main crack path in a slow bend specimen (figure 5.6) tend to confirm that the larger grains show a greater propensity for cracking.

A similar argument can of course be produced for the influence of the size distribution of carbides (Curry and Knott, 1976) ie., the crack nucleation process may be dominated by a small fraction of large carbides. In order to introduce any effect of size distribution in the cleavage fracture models the critical level, say the 90 or 95

percentile must be determined. This can be done by quantitative metallography if cleavage fracture occurs in the uniform stress field in a tensile specimen (McMahon and Cohen, 1965). If, however, the presence of the hydrostatic stress component in front of a notch is required to reach the cleavage stress, fracture will occur in a stress gradient. Thus the probability of failure of a particular carbide or ferrite grain is dependent on the local tensile stress in addition to the actual carbide or grain size. The controlled rolled HSLA steels which frequently exhibit a non-uniform distribution both of grain size (figure 4.2) and carbide thickness can therefore not be expected to behave according to the models developed for ferrite pearlite steels.

Due to the poor fit between the observed values of the cleavage stress and the theoretical predictions based on the models by Cottrell and Almond et.al. (figure 5.3) a third analysis proposed by Brozzo et.al. (1977) was considered. This is simply a modified version of the Griffith equation (eqn. 2.2.19) using a microcrack of grain size dimension as the flaw size. The critical event in this mechanism is not to produce the ferrite microcracks as in the Cottrell and Almond models, but rather to extend the ferrite microcracks accross the grain boundaries. The flaw size was taken to be the average

cleavage facet size as determined from SEM fractographs from slow bend specimens of the T-L orientation. The size distribution of the cleavage facets determined by the line intercept method is shown in figure 5.4. In the fine grained polygonal material, steel A, the cleavage facet size is about twice the average grain size indicating a texture effect ie., only small angular deflections are necessary for the cleavage crack to propagate from one ferrite grain to the next. In steel C which exhibits a mixed polygonal - acicular microstructure the cleavage facet size observed represent an average value for the two structures. When the grain size was measured, however, only the polygonal structure was considered. It is thus reasonable to expect a value of the average cleavage facet size between the polygonal grain size and the acicular ferrite cleavage facet size.

When the experimental values of the cleavage stress are plotted versus the inverse square root of the effective grain size eg., cleavage facet size, as determined above (figure 5.5) the points fall very close to a straight line through the origin indicating a good fit with equation 2.2.19. In order to facilitate a direct comparison with data in the literature the results were reduced by a factor of 1.12 (Brozzo et.al., 1977). Using these data to calculate the effective surface

energy in the Griffith equation yields a value of 109 Jm^{-2} which is in very close agreement with the value of 120 Jm^{-2} deduced by Brozzo et. al. (1977) for bainitic steels.

Inherent in the model by Brozzo et.al. is the assumption that ferrite microcracks can nucleate at a stress level lower than the critical cleavage stress required for complete failure. It may thus be argued that in a test stopped immediately before failure the specimen should contain a fair number of microcracks in front of the notch or crack tip. In order to investigate this concept further the microcrack distribution in double notched bend samples (figure 3.2) of various root radii broken at -196^{o}C was studied in the SEM. The salient feature of these observations was however that no microcracks could be detected in front of the unbroken notch. It is thus concluded that the stress required to nucleate the ferrite microcracks must be of the same order of magnitude as the stress required for crack propagation. This is in agreement with the view of Knott (1977) who indicate that by decreasing the scale of the microstructure there may be a continuous transition from ferrite microcrack nucleation as the critical event in the fracture process to a mechanism where microcrack propagation is the crucial step.

In summary the cleavage failure models which introduce the scale of the microstructure through a Hall-Petch

relationship do not describe the experimentally determined values of the cleavage stress adequately for fine grained polygonal and acicular steels, although they show an excellent correlation between fracture stress and grain size for coarser grained structural steels. On the other hand theoretical predictions of the cleavage stress based on the Griffith equation show close agreement with experimental observation. The effective surface energy calculated from the Griffith equation is 109 Jm^{-2} which compares very well to the surface energy deduced by Brozzo et.al. (1977) for bainitic steels.

In attempting to describe the fracture toughness of a structural material it is important, as Ritchie et.al. (1973) have pointed out, to define both the critical cleavage stress σ_c and the distance X over which this stress is attained ahead of the crack tip. Assuming a sharp crack the toughness can then be described by eqn 2.2.20. When cracks or notches with a finite root radius are considered the stress distribution ahead of the crack, and thus the value of X, will change. To incorporate this effect it is convenient to introduce the concept of a process zone. For cleavage failure the process zone can be defined as the volume of material in front of the notch or crack tip where the condition for microcrack formation is fullfilled. The size of the process zone will therefore scale with the

radius of the crack tip as deduced by Malkin and Tetelman (1971) (eqn. 2.2.21) and by Gerberich and Guest (1970) for the elactic plastic stress distribution in a notched bar.

The experimental values of fracture toughness determined for steel A and C (figure 5.2) do not correlate with the Malkin and Tetelman analysis (eqn. 2.2.21). Although there is a slight dependence on notch root radius it is much less severe than predicted from eqn 2.2.21. Further there does not seem to be a lower shelf in the K_{IC} versus $\sqrt{\rho}$ plot and thus no well defined lower limit of the root radius or limiting crack sharpness (ρ_o). It should here be noticed that the range of root radii tested is fairly small (0-~300μm) and that a rapid increase in fracture resistance may occur at larger root radii. This was observed by Ritchie et al (1976) who found large variations in ρ_o in a 4340 steel austenitized at different temperatures. However, due to the fine scale of the microstructure in the present materials ρ_o-values below 100 μm were expected (Malkin and Tetelman, 1971).

The trend from the present data is a continuous increase in fracture resistance with increasing notch root radius starting from ρ=o (fatigue precracked specimens), thus resembling the results from Heald et.al. (1972 b). This model is a modified version of equation 2.2.10 (Heald et.al. 1972 a) where the influence of the notch root radius on stress distribution is taken into account. For small values of (K_{IC}/σ_u), where σ_u is the applied stress at

instability, the final equation is written

$$K_A(\rho) = \frac{K_{IC} + \sigma_u\sqrt{\pi\rho}}{(1 + \sqrt{(\rho/a)})} \qquad 5.1.1$$

where a is the crack length.

Values of $K_A(\rho)$ have been calculated according to this model taking σ_u equal to twice the ultimate tensile strength (Heald et.al., 1972 b) for the notch bend test. The use of $\sigma_U = 2\ \sigma_{UTS}$ in the failure condition can be rationalized in the following way. Failure is expected when the stress in the outer fibers reaches a critical stress level. In the case of cleavage this stress level is given by the cleavage stress. The cleavage stress-values determined for the present materials are close to twice the ultimate tensile stress observed at -196°C. Thus justifying use of the Heald model without corrections. Further the value of K_A is rather insensitive to changes in σ_U, e.g. decreasing the value of σ_U by a factor of two will only change the K_A-value by about 4%. The choice of σ_U-value will therefore not influence the prediction of the apparent toughness to a large extent.

The value of the fracture toughness determined for the fatigue precracked samples are used for K_{IC}, thus making the model semi empirical. The calculated values of K_A for larger root radii are however in very good agreement with the experimental results (figure 5.2). It seems that in the present case the variation of the apparant fracture toughness with the notch root radius is satisfactorily explained by the Heald model by modifying the stress distribution in front of crack tip to account for the finite notch root radius. However the basic problem of relating the fracture toughness K_{1C} to the scale of the microstructure still remains to be considered.

The low temperature fracture toughness values of 49 and 40.5 $MNm^{-3/2}$ for steel A and C respectively are in very good agreement with data from Curry and Knott (1976) who have investigated the influence of grain size on the resistance to cleavage fracture . By extrapolating their data to the actual grain size K_{1C}-values of 53 and 44 $MNm^{-3/2}$ would be predicted for steel A and C respectively. Thus a continuous increase in toughness seem to be observed when the grain size is reduced further below 12 μm which was the smallest grain size considered by Curry and Knott.

At this point it is of interest to calculate the extent of the process zone or the characteristic distance for the materials. Assuming a linear elastic stress distribution in front of the crack tip the characteristic distance is given by (Rawal and Gurland)

$$X = \frac{1}{2\pi} \left(\frac{K_{1C}}{\sigma_c}\right)^2$$

This yields characteristic distances of 57 μm and 59 μm for steel A and C respectively. Although the use of linear fracture mechanics in determining the process zone size may seem a rough approximation similar results are obtained when the finite element analysis due to Curry and Knott is used. The important results that emerges from these calculations are that the size of the process zone is substantially smaller than those calculated by Curry and Knott for materials with similar grain size. This is attributed to the higher level of the critical cleavage stress observed in the present materials. Further the characteristic distance seems to have attained a constant value, i.e., the grain size in steel A and C is different by a factor of two whereas the extent of the process zone is fixed. Again this behaviour corresponds to that reported by Curry and Knott for lower strength material, except that in the present case the value of the characteristic

distance is reduced by a factor of three.

The values determined for the characteristic distance in the present investigation of fracture behaviour of controlled rolled HSLA-steels and values for other structural steels reported in the literature can be rationalized in the following way. In order for cleavage failure to occur at a crack tip two conditions must be met. First the maximum tensile stress must exeed the critical cleavage stress throughout the process zone. This is usually obtained by stress amplification due to plastic constraint at the crack or notch tip, requiring a plastic zone size sufficient to accomodate the cleavage process. In addition the characteristic distance must be greater than the microstructural unit governing the cleavage process, eg., grain size or effective grain size (Ritchie et al, 1973) such that at least one whole grain will experience the cleavage stress. Thus for very coarse grained materials it is reasonable to assume that the process zone size will scale with the microstructure (Curry and Knott, 1976). For finer grained materials the latter condition is always met and the size of the process zone will depend only on the scale of plasticity required to accomodate the cleavage process, ie., to attain the critical tensile stress through stress amplification.

Based on the above arguments a semi-quantitative

description of the fracture toughness can be deduced. For grain sizes greater than a critical value Xo the characteristic distance will scale with the microstructure eg., $x = nd$ where d is the grain size and n is a constant. Several attempts have been made to quantify the correlation between characteristic distance and grain size, n-values of 1.5 and 2 have been suggested by Tetelman et. al. (1968) and Ritchie et.al. 1973 respectively. Combining equations 2.2.19 and 2.2.20 the fracture toughness can now be expressed as

$$K_{1C} = \left(\frac{4E\gamma_{eff}}{a(1-\nu^2)}\right)^{X\,\frac{1}{2}} \qquad 5.1.2$$

where a is the flaw size and X the characteristic distance. If a is some multiple of the grain size as suggested by Brozzo et.al. (1977), eg., $a = m(\frac{d}{2})$, and further only coarse grained materials are considered equation 5.1.2 can be rewritten

$$K_{1C} = \left(\frac{8E\gamma_{eff}\ n}{(1-\nu^2)\ m}\right)^{\frac{1}{2}} \qquad 5.1.3$$

This equation indicate that the toughness is indepe nt of grain size. By introducing the value of $\gamma_{eff} = 1$ Jm^{-2} as determined in the current work and assuming that $(n/m) = 2$ for coarse grained materials (Ritchie et.al., 1973) a

K_{IC} value of the order of 20 $MNm^{-3/2}$ is obtained. This value is somewhat lower than the constant K_{IC} level of 25 $MNm^{-3/2}$ determined by Curry and Knott for coarse grained structural steels. However, considering the approximations made in the model the agreement is reasonable.

For fine grained materials the characteristic distance is constant eg., $X = X_o$, and equation 5.1.2 becomes

$$K_{IC} = \left(\frac{8E\gamma_{eff}\, X_o}{md\,(1-\nu^2)}\right)^{\frac{1}{2}} \qquad 5.1.4$$

Inserting the values for γ_{eff} and X_o from the present work and m=1, the solution of equation 5.1.4 is plotted versus grain size in figure 5.9. together with the result of equation 5.1.3. It is seen that these predictions are in qualitative agreement with the data of Curry and Knott (1976), eg., the fracture toughness is independent of grain size for large grained materials and shows a $d^{-\frac{1}{2}}$ relation for fine grain sizes.

The important result that emerges from the above considerations is that the low temperature fracture toughness is determined by the value of the cleavage stress and the process zone size. The experimental observations suggest that the process zone is independent of the scale of the microstructure for fine grained materials. Hence the fracture toughness will be governed by the magnitude of the critical cleavage stress, and thus by the microstructural features controlling this stress level.

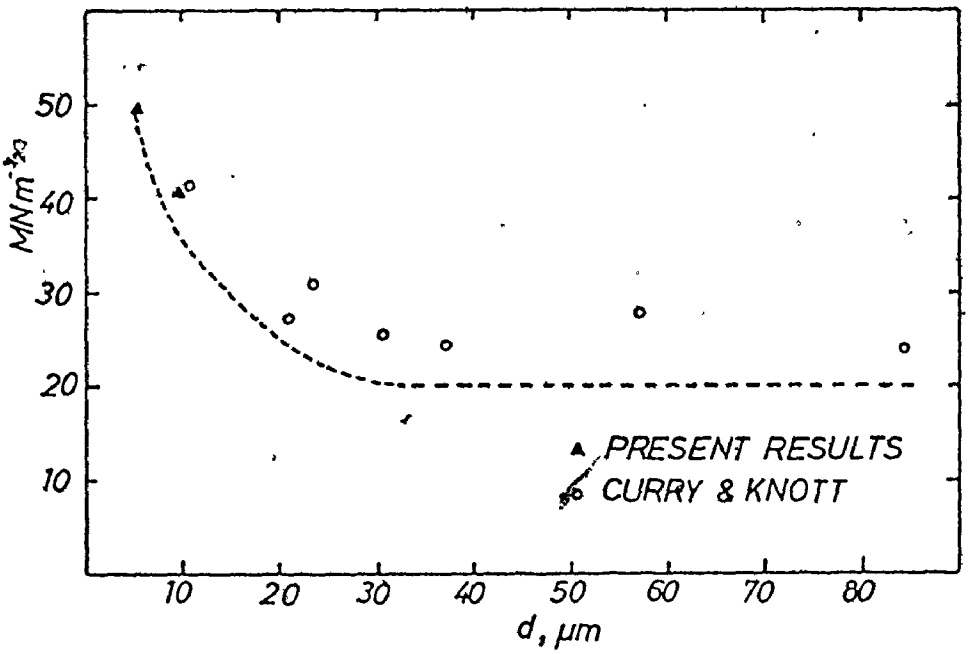

Figure 5.9: Diagram showing fracture toughness for steel A and C as a function of grain size. Data from Curry and Knott (1976) are included for comparison. The dotted lines represent theoretical predictions from equations 5.1.3 and 5.1.4.

TABLE 5.1

CLEAVAGE BEHAVIOUR IN THE SLOW BEND TEST

STEEL	CRITICAL TEMPERATURE, T_{gy} (°C)	YIELD STRESS (MPa)	CLEAVAGE STRESS (MPa)
A	- 170	965	2620
B	- 168	930	2490
C	- 147	905	2170

5.2 DUCTILE FAILURE

The basic mechanisms of ductile failure by void nucleation and growth were reviewed in chapter two. It is, however, pertinent to the understanding of the microstructural aspects of fibrous fracture to briefly consider the parameters which determine the fracture resistance prior to embarking on a detailed discussion of the results.

In broad terms there are four types of factors that have to be considered to obtain a complete description of the fracture toughness. First, from a purely mechanics viewpoint, K_{1C}, since it is related to the square root of the energy release rate, should increase as the plastic zone size at the crack tip or, equivalently, as the crack opening displacement increases (eqn. 2.2.7). Second, there is sufficient evidence (Brown and Embury, 1973; Rice and Johnson, 1969; Smith and Knott, 1971) to suggest that the crack opening displacement should roughly equal both the spacing of inclusions and second phase particles which determine the hole spacing and the size of the intensely deformed plastic zone, referred to as the process zone in ductile failure, at the crack tip. Thus K_{1C} should decrease with decreasing spacing of particles, and hence with increased volume fraction at a fixed particle size. Third, K_{1C} should be lower in high strength material or materials which show a greater tendency for strain

localization than would be expected from extrapolation from lower strength due to the occurrence of plastic instabilities and failure along characteristic slip paths. Finally, crack tortuosity and crack branching should increase the apparent fracture toughness simply because of the increase in surface area and plasticity, and hence the energy consumed per unit projected area. The latter effect has received little attention in the literature and has not been incorporated into any of the theoretical relations for K_{1C}.

In the following section the tensile ductility and the fracture resistance as measured by the COD test are reported for the three steels investigated. The results are then interpreted in terms of the microstructural features, eg., inclusion morphology and nonferritic transformation products, described in chapter four.

5.2.1 Results

The occurrence of ductile failure in controlled rolled HSLA-steels has been studied using both tensile specimens and notched bend specimens of various notch acuity. The room temperature tensile properties of the three steels are summarized in table 5.2. Both longitudinal and transverse tensile properties have been determined in order to correlate the tensile behaviour to the fracture properties determined from COD-specimens in the T-L orientation

TABLE 5.2

TENSILE PROPERTIES AT ROOM TEMPERATURE

STEEL	ORIENTATION	YIELD STRESS(MPa)	ULTIMATE TENSILE STRESS(MPa)	TRUE FRACTURE STRAIN
A1	L	472	608	1.5
	T	ND[x]	ND	ND
A2	L	476	613	ND
	T	461	589	1.2
B	L	507	769	0.9
	T	500	639	0.8
C	L	506	732	ND
	T	465	685	0.6

x Not determined

TABLE 5.3

FRACTURE PROPERTIES

	CHARPY FT. LB/% SHEAR		DWTT[x] (% SHEAR)		
	-15°C	-35°C	-15°C	-35°C	-45°C
STEEL A1	92/100	91/100	100	100	-
STEEL A2	112/100	104/100	99	100	-
STEEL B	77/100	73/100	95	88	75
STEEL C	35/100	35/100	100	100	92

x Specimen oriented 40° to rolling direction.

(figure 3.2). Large variations in fracture strain, measured as reduction in area, are noticed both between the different steels and from testing the same material in different orientations.

Various methods are currently being used to assess the fracture resistance in line pipe steels. For example Charpy tests and drop weight tear tests (DWTT) are required, by the American Petroleum institute. Although these tests describe the fracture resistance and are extensively used by the steel industry the results are not easily interpreted in terms of the detailed fracture mechanism. In the present case Charpy and DWTT data were supplied by the steel producer and are reported in table 5.3. These data can not be correlated directly to K_{1C} or COD values, except by empirical relations. They do, however, serve as valuable means of comparing the fracture resistance of various materials. Further it should be noted that the DWTT specimens are oriented at 40^{o} to the rolling direction to simulate a crack running along the axis of a spiral welded pipe.

In order to determine the fracture resistance for fibrous fracture COD tests were performed at room temperature using the rubber impregnation technique (figure 3.6) to determine the critical value of the crack opening displacement at crack initiation. Fatigue precracked

specimen were used as recommended by Knott (1973). To obtain further information about the detailed fracture process eg., the influence of the process zone size, . specimens with various notch root radii were broken. The results of these tests are plotted in figure 5.10 as crack opening displacement versus notch root radius ρ. The characteristic features of these data are a linear dependence on root radius for large values of ρ and a constant COD value for smaller root radii. The minimum COD value appears to be strongly dependent on the cleanliness of the material. Further the fracture strain in a notched specimen can be calculated from the slope of a COD versus ρ plot (Hahn et al, 1976) according to Equation no. 5.2.2. The results of this calculation are reported in figure 5.10. To compare these results to the fracture strains in tension it is necessary to convert the data to true strain values. The values for the notch ductility for the three steels are reported in table 5.4. It should be noticed that the strain value for steel B is calculated from one data point only and may thus deviate substantially from the true notch ductility.

Due to the complexity of the microstructures in the controlled rolled HSLA-steels it is of interest to investigate the role played by the various microstructural components in the fracture process. Thus double notched bend samples of various root radii were broken, and

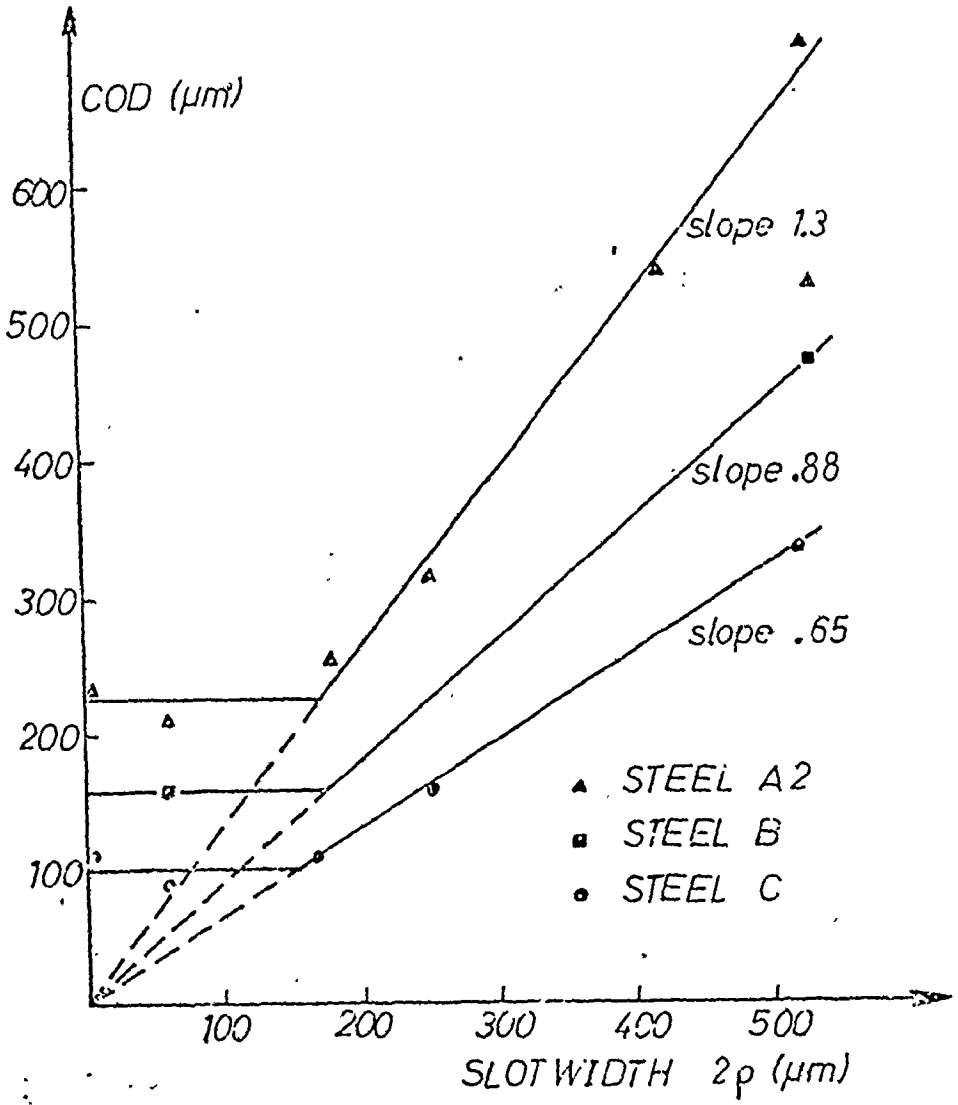

Figure 5.10: Diagram showing COD values determined from four point bending specimens with various notch root radii.

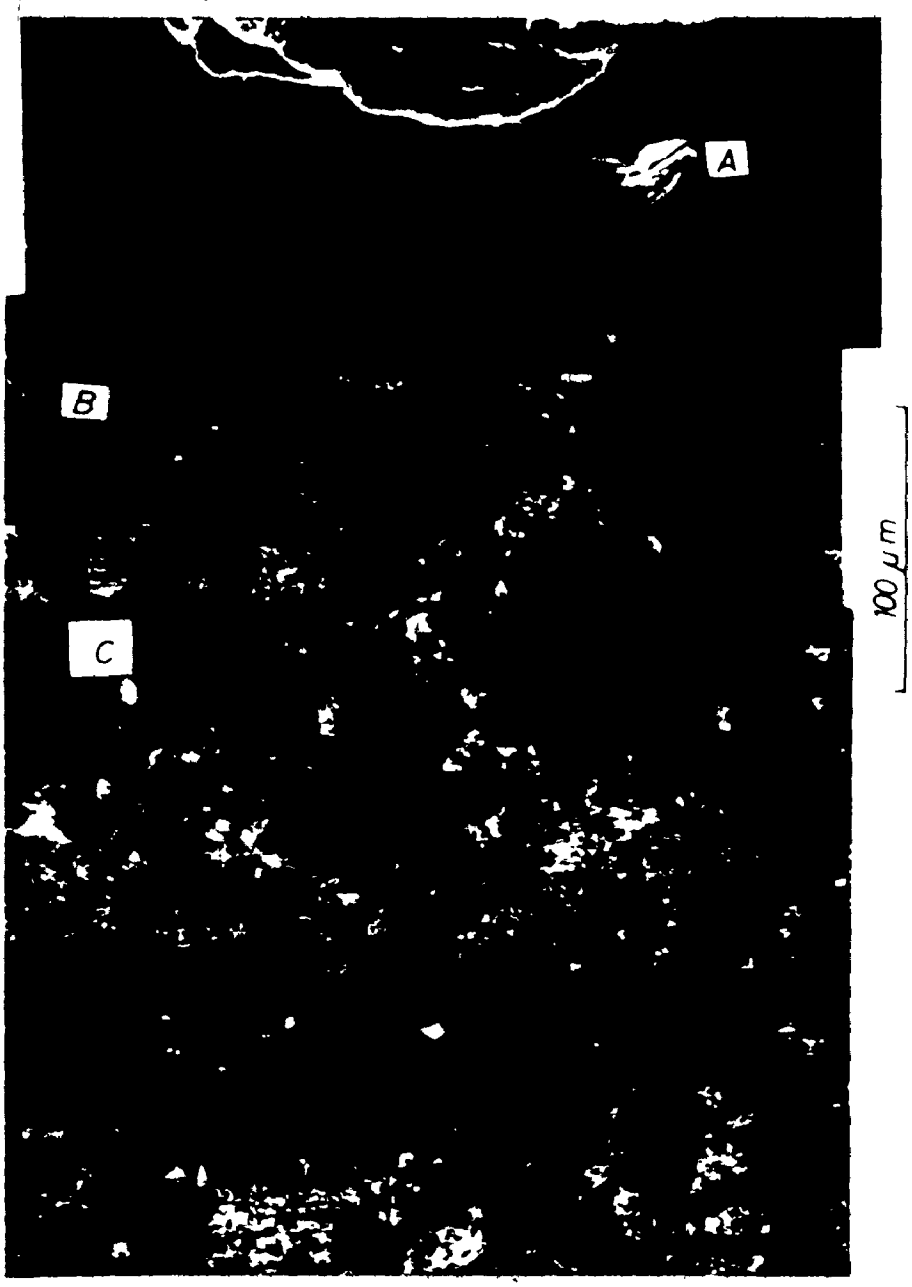

Figure 5.11: Composite micrograph (SEM) showing voiding ahead of the unbroken notch in a double notched slow bend specimen. (steel A). Voids are observed both at inclusions (A) and at carbides (B). Extensive void linkage has occurred at (C).

metallographic sections prepared. Both nonmetallic inclusions, martensite-austenite islands and cementite particles were found to participate in the fracture process by serving as nucleation sites for voids. This is demonstrated in figures 5.11 and 5.12. In steel A which showed the greatest notch fracture strain, extensive linking of voids formed at grain boundary carbides was observed (figure 5.11).

Further information on the behaviour of the various nonferritic phases and inclusions was obtained by determining the strain gradient in front of the unbroken notch in a double notched bend specimen. This was done by measuring the microhardness of the material in the plastic zone as a function of the distance from the notch root. From these curves (figure 5.13) the critical strain for void nucleation in a crack tip stress field could be estimated. In the case of sulphides and oxysulphides voiding was observed after a strain of about 0.1 whereas the nucleation strain for the martensite austenite constituent and the cementite particles was of the order of 0.3. Thus the fracture event seem to be dominated by the distribution of the non metallic inclusions, but the carbides and the M/A-phase are playing an important role in the terminating stage of the fracture process.

The process of void coalescence with the crack tip is illustrated in figure 5.14 which indicates that plastic

Figure 5.12: SEM-micrograph showing details of void formation at cementite particle ahead of notch in steel C. (6000x magnification).

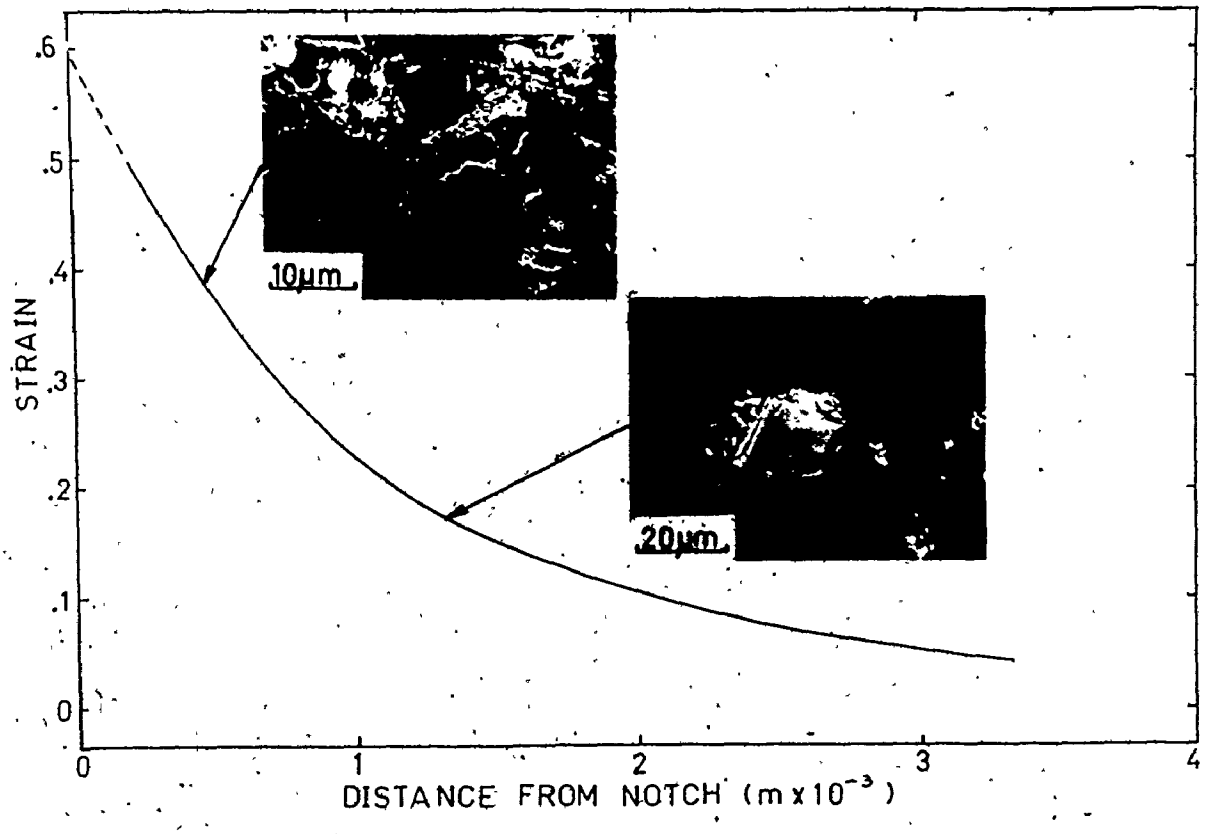

Figure 5.13: Strain gradient in front of unbroken notch in a double notched bend specimen determined from micro hardness measurements. The inset micrographs indicate the critical strain level for nucleation of voids at nonmetallic inclusions and M/A-islands respectively.

instability and strain localization along characteristic slip paths becomes important in the coalescence stage in HSLA-steels.

5.2.2 Discussion

For materials with a uniform inclusion distribution the fracture strain in tension may be estimated from theoretical models such as the Brown and Embury model (1973). However, characterizing the heterogeneities which represent the void nucleation sites in a structural material is a major problem when attempting to interpret the mechanical properties in terms of a theoretical model. This is clearly demonstrated by calculating the fracture strain according to the model suggested by Brown and Embury (1973), viz.

$$\varepsilon_f = \varepsilon_n + \ln \left(\sqrt{\frac{\pi}{6V_f}} - \sqrt{\frac{2}{3}} - 1 \right) \qquad 5.2.1$$

Using a nucleation strain (ε_n) of 0.1 and the volume fraction of inclusions reported in table 4.4 fracture strains of the order 3 are obtained. This is about three times the observed values for the true fracture strain determined from the reduction in area (table 5.2).

There may be several reasons for this deviation between theoretical predictions and experimental observations. First the nonuniform inclusion distribution may reduce the fracture strain in tension substantially. If the particle

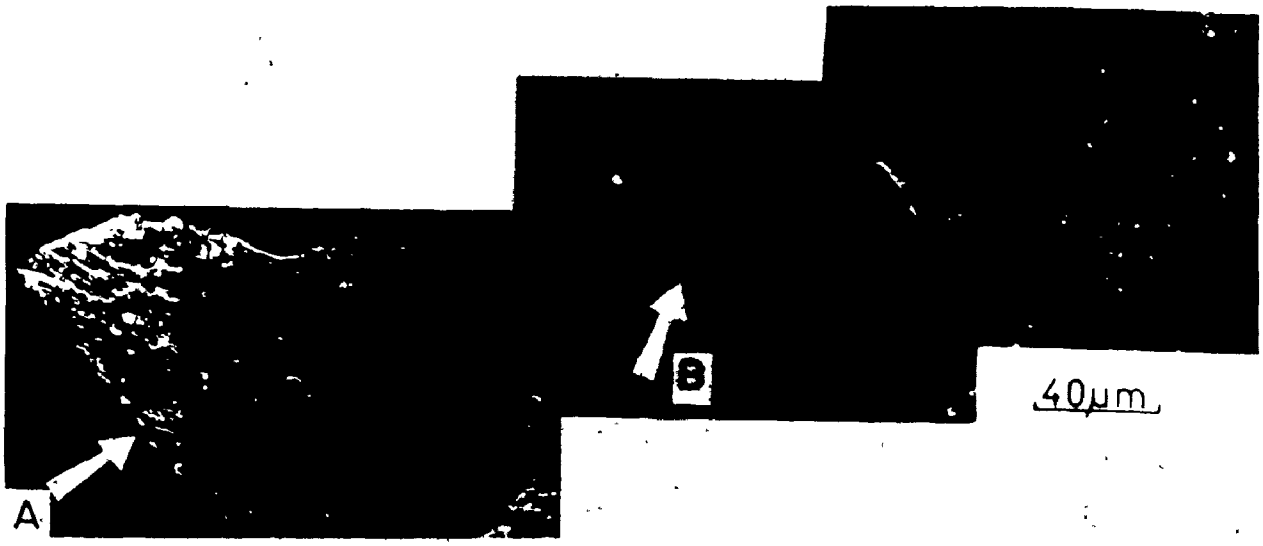

Figure 5.14: Composite micrograph (SEM) showing nickel plated section of notch tip region of COD speciment (steel A). Arrows indicate void coalescence by localized shear at the fracture surface (A) and shear band starting at notch tip (B).

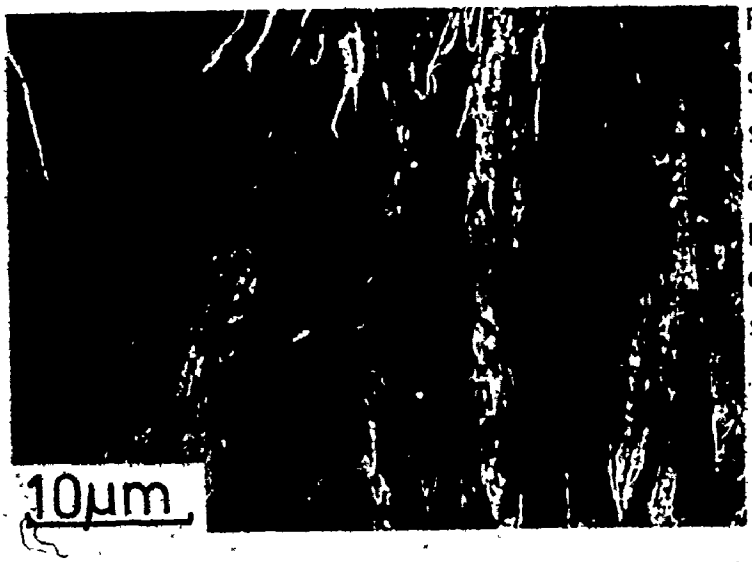

Figure 5.15:

Scanning electron micrograph showing voiding at M/A-phase and carbides in a nickel plated section of the neck of a tensile specimen from steel C.

spacing is reduced locally the nucleation strain will decrease due to overlap in the stress fields around the particles as described by Argon et.al. (1975,b). Further the local growth strain is reduced (Brown and Embury, 1973) leading to the formation of large voids or internal flaws. It has been suggested (LeRoy, 1977) that the further deformation tends to localize in front of the super voids and that these expand as a large crack. The macroscopic reduction in area associated with this final stage of fracture is thus very small, and the overall fracture strain will be substantially smaller than predicted from a model based on a uniform inclusion distribution.

In addition to the effects that can be ascribed to the non uniform inclusion distribution most HSLA-steels contain various other phases which may serve as nucleation sites for voids. In the present materials both islands of the M/A-phase and cementite particles have been observed to produce voiding (figure 5.15). The nucleation strain for voids at the M/A-islands is about 0.3-0.4 as compared to 0.1 for the sulphides. Thus the initiation of fracture will be dominated by the distribution of non-metallic inclusions, but at larger strains the presence of non ferritic transformation products may become increasingly important by reducing the strain required to terminate the fracture process. The lower fracture strain observed

in steel B, compared to steel A2 of the same inclusion content, can be understood in terms of the above argument. According to table 4.2 the M/A content of steel B is about 12% which is almost four times the amount found in steel A2.

The occurrence of elongated inclusions and inclusion sheets (figure 4.18 and 4.19) give rise to anisotropy in the fracture strain (table 5.2). This effect is however difficult to incorporate in any theoretical model and can only be treated in qualitative terms. In general inclusion stringers oriented normal to the tensile axis are the most severe as they will serve as internal flaws after decohesion at the particle matrix interface. This aspect of fracture is treated in more detail in the section on delamination.

Recently there have been much evidence (Smith and Knott, 1971; Hahn et.al. 1976) to suggest that fibrous fracture initiation occurs at a constant value of strain at the crack tip as indicated by Cottrell (1965). The crack opening displacement is then given by

$$COD = 2\rho\ \varepsilon_f \qquad 5.2.2$$

where ρ is the crack tip radius and ε_f a measure for the notch ductility. The data reported in figure 5.10 seem to fit equation 5.2.2 very well for large values of ρ.

It has been suggested (Claussing, 1970) that the notch ductility as determined from COD-data should equal the plane strain ductility for a material and evidence for this correlation has been reported by Hahn et.al. 1976. The plain strain ductility was not determined in the present case, but it is evident by comparing the notch ductility (table 5.4) and tensile ductility (table 5.2) that the stress state plays an important role in determining the fracture strain. This is in accord with previous results of Bridgeman (1952)) that void nucleation is retarded by applying hydrostatic pressure, and further that the growth of voids may be accelerated by the presence of a hydrostatic tensile stress component (McClintock, 1968; Rice and Johnson, 1969).

The detailed mechanism of ductile fracture by nucleation and growth of voids at heterogeneities in the microstructure is the same in tensile and COD tests. Thus the notch ductility is expected to show a similar dependence on the microstructure as the tensile ductility. It is evident from figure 5.10 that reducing the inclusion content and use of inclusion shape modification greatly improves the notch ductility as calculated from the slopes of the curves. The effect is however more obvious in terms of the minimum COD-value.

The minimum COD-value is determined by the spacing of the inclusions or second phase particles serving as

sites for void nucleation (Smith and Knott, 1971; Rice and Johnson, 1969; Hirth and Froes, 1977). Hirth and Froes have shown that most of the plastic deformation accompanying crack propagation occurs in a narrow zone close to the crack tip. The intense deformation close to the crack tip takes place during the void coalescence stage in the fracture process, and the width of the zone should then be of the same size as the inclusion spacing (Brown and Embury, 1973). It follows directly from the Brown and Embury model that the COD-value will scale with the inclusion spacing. The same result is obtained by considering an energy balance. If it is assumed that most of the fracture energy is consumed in a narrow zone of width L the energy release rate can be written (Hirth and Froes, 1977)

$$G_{1C} = L\ \sigma_y\ \varepsilon_f \qquad 5.2.3$$

It then follows from equation 2.2.9 that

$$COD = L\varepsilon_f \qquad 5.2.4$$

ie., assuming a constant fracture strain the crack opening displacement is directly related to the inclusion spacing.

In deducing the above relations a uniform inclusion distribution is assumed. If, however, clustering of the inclusions occurs the critical event in crack propagation

TABLE 5.4

NOTCH BEND BEHAVIOUR AT ROOM TEMPERATURE

Steel	Inclusion aggregate spacing(μm)	Notch ductility from figure 5.10	COD (μm)	
			Experimental	Calculated (eqn. 5.2.4)
A2	199	0.83	213	165
B	200	0.63	159	126
C	170	0.50	101	87

will be to link the supervoids formed at the inclusion clusters. Hence the width of the process zone or the intensely deformed zone will not scale with the average inclusion spacing but rather with the spacing of the clusters, and the COD values are expected to increase accordingly. In chapter four the spacing of inclusion clusters in the rolling direction was found to be about four times the average inclusion spacing. Using this value for the process zone size and the notch ductility determined from equation 5.2.2 the minimum COD-value for a sharp crack can be estimated. Table 5.4 compare calculated and experimentally determined COD-values. Although there is a reasonable correlation between calculated COD values and experiments the analysis is at best semiquantitative due to the difficulties in establishing statistically significant values of the inclusion spacing.

In addition to the difficulties in characterizing the inclusion morphology in a quantitative manner other microstructural features such as the M/A-constituent and the cementite distribution may play an important role in determining the fracture resistance. In figure 5.13 it is seen that voids nucleate at the M/A-islands after straining to about 0.3. Further the strain required for coalescence of the voids nucleated at the M/A phase is small because of the large volume fraction of this

constituent. The nonferritic transformation products will therefore tend to accelerate the process of void coalescence. This is illustrated in figure 5.16 a,b which show the fracture appearance of steel C. The fracture process is dominated by the elongated manganese sulphides which appear as long stringers on the fracture surface. The remaining ligaments between the large inclusions are however deformed sufficiently to produce voiding at the nonferritic transformation products as revealed by the special etching technique described by Chessnut and Spurling (1977) (figure 5.16 b). This results in a fracture surface (figure 5.16 a) characterised by long featureless bands from the MnS stringers, and between the large inclusions, ridges covered with fine dimples from voiding at the non ferrite transformation products are observed.

The effect of the non ferritic transformation products on the ductile failure behaviour is difficult to incorporate in any quantitative model because the plastic inhomogeneity associated with the M/A-constituent and the cementite aggregates depends on the local carbon content, the degree of autotempering and the dispersion of the carbides. Hence, although the non ferritic regions may serve as sites for void nucleation the ductility does not decrease in proportion to the volume fraction of the non ferritic phases.

The linking of voids by localized shear (figure 5.14)

Figure 5.16.a: SEM-fractograph of COD-specimen from steel C. Long ridges of fibrous failure form between MnS-stringers.
(660x magnification)

Figure 5.16.b: SEM-micrograph showing section of the ridges seen in figure 5.16.a. Voiding at M/A-islands and carbides is seen to accelerate the coalescence of large voids.
(2600x magnification)

is a commonly observed feature in HSLA-steels (Embury et al, 1977). The phenomenon is usually associated with materials with higher strength and lower workhardening capasity (Ernst and Spretnak, 1969; Hirth and Froes, 1977). The occurrence of plastic instability by localized shear along characteristic slip paths clearly imposes limitations on the fracture resistance of HSLA steels in terms of the COD value which can be attained. Although current models of ductile failure indicate a proportionality between the COD value and the inclusion spacing. (equation 5.2.3) the constant of proportionality (the fracture strain ε_f in eqn. 5.2.3) may be severely reduced in materials of low work hardening capasity, thus placing some restrictions on the benefits to be derived from inclusion control at higher strength levels (Hirth and Froes, 1977).

The objective of the COD measurement is twofold. Firstly it provides a means of evaluating the influence of various microstructural features on the fracture resistance, and is thus a useful screening test for comparing the fracture of various materials. Further there is evidence that the COD-value, obtained from small scale specimens which suffer general yield, may be related to the fracture toughness or K_{IC}-value by relations similar to equation 2.2.7 (Knott, 1977). This however requires a detailed knowledge of the stress and strain distribution in front

of the crack tip. However, prior to discussing the stress and strain distribution it is of importance to consider briefly the physical processes occuring at the crack tip.

It has been shown in the last section that the fracture events which limit the COD-value are nucleation, growth and coalescence of voids in the process zone. In equation 5.2.4 an attempt has been made to express the COD-value in terms of the width of the extensively deformed zone (L) and the notch ductility (ε_f). The latter is governed by metallurgical factors such as the size and distribution of inclusions, whereas the former also is strongly dependent on geometrical factors. For large values of the notch root radius L is effectively the slot width. As the root radius decreases, however, and a sharp crack configuration is approached the width of the process zone will be governed by metallurgical factors such as the inclusion spacing or the inclusion aggregate spacing. Thus the COD-value becomes independent of geometry at small values of the notch root radius as seen in figure 5.10. According to the experimental data the critical values of L or $2\rho_o$ are 150 μm for steel C and about 170 μm for steels A and B. This is in reasonable agreement with the inclusion aggregate spacing listed in table 5.4. Thus for a sharp crack both the notch ductility and the size of the process zone are determined by micro-

structural features and are independent of geometry. This has been confirmed in recent experiments by Lereim (1977) who found, by altering the specimen dimensions and the crack tip geometry, that the COD-value is independent of the plastic zone size and geometrical factors in specimens suffering extensive yielding prior to failure.

Assuming that the critical fracture event occurs close to the crack tip the hydrostatic stress component at this point is small and the material is undergoing plane strain, plane stress deformation, eg. $\varepsilon_z = 0$ and $\sigma_x = 0$ (figure 3.7). The fracture strain in this condition has been measured by Claussing (1970) and Sailors (1976) who found a ratio between the plane strain fracture strain and the tensile fracture strain of 0.7 and 0.6 respectively for a 500 MPa yield strength material. Using a ratio of 0.65 the plane strain fracture strains can be calculated from the tensile fracture strains in table 5.2 which yields values of 0.8, 0.5 and 0.4 for steels A2,B and C respectively. Comparing these values to the notch ductility determined from the COD tests (table 5.4) a quite good agreement is observed. There is, however, a trend that the experimentaly determined notch ductility values are higher than those predicted from a plane strain model. This may be explained in terms of the detailed fracture process occurring at the crack tip. When void nucleation and

growth start in front of the crack tip there will be a loss of plastic constraint in the remaining ligaments. Thus there will be a local transition from the plane strain condition to a strain state resembling that of fracture in a tensile specimen. Although the process zone apparently is deforming in plane strain there may be a local loss of constraint towards the termination of the fracture process leading to somewhat higher fracture strains than expected in plane strain.

Good agreement is also observed between the notch tip fracture strain determined from the COD-specimens and the fracture strain values obtained from microhardness measurements in front of the notch root in the double bend specimens (figure 5.13). The coincidence of fracture strain values determined from independent experiments and fracture strain values estimated from the plane strain deformation model indicate that the process zone is subjected to plane strain deformation and that the loss of plastic constraint is not significant until very late in the fracture process.

In attempting to estimate the fracture toughness from COD measurements the stress distribution in front of the crack tip must be considered. The fracture toughness is usually expressed by relations such as equation 2.2.7. This, however, neglects both the influence of workhardening and the effect of plastic constraint on the crack tip stress distribution. The plastic constraint factor which should be

applied is criticaly dependent on where the fracture event is nucleated relative to the crack tip. If fracture is initiated at the very tip of the crack the material is subjected to biaxial stretching and the constraint factor is 1.15 according to the von Mises yield criterion. If, however, fracture is initiated further away from the crack tip the triaxiality and thus the plastic constraint factor is increasing. Sailors (1976) calculated a constraint factor of 1.3 for high strength materials with negligible work hardening rates, thus indicating that fracture is occurring in the large strain region very close to the crack tip.

A work hardening factor (H) can be estimated by generating rigid plastic flow curves with the same plastic work over strain ratio as for the actual material (Sailors, 1976). Assuming that the material obeys a power law hardening function the work hardening factors can be expressed in terms of the n-value, eg.

$$H = \frac{1}{n+1}\left(\frac{\varepsilon_f}{0.002}\right)^n \qquad 5.2.5$$

Using n-values of 0.1 which is typical for controlled rolled HSLA-steel and the notch ductility data from table 5.4 equation 5.2.5 yields work hardening factors of 1.66, 1.62 and 1.58 for steels A2, B and C respectively.

Combining the plastic constraint factor and the work hardening factor the effective stress in the process

zone is of the order of 2.1 σ_y. Inserting this value for the effective flow stress and the COD-values from table 5.4 in equation 2.2.7 the following K_{IC}-values are calculated: 215 $MNm^{-1/3}$, 200 $MNm^{-3/2}$ and 150 $MNm^{-3/2}$ for steels A2, B and C respectively. Controlled rolled plate for line pipe applications is normally produced in gauges insufficient for valid K_{IC}-measurements. Thus it is difficult to make a direct comparison between estimated and experimentally determined K_{IC}-values. The calculated K_{IC}-values are however, of the same magnitude as those reported for A533B steel which is of the same strength level and shows similar notch ductility properties as steel A2 and B (Knott, 1977). A reasonable agreement is therefore expected between calculated and experimentally determined K_{IC}-values.

5.3 DELAMINATION

In the transition range between ductile and brittle failure figure 2.2., splitting or delamination is often observed along planes parallel to the rolling plane in controlled rolled plate and sheet. Characteristic features of the delamination fracture are illustrated in figure 5.17. The occurrence of delamination is due to planes of weakness oriented parallel to the rolling plane. The origin of these planes has been described in the literature in terms of cleavage on (100) planes oriented parallel

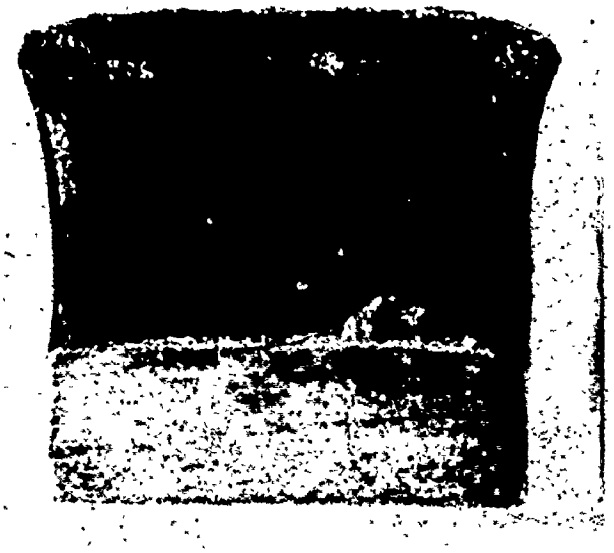

Figure 5.17.a: Photograph showing delamination in fractured charpy specimen.

Figure 5.17.b: Photograph showing the occurence of delamination in the neck of a tensile specimen.

to the rolling plane, grain boundary decohesion or decohesion along sheets of inclusions.

It is often assumed that delamination occurs under the action of the stress component normal to the delamination plane. However, many delamination fractures occur after large plastic strains, eg. in the neck of a tensile sample. An attempt has thus been made to quantify the through thickness properties of the materials using tests involving various states of stress and strain. The tests includes short transverse tensile tests, and a Bridgeman calculation to find the transverse stress in a longitudinal tensile specimen, in addition notched bend tests were used to determine the critical value of the stress component required to produce delamination at various temperatures.

5.3.1 Results

The results obtained from the investigation of the delamination behaviour of HSLA-steels are based on a variety of tests on steel A1 and B. Steel A1 (referred to as steel A in the further discussion) has the highest volume fraction of rare earth oxysulphides and exhibits a non uniform inclusion distribution.

By detailed optical and SEM metallography splits were found to propagate along two sources of weakness either ferrite grain boundaries as described by Herø et.

al. (1975) or along sheets of inclusions (Embury et.al. 1977). Figure 5.18 shows a sectioned slow bend specimen where the splits are seen to propagate preferentially along inclusion sheets. Details of the crack path and fracture surface are also shown. Figure 5.19 shows the fracture appearence after delamination along the ferrite grain boundaries. The scale of the features seen on the fracture surface correspond to the ferrite grain size in the material, hence excluding the possibility of failure along the austenite grain boundaries.

In order to develop fracture criteria for these failure mechanisms mechanical tests involving various states of stress and strain were performed. The normal stress acting across the plane of weakness at failure was then determined. In addition it became apparant during the experimental programme that the materials resistance to plastic deformation, as expressed by the maximum shear stress at failure, was an important parameter. Further the influence of strain on the delamination behaviour was determined by deforming through thickness specimens in compression to strains of about 0.5 before remachining and testing in tension.

Results for the three types of test used are summarised in figures 5.20 a, b and 5.21 a, b. The critical values of normal stress at failure are shown

Figure 5.18.a: Optical micrograph showing delamination in nickel plated section of Charpy specimen from steel A.

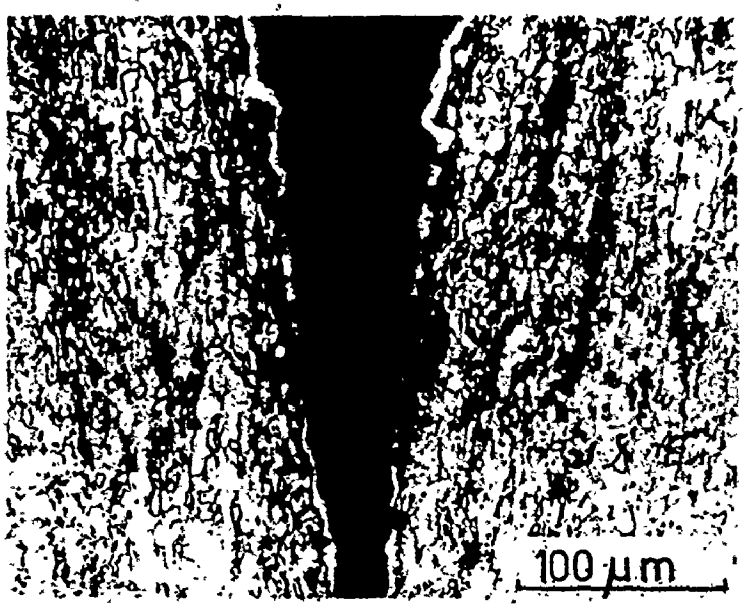

Figure 5.18.b: Optical micrograph showing detail of fracture path in figure a. Large inclusions are seen in the fracture surface between the nickel plating and the matrix.

Figure 5.18.c: SEM-micrograph showing fracture surface of delamination failure propagating along an inclusion sheet. (2000x magnification).

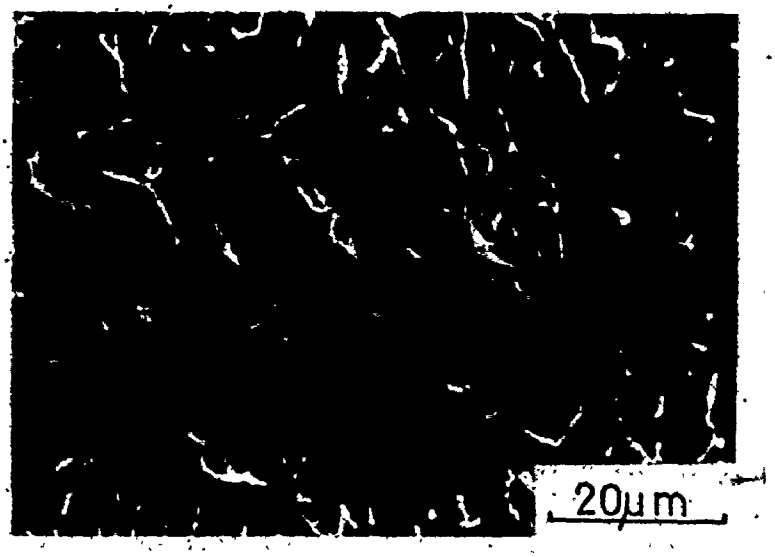

Figure 5.19: SEM-micrograph showing fracture surface of delamination failure propagating along ferrite grain boundaries.

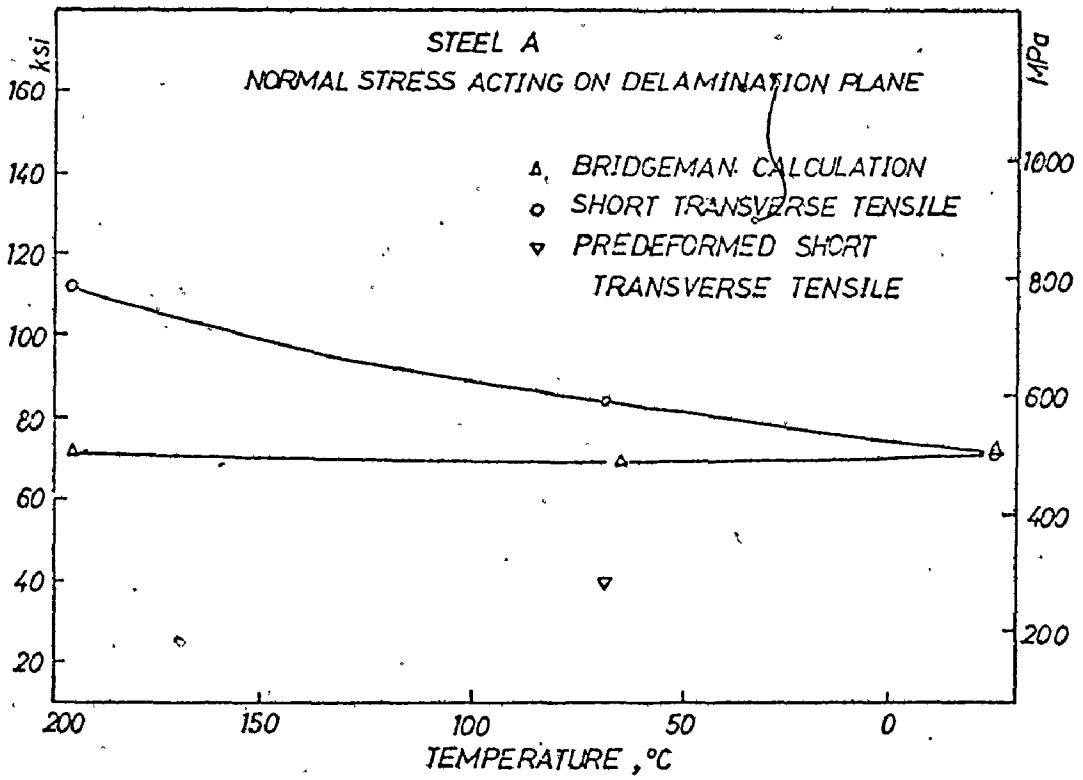

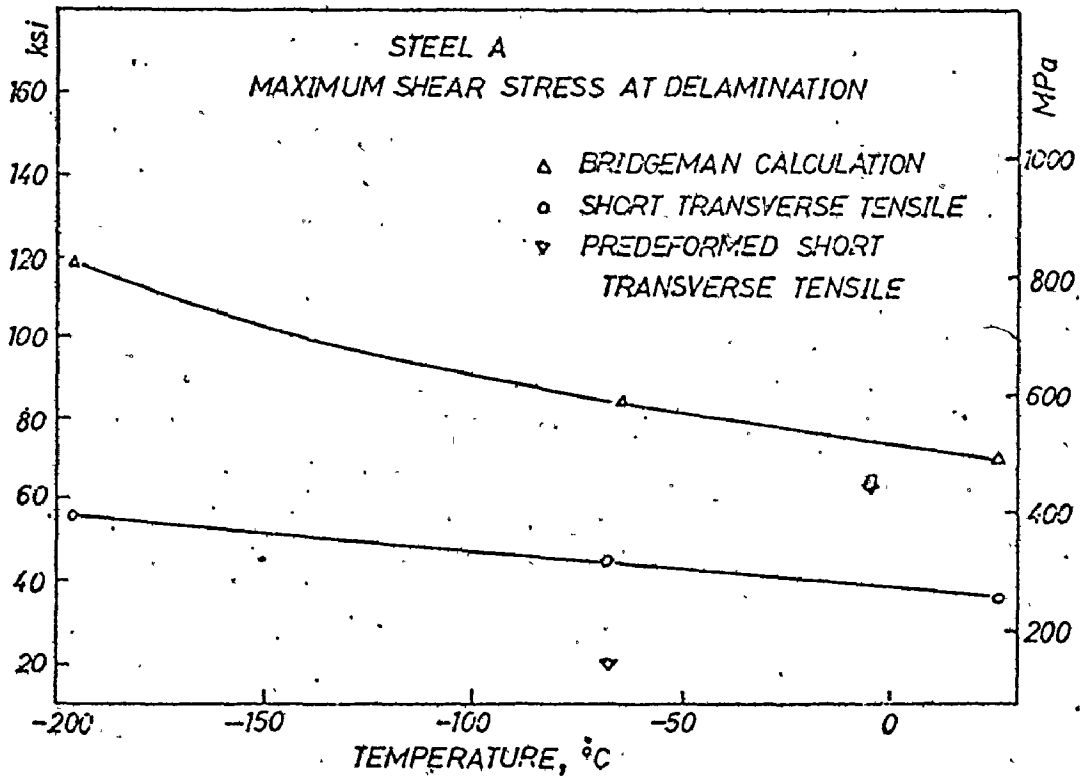

Figure 5.2: Diagram showing stress at the onset of delamination for various test specimens and temperatures.

a: normalstress acting on delamination plane.

b: critical value of the maximum shear stress at delamination.

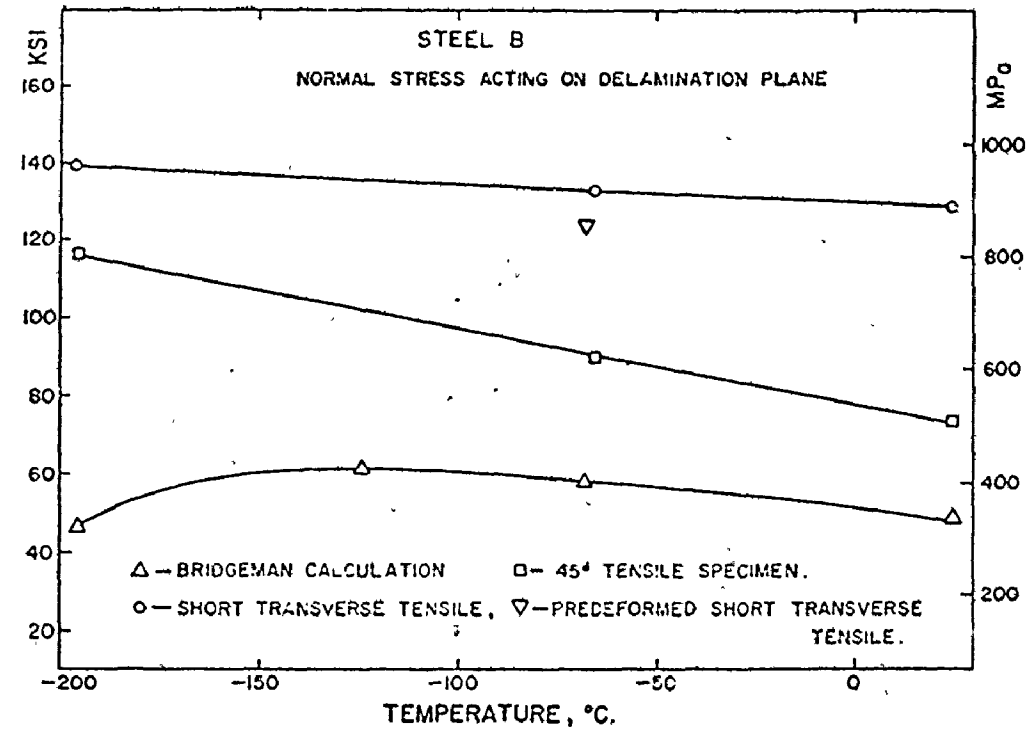

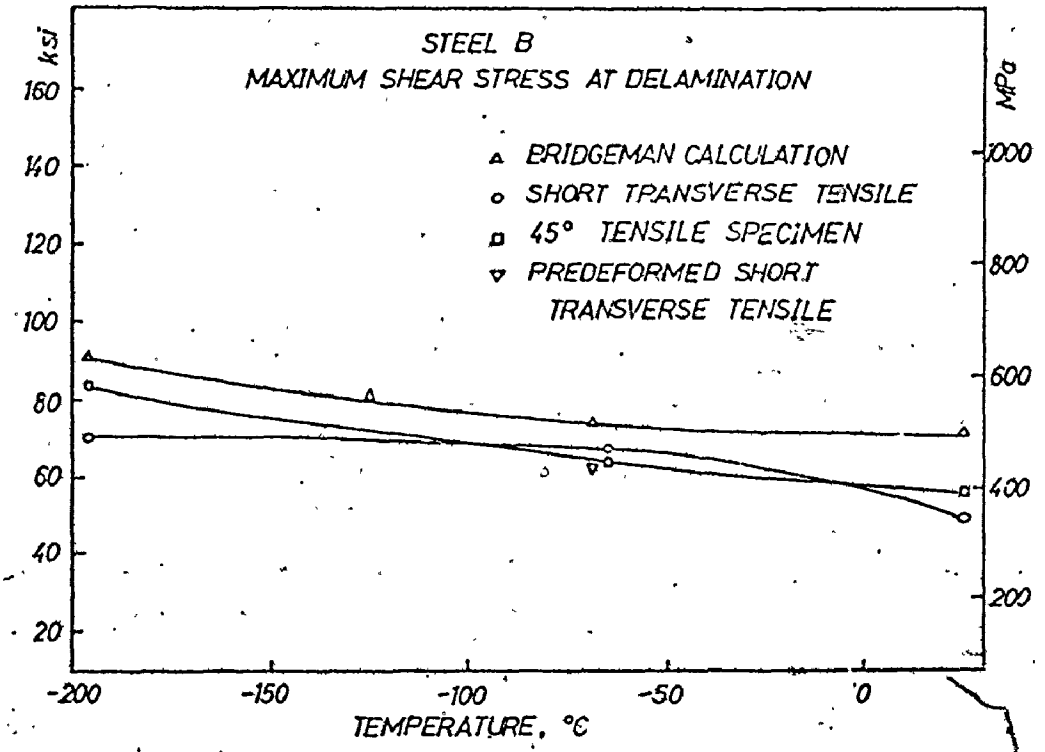

Figure 5.21: Diagram showing stress at the onset of delamination for various test specimens and temperatures.
a: normalstress acting on delamination plane.
b: critical value of the maximum shear stress at delamination.

in figure 5.20 a and 5.21 a for steel A and B respectively. Results from the through thickness tensile tests, the Bridgeman calculation from longitudinal tensile tests, and the slow bend test performed at various temperatures between -196°C and room temperature are included. In figures 5.20 b and 5.21 b the critical values of shear stress at delamination are evaluated for the same tests. The salient features revealed by these experiments are that in steel B, which is the material of low sulphur content, there is no correlation between normal stress at failure from one test to the other. In this material the fracture path in all cases appeared to follow the ferrite grain boundaries, i.e., the fracture mechanism was the same. There is however, a major difference between the Bridgeman test and the short transverse tensile test in terms of strain to failure. In the longitudinal test used for the Bridgeman calculation the true strain to failure varied from 0.5 to about 1.0 depending on temperature, whereas the short transverse specimens usually failed after straining to 0.2 or less.

The results for steel A are more complex because two sources of delamination were observed in this material. In the short transverse tests the dominant mode of failure was by decohesion of aggregates of inclusions, whereas both in the necked portion of the longitudinal tensile

specimens and in the notched bend tests the grain boundary failure mode occurred.

In order to show the influence of precompression the values of shear and normal stress at failure for specimens tested at -68°C are reported in table 5.5. For steel A, the material containing the largest fraction of oxysulphides, the fracture stress dropped by a factor of two to 280 MPa which is about one third of the flow stress in the workhardened condition. In steel B there was no significant decrease in fracture stress after deforming the samples in compression.

To further investigate the concept of a critical shear stress, tensile specimens were cut with the axis at 45 degrees to both rolling plane normal and rolling direction, thus aligning the plane of weakness parallel to the plane of maximum shear stress.

At room temperature these specimens exhibited localized shear failure at very low strains and before any sign of geometric instability (figure 5.22). The shear stress at failure however, is comparable to the shear stress in the neck of the short transverse specimens. At lower temperatures the mode of failure changes from localized shear to a mixed mode involving shear and cleavage at -65°C to pure cleavage at -196°C.

Figure 5.22:

Photograph showing fracture surface of 45^{o} tensile specimen after failure at room temperature.

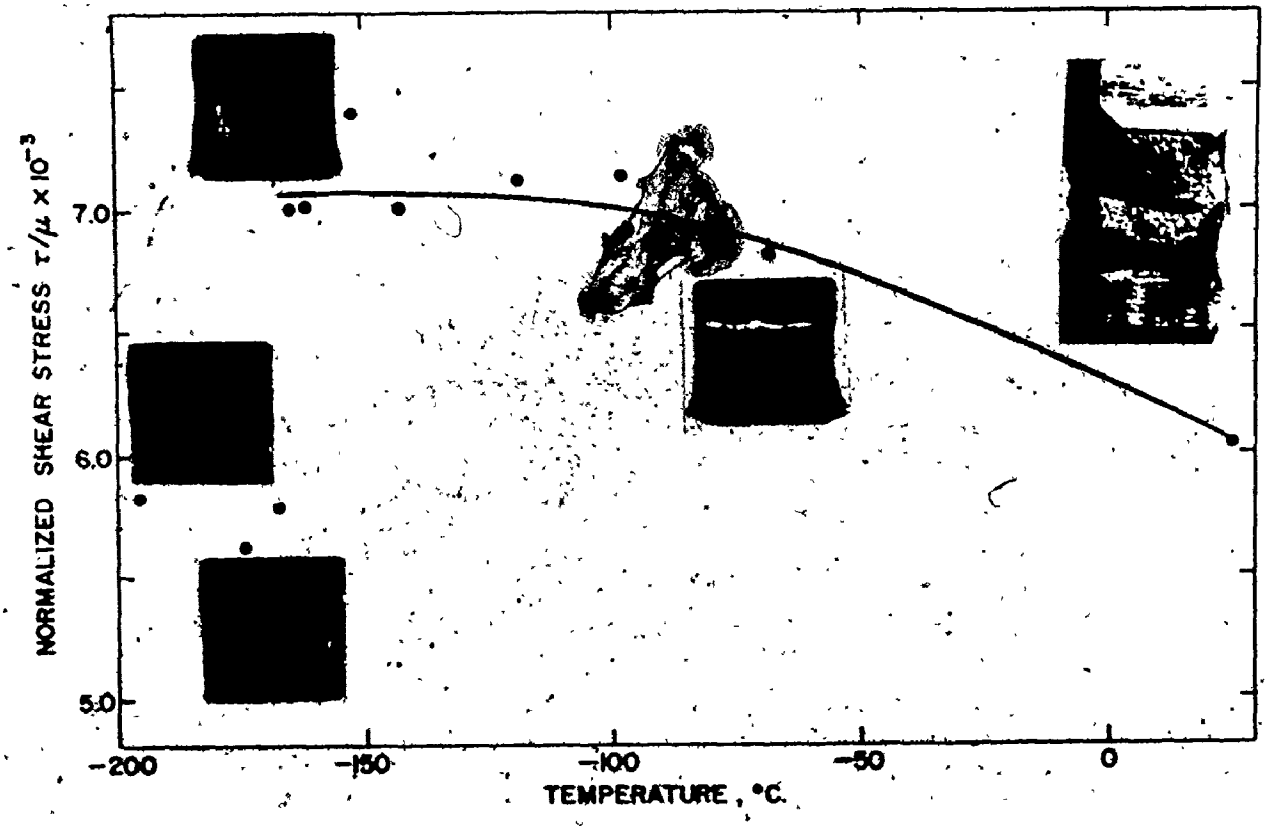

Figure 5.23: Diagram illustrating the propensity for delamination and the variation in maximum shear stress as a function of temperature.

5.3.2 Discussion

The detailed metallography on sectioned test specimens and observation of fracture surfaces revealed two mechanisms of delamination failure, e.g., decohesion along inclusion sheets and crack propagation along ferrite grain boundaries. The former does not represent the traditional form of lamellar tearing along elongated inclusions but is due to the agglomeration of rare earth oxysulphides in the melt which are subsequently rolled out to form sheets of inclusions (Embury et.al., 1977). Inclusion sheets exceeding 5 mm in length were frequently observed on the fracture surface of through thickness tensile samples.

Propagation of splits along ferrite grain boundaries was first described by Herø et.al. (1975) who attributed the delamination failure to extensive precipitation of cementite on ferrite grain boundaries during the austenite-ferrite transformation. Transmission electron microscopy did not reveal the same degree of grain boundary precipitation in the present materials as observed by Herø et.al. However, the extensive voiding at ferrite grain boundaries observed in front of the notch in the double notched bend specimens indicate that the grain boundaries represent a plastic inhomogeneity (figures 5.11 and 5.13). Further the propensity to delamination was greatly reduced after

annealing the steels at 600°C for 24 hours to spherodize the grain boundary carbides. Recrystallization of the ferrite did not seem to occur at this annealing temperature. Hence, the delamination failure seems to be associated with the occurrence of grain boundary cementite.

Although cleavage facets were observed occasionally on the delamination fracture surface they only represented a small area fraction of the surface. Cleavage fracture is therefore not considered a significant fracture mechanism for delamination. This is in accord with the crystallographic texture observed which only show very weak {100} components in the rolling plane (figures 4.15 and 4.16). Cleavage may however be a possible splitting mechanism in materials with a strong 100 texture component (Miyoshi et. al. 1974).

Except for the occurrence of a non uniform inclusion distribution in the present materials delamination failure is attributed to the banded carbide distribution commonly observed in controlled rolled HSLA-steels (figure 4.5). The morphology and distribution of the carbon rich phases depends criticaly on the detailed transformation kinetics of the material as described in chapter 4. Thus the occurrence of elongated austenite grains before transformation tend to produce a non uniform or banded carbide distribution. (Herø et.al., 1975; Hornbogen and

Beckmann, 1976). On straining decohesion tends to occur at the interface between the grain boundary carbides and the ferrite matrix in the carbon rich bands thus producing planar weak areas parallel to the rolling plane where splits may form.

Having established the mechanisms by which delamination occurs it is of interest to formulate criteria for failure. This requires a detailed knowledge of the state of stress and strain at delamination.

It was found that when the normal stress acting on the plane of weakness was calculated for the various test geometries very poor correlation was obtained between the delamination stresses from one test to the other (figure 5.21 a). To investigate whether this was due to different levels of strain in the longitudinal and short transverse test specimens predeformed specimens were tested.

No significant decrease of the fracture stress was observed in steel B after deforming the samples in compression (table 5.5) thus indicating that delamination by the grain boundary decohesion mechanism is insensitive to the level of strain. In steel A, however, the fracture stress was reduced by a factor of two after compression (table 5.5). The effect of prestraining in this case appears to be the introduction of damage in the inclusion containing material by opening up voids along the inclusions.

The inclusion sheets will then act as internal flaws in the material when subjected to tension. Assuming the fracture toughness of the material in the prestrained condition to be of the order of 50 $MNm^{-3/2}$ at $-68^{o}C$ and introducing a flaw size of 4 mm which was often observed, linear elastic fracture mechanics yields a critical stress of 240 MPa which is in good agreement with the observed values.

As there was no effect of prestrain on the short transverse fracture in steel B, the difference between splitting stress for longitudinal and short transverse tensile test cannot be due to the difference in fracture strain. This suggests that for the grain boundary initiated delamination mode the propagation of the splits under the action of a normal stress component may not be the critical event for delamination failure. The alternative is to consider nucleation of voids or decohesion at the grain boundary carbides as the critical event in the onset of delamination.

In this case, delamination is competitive with continued plastic flow and is thus expected to occur at a critical level of resistance to plastic deformation, i.e., at a critical level of the flow stress. The flow stress of the material is characterized by the maximum shear stress at failure, i.e., the radius of the expanded von

Mises yield surface.

From table 5.5 it is seen that there is good agreement between the various test methods in terms of the critical shear stress when the delamination fractures are propagating along the ferrite grain boundaries. Thus confirming the theory of a critical shear stress criterion.

Further the results from tensile tests oriented at 45^{o} to both the rolling plane normal and the rolling direction indicate that the critical shear stress at failure is independent of orientation, although the mode of failure changes to pure shear failure (figure 5.22) when the plane of weakness is oriented parallel to the maximum shear stress.

The change in failure mode from pure shear along the planes of weakness at room temperature to a partial cleavage failure at $-65^{o}C$ and complete cleavage fracture at liquid nitrogen temperature suggest that the occurrence of delamination due to nucleation of colinear arrays of voids parallel to the rolling plane must be considered in relation to other fracture modes. At low temperatures the stresses close to the tip of a notch become sufficient to produce cleavage failure and at high temperatures the yield stress of the material is sufficiently low so that the critical stress for delamination is not attained. Thus in a Charpy V-notch sample there should be a range

TABLE 5.5

DELAMINATION BEHAVIOUR AT - 68°C

	Material	Notch bend Test[x]	Bridgeman calculation	Short Transverse Tensile	Short Transverse Tensile, Pre-deformed in compression
Normal Stress (MPa)	A	1680	490	588	280
	B	2060	494	995	875
Maximum shear stress (MPa)[xx]	A	466	595	298	140
	B	568	518	497	442

[x] from equation 3.3

[xx] $\tau = \frac{1}{2} (\sigma_{max} - \sigma_{min})$

in temperature over which delamination is observed. The critical temperature range for delamination will depend on the competing fracture mechanisms and how they respond to changing temperature and stress state. Thus delamination is observed at different temperatures in notched bend tests and tensile tests. This result is in accord with data reported in the literature and is sketched in a semiquantitative manner in figure 5.23 which illustrates the occurrence of delamination in sub size Charpy specimens as a function of temperature. The curve shows the shear stress at the onset of delamination for various test temperatures, and the tendency to form splits is indicated by photographs of the fracture surface at representative temperatures. The correlation between splitting intensity and shear stress is clearly demonstrated in figure 5.23. Further the transition to ductile failure and fewer splits at lower levels of the flow stress is apparent at higher temperatures.

Although it is currently not established whether delamination plays a deleterious role in terms of the dynamic toughness, it does promote the occurrence of a sloping shelf energy region which is of importance if one of the design criteria specified for HSLA steels in pipeline use is the value of the CV100 parameter, i.e.

the Charpy energy at 100% shear failure. Also it is clear that the specification of the critical stress condition for delamination is pertinent to the occurrence of delamination in the form of lamellar tearing in welded constructions where the fracture may initiate under a combination of applied and residual stresses.

The observation that delamination can arise either from decohesion in the vicinity of grain boundaries or arrays of oxy-sulphides strongly suggest that control of these microstructural features is of major importance. This requires strict attention both to the desulphurisation, deoxidation and reoxidation reactions in the steel-making process and a much more detailed understanding of the carbon redistribution involved in the formation of a fine scale ferrite. The observation that the formation of grain boundary carbides is much greater in 0.06% C steel than 0.025% C steel (Brozzo et.al., 1977) and the variation of carbide morphology with section size and subsequent low temperature annealing (Herø et.al., 1975) strongly suggest that optimisation of cooling rate and section size may present future difficulties in the application of control rolled HSLA steels from the viewpoint of the attainment of adequate through thickness properties.

6. CONCLUDING DISCUSSION

The experimental results outlined in the preceeding chapters raise questions of interest both in defining the critical fracture parameters for HSLA-steels and in regard to the optimisation of the microstructures of these materials from the viewpoint of fracture resistance.

Prior to embarking on a discussion of the fracture modes and the criteria which govern their occurrence the microstructural features which appear detrimental to the fracture resistance will be briefly reviewed.

The occurence of islands of the martensite austenite phase can lead to deleterious effects because in some cases at low temperatures these phases can act as nuclei for cleavage cracks (Embury et.al., 1976) and at higher temperatures voids may form in the highly strained region close to the crack tip, thus reducing the fracture toughness of the material (figure 5.13).

The sulphide inclusions modified by rare earth additions exert a major effect on ductility by virtue of their distribution. It appears that with rare earth additions to the ladle the sulphide modification process and the re-oxidation reactions occur simultaneously resulting in a very complex arrangement of both sulphides and oxidation products. Frequently these products are

aggregated to form large areas of agglomerated inclusions which represent one source of lamellar tearing in the HSLA-steels.

Further in attempting to rationalize the relationship between inclusion distribution and critical fracture parameters, such as fracture strain or COD values it is important to realize that the inclusions are not randomly dispersed and that the ductility depends both on the nearest neighbour distance in the aggregates and the mean spacing of the aggregates.

During the transformation of austenite to ferrite after controlled rolling extensive precipitation of carbides may occur on ferrite grain boundaries aligned parallel to the rolling plane. These carbides also serve as sources of delamination, but the process is operative at higher stresses than in the case of the inclusion sheets.

Plastic collapse by strain localization is frequently observed in HSLA-steels. This leads to the occurrence of shear failure in a manner similar to that observed in higher strength materials. The linking of voids by a localized shear process represent a premature failure which may severly reduce the COD-value or the fracture toughness predicted from a fibrous fracture model.

6.1 CLEAVAGE FAILURE

In the case of brittle failure it is found that the fracture resistance is determined by the cleavage stress and the size of the process zone. For coarse grained materials the latter will scale with the grain size as outlined by Ritchie et.al.(1973) and Curry and Knott (1976). For grain sizes below about 40 μm, however, the process zone size becomes independent of the scale of the microstructure and is determined by the plasticity required to attain the critical cleavage stress. Hence the fracture toughness will be governed by the magnitude of the cleavage stress and thus by the microstructural features which control σ_c. Using this semiquantitive model it has been possible to predict the grain size dependence of K_{IC} both for coarse and fine grained materials (figure 5.9).

The present results emphasize the importance of the critical cleavage stress in determining the low temperature fracture resistance, and hence the need of understanding the detailed mechanism by which cleavage failure is nucleated. In general two conditions must be met for cleavage fracture to occur. Firstly the applied stress must be sufficient to cause microcracking either by a dislocation mechanism (Cottrell, 1958) or by a carbide cracking mechanism (Almond et.al., 1969), secondly the microcracks must be of a size sufficient to supply the extra energy required to extend the microcracks past the grain boundaries (equation 2.2.19). In the present materials the distribution of the cementite particles seems to satisfy

the condition for nucleation of microcracks, although both the average grain size and the average carbide distribution is smaller than expected from the recorded values of the critical cleavage stress. Thus the critical event in cleavage failure is extending the microcracks into the neighbouring grains. This condition can be expressed by a modified version of the Griffith equation (2.2.19) in terms of an effective ferrite grain size, eg. the cleavage facet size. The average microcrack size or cleavage facet size exceeds the ferrite grain size by a factor of about two, although substantially larger cleavage facets are observed occasionally (figure 5.8). This indicates that in addition to the scale of the microstructure, texture effects may be important in determining the microcrack size and thus the critical cleavage stress.

In order to improve the low temperature fracture properties it is therefore important to avoid microstructural constituents which may reduce the critical cleavage stress. In particular it is important to obtain a fine and uniform ferrite grain size or covariant packet size. The effect of texture on the microcrack size and distribution has not been investigated in any detail. The present results do, however, suggest that this parameter may be of importance in determining the critical cleavage stress and that attention should be a focused on texture effects in future investigations of the cleavage fracture process.

6.2 DELAMINATION

Delamination failure was commonly observed when testing the materials in the temperature regime between ductile and brittle fracture (figure 2.2). The occurrence of delamination was attributed to the presence of either inclusion sheets produced by rolling materials containing large inclusion aggregates, or cementite particles precipitated at the ferrite grain boundaries. In the former case splits propagated along the inclusion sheet under the action of the stress component normal to the rolling plane. In the latter case, however, there is a competition between continued plastic flow at the grain boundaries and nucleation of voids at the grain boundary carbides. Since the carbides are acting as barriers to the plastic deformation strain gradients and hence stress concentrations will build up at the particles until voiding occurs. If the macroscopic flow stress is increased either by decreasing the temperature or by prestraining the material, continued plastic flow is impeded and the propensity to delamination is increased (figure 5.23).

In materials with a banded carbide distribution planar arrays of voids are formed and delamination may occur due to the normal stress acting on the void sheet. However, void nucleation is the critical event and thus the condition for delamination can be expressed by a shear stress criterion, or effectively by the flow stress in shear.

The local shear stress may represent the combined effect of the applied stress and internal stresses in the material. Internal stresses may be present either as residual stresses due to the phase transformation or they may be generated during straining if textural banding occurs on a microscopic level (Chao, 1977). Large residual stresses may also be produced during welding of heavy sections.

Textural banding in HSLA steel may arise if the austenite is allowed to recrystallize partially before transformation, which emphasizes the importance of controlling the rolling schedule such that duplex microstructures are avoided.

6.3 DUCTILE FAILURE

At higher tempratures the failure mode is by fibrous rupture and the condition for failure is the attainment of a critical strain rather than a critical stress. Failure occurs by nucleation and growth of voids at second phase particles which are introduced in the material either in the steelmaking process or during the austenite-ferrite transformation.

The resistance to fibrous fracture in the HSLA-steels investigated is found to be dominated by the spacing and distribution of the non metallic inclusions formed in the melt. In particular the sulphides and oxysulphides. The use of rare earth additions to modify the sulphide shape may improve the fracture resistance substantially. However, this practice requires both a detailed knowledge of the

chemistry of the various compounds and a close control of the steelmaking process. It is found that inclusions formed during the deoxidation process are small and evenly distributed, whereas inclusions formed by reoxidation of the rare earth sulphides are large and often agglomerated in clusters. During rolling both the shape and the distribution of the inclusion aggregates will change. If the aggregates are large, sheets of very high inclusion density will form parallel to the rolling plane resulting in poor short transverse properties.

In clean materials with a large spacing between the nonmetallic inclusions the presence of the M/A constituent may be important as a void nucleating agent. Further, failure by strain localization and plastic collapse is frequently observed in these materials (figure 5.14). Hence indicating that there may be a limit to the benefits that may be attained from reduction of the inclusion content and the use of sulphide shape control in structural steels.

Testing the fracture resistance of structural steels represent a major engineering problem. Due to the size requirements of the test specimens (eqn. 2.2.5) K_{IC}-measurements according to ASTM E399 are tooexpensive for quality control purposes. Further these materials are not normally produced in gauges sufficient to meet the size requirements. However, the present results indicate that the COD-test may be a valuable tool in evaluating the fracture resistance for low and medium strength structural steels.

In the case of ductile failure the COD-values are found to be independent of the extent and pattern of the plastic zone (Lereim, 1977). This is contradictory to the results of linear elastic fracture mechanics where proportionality between the COD-value and the plastic zone size is expected (eqn. 2.2.23). In the fully plastic case, however, the COD-value is determined by the extent of the process zone. Hence the COD-value is limited solely by metallurgical features, such as volume fraction and distribution of inclusions, flow properties etc.

Although the amount of plasticity experienced in the failure of structural members and the COD test specimen may be vastly different the foregoing arguments indicate that the critical crack opening displacement is constant and independent of geometrical factors. Thus it is possible that the COD-value may be used as a design parameter. This will allow an evaluation of the fracture resistance from simple and inexpensive small scale tests requiring little advanced testing equipment.

Further the COD test allows the fracture resistance to be determined locally in materials exhibiting large gradients in fracture resistance. This is of importance in welded structures where the fracture properties of both the weld-metal and the heat affected zone may be evaluated. Similar problems exist in materials suffering radiation damage where it is of interest to determine the fracture resistance both in terms of the position in the plate and

as a function of exposure time at a given location. Both in the case of welded structures and radiation damaged materials small scale tests are required in order to locate the crack tip in the structural constituent of interest.

Considering the potential savings and the additional information that may be obtained from the COD-test compared to conventional fracture toughness testing, it is important to achieve a better understanding of the fracture event occuring in small scale specimens.

6.4 SUGGESTIONS FOR FUTURE WORK

In view of the increased interest in dual phase materials which make deliberate use of a high volume fraction of the M/A-constituent (Bucher and Hamburg, 1977) it is important to attain a better understanding both of the transformation mechanism by which this phase is formed and of the role played by the M/A-constituent in determining the fracture resistance of the material.

The dual phase steels exhibit a very high initial work hardening rate which may be beneficial both in plate material where it can balance the detrimental influence of the Bauschinger effect in the pipe forming operation and in sheet forming applications where a better formability may be attained with no reduction in the final product strength. Considering the potentially deleterious effects of the M/A constituent on the fracture resistance the successful use of these materials depends strongly on the steel producer being

able to make a material with a given volume fraction, size and distribution of the second phase. This, of course, requires a detailed knowledge of the transformation behaviour of controlled rolled HSLA-steels in terms of predicting the hardenability from the steel chemistry and processing schedule. Further in the heat treated dual phase material it is important to delineate the effect of the local carbon content and dispersion of the carbides on the plastic inhomogeneity of the M/A-phase.

Thus there is a great impetus for further work both on the transformation kinetics and on the mechanical response of the martensite-austenite constituent. Particularly in view of the growing interest in dual phase materials for automotive applications this area will become of major importance in the future.

In the present work only the static fracture toughness or the resistance to fracture initiation has been considered. Over the last few years, however, the dynamic fracture resistance or the materials ability to stop a running crack has been of growing concern. Recent work by Hahn et.al. (1975) suggests that the fracture resistance varies strongly with crack velocity and that in some cases there is a minimum in the dynamic fracture toughness for a given crack velocity.

The microstructural features which govern the dynamic fracture properties have been offered little attention in the past, and alloy development has, at the best, been based on the static fracture resistance, K_{1C}. Thus the posibility exists that materials which have been designed to yield optimum static fracture properties may show poor crack arrest abilities.

This problem is of major importance in the application of HSLA-plate for pipelines. In pipelines carrying pressurized gas the velocity of a running crack may substantially exeed the rate by which the line can be depressurized, hence there will be no reduction in the driving force for crack propagation. As this example shows there is great impetus for improving the understanding of the mechanisms by which energy is consumed during fast fracture and crack arrest. In this field extensive research efforts are required to delineated the influence of metallurgical variables on the materials crack arrest properties.

The present work indicates, in a semiquantitative manner, the influence of a variety of microstructural features on the basic modes of failure which are important in the application of HSLA-steels. The need for relations which enable tolerable flaw sizes and critical stress levels to be predicted in a quantitative manner under general yield conditions is however apparent. Currently the J_{1C} and COD approach looks promising but further work is required to establish the limits within which these tests can be used satisfactorily. It is characteristic for many of the low and medium strength structural materials that they are never used in thicknesses resembling those required for valid K_{1C}-testing. Hence a valid K_{1C}-value according to the ASTM standard may be too conservative as a design criterion for the actual structure. The approach suggested by Heald et al (1972) where an apparent fracture toughness modified for the section size may be useful in this regard, but again further work is required on a broad

range of materials to assess the limits for use of the model.

In the final discussion some of the areas in which further research efforts are required have been emphasised. It is evident from the preceding arguments that several challenging problems, both in terms of microstructural features and with regard to the detailed fracture mechanisms, have to be considered before a complete understanding of the fracture behaviour of controlled rolled HSLA-steels is achieved.

7. REFERENCES

Akamatsu, T., Sakamoto, T., Taumi, M and Watanabe, K.:
Trans ISIJ. 16, 1976, 241

Almond, E.A., King, J.T. and Embury, J.D.:
Metallography, 3, 1970, 1

Almond, E.A., Timbres, D.H. and Embury, J.D.:
"Fracture 1969", Proc. Second Int. Conf. on Fracture,
p 253, Chapman and Hall, London, 1969.

Almond, E.A., Timbres, D.H. and Embury, J.D.:
Can. Met. Quart, 8, 1969, 51

Argon, A.S., Im, J. and Needleman, A.:
Met. Trans. 6A, 1975, 815

Argon, A.S., Im, J. and Safoglu, R.:
Met. Trans. 6A, 1975, 825.

Ashby, M.F.:
Phil. Mag., 14, 1966, 1157

Baird, J.D. and Preston, R.R.:
"Proc. Processing and Properties of Low Carbon Steel",
p1 Edited by J.M.Gray. AIME, New York, 1973.

Beauchamp, E.R.:
"High Strength Low Alloy Steels for Arctic Pipelines, with
Special Emphasis on the New Manganese - Columbium - Molybdenum
Grades". Report. Noranda Research Center, 1973.

Bilby, B.A., Cottrell, A.H. and Swindon, K.H.:
Proc. Roy. Soc. A272, 1963, 304

Biss, V. and Cryderman, R.L.:
Met. Trans. 2A, 1971, 2267

Boyd, J.D.:
Canada Centre for Mineral and Energy Technology.
Report No. ERP/PMPL - 75 - 13 (R), 1975.

Boyd, J.D.:
Met.Trans. 7A, 1976, 1577.

Bramfitt, B.L. and Marder, A.R.:
"Proc. Processing and Properties of Low Carbon Steel".
p 191, Edited by J.M.Gray, AIME, New York, 1973.

Brandon, D.G.: "Modern Techniques in Metallography".
Butterworths, London, 1966.

Bridgeman, P.W.:
Studies in Large Plastic Flow and Fracture.
McGraw-Hill, 1952.

Brown, L.M. and Embury, J.D.:
"Proc. Third. Int. Conf. Strengthening of Metals and Alloys". p 164,
Cambridge, 1973.

Brozzo, P., Buzzichelli, G., Mascanzoni, A. and Mirabile, M.:
Met. Sci. J. 11, 1977, 123.

Bucher, J.H. and Hamburg, E.G.:
Society of Automotie Engineers,
Publ. No 770164, 1977.

Chao, H.C.:
Paper presented at the AIME Fall Meeting. Chicago 1977.

Chessnut, J.C. and Spurling, R.A.:
Met. Trans. 8A, 1977, 216.

Chipperfield, C.G. and Knott, J.F.
Metals Technology 2, 1975, 45.

Christian, J.W.: "Strengthening Methods in Crystals".
Edited by Kelly, P.M. and Nicholson, R.B. p. 261,
Elsevier, Amsterdam, 1971.

Claussing, D.P.:
Int. J. Fract. Mech 6, 1970, 71.

Clayton, J.Q. and Knott, J.F.:
Metal Science. 10, 1976, 63.

Coldren, A.P. and Mihelich, J.L.:
in "Molybdenum Containing Steels for Gas and Oil Industry
Applications", published by Climax Molybdenum Co., Ann Arbor, 1977.

Coldren, A.P., Cryderman, R.L. and Smith, Y.E.:
"Proc. Processing and Properties of Low Carbon Steel",
Edited by J.M. Gray, p 169, AIME, New York, 1973.

Coleman, T., Dulieu, D., and Gouch, A.:
"Proc. Third, Int. Conf. Strenthening of Metals and Alloys".
p. 70, Cambridge, 1973.

Cottrell, A.H.:
Trans. AIME, 212, 1958, 192.

Cottrell, A.H.:
Proc. Roy. Soc. A285, 1965, 10.

Curry, D.A. and Knott, J.F.:
Met. Sci. J. 10, 1976, 1.

Davenport, A.T., Miner, R.E. and Kot, R.A.:
"Hot Deformation of Austenite".
TMS-AIME, Cincinnati, 1977.

Eagan, G.R.:
Eng. Fract. Mech. 5, 1973, 167.

Embury, J.D., Evensen, J.D, and Filipovic, A.:
"Fundamental Aspects of Structural Alloy Design".
Edited by R.K.Jaffe. Plenum Press, 1977.

Ernst, R.H. and Spretnak, J.W.:
Trans. ISIJ. 9, 1969, 361.

Fukuda, M., Hashimoto, T., and Kunishige, K.:
The Sumitomo Search, 9, 1973, 8.

Gerberich, W.W. and Guest, P.J.:
Int. J. Fract. Mech, 6, 1970, 98.

Glover, A.G., McGrath, J.T., Winkler, M.J. and Weatherly, G.C.:
Canadian Welding Development Institute, Report:
"The influence of Cooling rate and Composition on Weld Metal Microstructures in a C/Mn and a HSLA Steel". Toronto, March 1977.

Gray, J.M.:
"Metallurgy of HSLA Pipeline Steels",
Molybdenum Corp. of America, Rep. No 7201, 1972.

Green, A.P. and Hundy, B.B.:
J. Mech. Phys. Sol. 4, 1956, 128.

Griffis, C.A.:
J. Pres. Ves. Techn. 1975, 278.

Griffiths, J.R. and Owen, D.R.J.:
J. Mech. Phys. Sol. 19, 1971, 419.

Habraken, L.J. and Economopoulos, M.:
Symposium: "Transformation and Hardenability in Steels".
Published by Climax Molybdenum Co. 1969.

Hahn, G.T., Hoagland, R.G. and Rosenfield, A.R.:
Met.Trans. 7A, 1976, 49.

Hahn, G.T., Hoagland, R.G., Kanninen, M.F. and Rosenfield, A.R.:
Eng. Fract. Mech. 7, 1975, 583.

Hahn, G.T., Owen, W.S., Averbach, B.L. and Cohen, M.:
"Fracture" p. 91, Wiley, New York, 1959.

Heald, P.T., Spink, G.M. and Worthington, P.J.:
Met.Sci. Eng. 10, 1972, 129.

Heald, P.T., Spink, G.M. and Worthington, P.J.:
Central Electricity Generating Board, Report No.
RD/L/N 172/72, 1972.

Herø, H., Evensen, J.D. and Embury, J.D.:
Can. Met. Quart. 14, 1975, 117.

Hill, R.: "Mathematical Theory of Plasticity".
p 245, Oxford University Press 1950.

Hirth, J.P. and Froes, F.H.:
Met. Trans, 8A, 1977, 1165.

Hornbogen, E. and Beckmann, K.D.:
Arch Eisenhüttenwesen, 47, 1976, 553.

Inagaki, H.:
Trans. ISIJ. 17, 1977, 166.

Johansen, T.H., Christensen, N., and Augland, B.:
Trans AIME, 239, 1967, 1651.

Jones, A. and Walker, B.:
Metal Science. 8, 1974, 397.

Kallend, J.S., Morris, P.P. and Davis, G.J.:
"Hot Deformation of Austenite".
TMS-AIME, Cincinnati, 1977.

Kirkaldy, J.S.:
Met. Trans. 4, 1973, 2327.

Kirkaldy, J.S., von Destinon-Forstmann, J. and Brigham, R.J.:
Can.Met.Quart, 1. 1962, 59.

Klevebring, B.I.:
Scand. J. Met. 3, 1974, 102.

Knott, J.F.: JISI 204, 1966, 104.

Knott, J.F.:
"Fundamentals of Fracture Mechanics".
Butterworths, London, 1973.

Knott, J.F.:
"Fracture 1977". Proc. Fourth. Int. Conf. on Fracture,
p 1-61, University of Waterloo Press. Waterloo 1977.

Landes, J.D. and Begley, J.A.:
"Test Results from J-integral Studies".
ASTM STP. 560, Part II, p. 170, ASTM, Philadelphia, 1974.

Lange, E.A.:
"Dynamic Fracture-Resistance Testing and Methods for Structural Analysis".
NRL Report 7979, Washington D.C. 1976.

Le Bon, A., Rofes-Vernis, J. and Rossard, C.:
Metal Science 9, 1975, 36.

Le Roy, G.:
Private Communications, McMaster University, 1977.

Lereim, J.:
Private Communications, McMaster University, 1977.

Lindley, T.C., Oates, G. and Richards, C.E.:
Acta Met. 18, 1970, 1127.

Lotter, U., Meyer, L. and Knorr, R.D.:
Arch. Eisenhüttenwesen, 47, 1976, 289.

Low, J.R.: "Relation of Properties to Microstructure" p 163, ASM, 1954.

Lu, W-K. and McLean, A.:
Metals and Materials 8, 1974, 452.

Luyckx, L., Bell, J.R., McLean, A. and Korchynsky, M.
Met. Trans. 1, 1970, 3341.

Luyckx, L.: Presented at the Annual ASM Materials Science Symposium.
Cincinnati, 1975.

Malkin, J. and Tetelman, A.S.:
Eng. Fract. Mech. 3, 1971, 151.

Matsuda, S., Inone, T., Mimura, H., and Okamura, Y.:
Trans ISIJ 12, 1972, 325.

McClintock, F.A.:
Ductility, p 255, ASM, Ohio, 1968.

McCutcheon, D.B., Trumper, T.W. and Embury, J.D.
Rev.Met. 1976, 143.

McLean, A. and Kay, A.:
"Micro Alloying 75". Proc.Int.Symp. HSLA-steels, p. 215, Washington 1975.

McMahon, C.J. and Cohen, M.:
Acta. Met. 13, 1965, 591.

Miyoshi, E., Fukuda, M., Iwanaga, H. and Okazawa, T.:
Conf. on Crack Propagation in Pipelines.
Inst. of Gas, UK, March 1974.

Oates, G.:
JISI 207, 1969, 353.

Ohmori, Y.: Trans ISIJ. 15, 1975, 194.

Ohmori, Y., Ohtani, H., and Kunitake, T.:
Met. Sci. 8, 1974, 357.

Parrini, C., Pizzimenti, N. and Pozzi, A.
Micro Alloying 75". Proc. Washington 1975.

Pickering, F.B.:
Symposium: Transformation and Hardenability in Steels,
p 109, published by Climax Molybdenum Co. 1967.

Pickering, F.B.:
"Micro Alloying 75". Proc.Int.Symp. HSLA-steels, p 9, Washington 1975.

Rawal, S.P. and Gurland, J.:
Met. Trans. 8A, 1977, 691.

Rice, J.R. and Johnson, M.A.:
"Inelastic Behaviour of Solids".
edited by Kanninen M.F., Adler, W.F., Rosenfield, A.R.,
Jaffe, R.I., McGraw-Hill, 1969.

Ritchie, R.O., Francis, B. and Server, W.L.:
Met. Trans. 7A, 1976, 831.

Ritchie, R.O., Knott, J.F. and Rice, J.R.:
J.Mech. Phys. Sol. 21, 1973, 395.

Robinson, J.N. and Tetelman, A.S.:
Eng. Fract. Mech. 8, 1976, 301.

Sailors, R.H.:
ASTM, STP 605, 1976, p. 34.

Sekine, H. and Maruyama, T.:
Proc. Third. Int. Conf. on Strengthening of Metals and Alloys: p 85, Cambridge 1973.

Shewmon, P.G.:
"Transformations in Metals", p 210,
McGraw-Hill, 1969.

Shewmon, P.G.:
"Diffusion in Solids".
McGraw-Hill, 1963.

Smith, E.:
Proc. Conf. Physical Basis of Yield and Fracture, p 36.

Inst. Phys., Phys. Soc., Oxford 1966.

Smith, R.F. and Knott, J.F.:
Practical Applications of Fracture Mechanics in Pressure Vessel Technology.
Inst. Mechn. Engrs. 1972.

Speich, G.R. and Dabkowski, D.S.:
"Hot Deformation of Austenite".
TMS-AIME, Cincinnati, 1977.

Tada, Paris, and Sih,
Handbook of Stress Analysis.

Tanaka, J., Tani, S., and Ouchi, C.:
Trans. ISIJ 15, 1975, 19.

Tegart, W.J., McG. and Gittins, A.:
"Hot Deformation of Austenite",
TMS-AIME, Cincinnati, 1977.

Tetelman, A.S., Wilshaw, T.R., and Rau, C.A.:
Int. J. Fract. Mech. 4, 1968, 147.

Tither, G., and Lauprecht, W.E.:
in "Molybdenum Containing Steels for Gas and Oil Industry Applications". published by Climax Molybdenum Co. Ann Arbor, 1977.

Thomason, P.F.:
J.Inst. Met. 54, 1969, 360.

Wells, A.A.:
Proc. Roy. Soc. A285, 1965, 34.

Wilson, W.G. and Wells, R.G.:
Metal Progress 1973, 75.

Woodhead, J.H. and Whiteman, J.A.:
"Processing and Properties of Low Carbon Steels"., Edited by J.M.Gray, p.145. AIME, New York, 1973.